MESON AND BARYON STRUCTURE IN A GENERALIZED NJL MODEL

by

JACEK SZWEDA

A dissertation submitted to Graduate Faculty in Physics in partial fulfillment of the requirements for the degree of Doctor of Philosophy, The City University of New York

1995

This manuscript has been read and accepted for the Graduate Faculty in Physics in satisfaction of the dissertation requirement for the degree of Doctor of Philosophy.

June 19, 1995
Date

Carl Shakin
Chair of Examining Committee

June 16, 1995
Date

Joseph B. Kiniger
Executive Officer

Carl Shakin
Carl M. Shakin

Louis S. Celenza
Louis S.Celenza

Peter M.L. Lesser
Peter Lesser

Ming-Kung Liou
Ming-Kung Liou

Ngee-Pong Chang
Ngee-Pong Chang

Supervisory Committee

THE CITY UNIVERSITY OF NEW YORK

Abstract

MESON AND BARYON STRUCTURE IN A GENERALIZED NJL MODEL

by

JACEK SZWEDA

Adviser: Distinguished Professor Carl M. Shakin

We use the Nambu-Jona-Lasinio (NJL) model to study the structure of mesons and baryons with particular attention given to an interpretation of the scalar-isoscalar (sigma) meson that plays an important role in nuclear structure studies and in the description of nucleon-nucleon scattering. To carry out this program, we generalize the NJL model to include the description of confinement. We also study nucleon structure based upon a quark-diquark model of the nucleon. It is found that scalar (T=0) diquark and the axialvector (T=1) diquark contribute approximately equal amplitudes in the nucleon wave function.

Acknowledgements

To Professor Carl M. Shakin, my thesis advisor, I wish to express my deepest gratitude for his valuable guidance and constant encouragement throughout this work.

I would also like to express my sincere gratitude to Professor Louis S. Celenza for many useful discussions and for help given to me during the course of this work.

I wish to acknowledge with gratitude the Department of Physics of Brooklyn College and the Research Foundation of CUNY for the financial support during the course of this work.

CONTENTS

Chapter 1

Introduction

1.1 General Survey

In this work we will discuss several topics. These are mainly concerned with the nature of the "sigma meson", a low-mass scalar-isoscalar interaction that plays an important role in nuclear structure studies [Ce 86] and in the description of a nucleon-nucleon scattering [Ma 89]. Since there is no experimental evidence for a low-mass sigma ($m_\sigma \approx 550$ MeV), the nature of this excitation is not understood. (Often sigma exchange is considered as representing "correlated two-pion exchange" [Du 77, Du 80].) In this work, we hope to clarify the nature of the sigma meson and explain how it can be an important degree of freedom for nuclear structure studies, while not appearing in the data tables. Our basic result is that, if the sigma momentum is timelike, the sigma is very strongly mixed into the two-pion continuum [Ce 93a, Ce 93b]. However, when the sigma meson's momentum is spacelike, the sigma is sufficiently far away from the two-pion continuum so as to be a distinct degree of freedom. (Note that the sigma meson used in nuclear physics studies is spacelike.)

For our studies we have made use of the Nambu-Jona-Lasinio model [Na 61] and have generalized the model to include a description of confinement [Ce 93c]. The generalized model has amplitudes with only physical cut structure, the cut structure

arising from the presence of on-mass-shell quarks being removed by the confinement model.

We continue our work by studying the structure of the nucleon in a quark-diquark model [Is 93a,Is 93b]. The use such a model greatly simplifies the study of a three-quark model of nucleon structure that would otherwise require a solution of the three-body Faddeev equations. Aside from simplifications created by the quark-diquark model, there are other reasons for believing that such a model may be important for nucleon structure. We may note that the work of Shuryak and collaborators [Sh 93] on hadronic current correlation functions provide results that are quite similar those of NJL model. Shuryak makes use of a random instanton vacuum that is supposed to provide a satisfactory model of the QCD vacuum. It is found that there is strong attraction in the scalar-isoscalar channel leading to a diquark with energy of about 400 MeV. Also found is a axial vector (T = 1) diquark of energy of about 900 MeV. (These results are similar to those obtained in the NJL model when one studies diquarks.) The fact that Shuryak's work makes a good fit to hadronic current correlation functions obtained in lattice simulation of QCD provides further confidence in Shuryak's model.

Some further support for strong quark-quark correlations in the nucleon comes from the study of deep-inelastic scattering [We 94]. In particular, the ratio of neutron to proton structure functions, $F_2^n(x)$ / $F_2^p(x)$ may be understood by noting that the scalar diquark is more strongly coupled and, therefore, describes a smaller object (with higher momentum components) than the axialvector diquark.

Further support for the use of the NJL model in our work comes from the

Lagrangian of chiral perturbation theory. It has been shown that the low-energy parameters, that specify the terms of order p^4 in the chiral Lagrangian are well reproduced by the effective chiral Lagrangian generated from the NJL model [Bi 93]. The correspondence is particularly satisfactory if one recognizes the fact that the NJL model will generate a rho meson. Indeed, it may be seen that the chiral Lagrangian may be modeled in a formalism that takes into account the low-energy resonances of QCD.

The plan of our work may be seen by inspecting the Table of Contents. We now proceed to a short review of applications of the NJL model to the study of meson structure [Vo 91].

1.2 The Nambu–Jona-Lasinio Model

The Nambu-Jona-Lasinio (NJL) model was constructed (pre-QCD) in 1961 [Na 61]. The theory was based on an analogy with the BCS theory of superconductivity and described the dynamics of nucleons interacting via a point-like interaction. The model was then reinterpreted as a dynamical theory of quarks. A review of the NJL model can be found in [Vo 91] and [Kl 92].

The Lagrangian density of the NJL model in a flavor-SU(2) version has the form:

$$\mathcal{L}(x)= \bar{q}(i\partial_\mu\gamma^\mu - m_q^0)q + \frac{G_s}{2}[(\bar{q}q)^2 + (\bar{q}i\gamma_5\vec{\tau}q)^2]. \qquad (1.1)$$

The mass m_q^0 is a current quark mass and is here taken to be the same for up and down quarks. The Lagrangian of the NJL model exhibits chiral symmetry, if $m_q^0=0$. The dynamical breaking of chiral symmetry can be observed in the model, if G_s is large enough. The constituent quark mass, which is usually found to be about 300 - 400 MeV, can be obtained by solving the gap equation:

$$m_q^{const} = m_q^0 + G_s n_c n_f \int \frac{d^4k}{(2\pi)^4} \mathrm{Tr}\left[\frac{i}{\not{p} - m_q^{cons} + i\epsilon}\right] . \qquad (1.2)$$

The low-lying mesons are found by solving a Bethe-Salpeter equation for a quark and antiquark in the scalar (σ) and the pseudoscalar (π) channel, for example. The T-matrices in these channels satisfy the equations:

$$T_S(q^2) = -G_s + G_s\, J_S(q^2)\, T_S(q^2) . \qquad (1.3a)$$

and

$$T_P(q^2) = -G_s + G_s\, J_P(q^2)\, T_P(q^2) . \qquad (1.3b)$$

The pion appears as the Goldstone boson of the theory. The functions $J_S(q^2)$ and $J_P(q^2)$ are the quark-loop integrals:

$$J_P(q^2) = in_c n_f Tr \int \frac{d^4p}{(2\pi)^4} [i\gamma_5 S_F(p+\frac{q}{2}) i\gamma_5 S_F(p-\frac{q}{2})] \ , \qquad (1.4)$$

and

$$J_S(q^2) = in_c n_f Tr \int \frac{d^4p}{(2\pi)^4} [S_F(p+\frac{q}{2}) S_F(p-\frac{q}{2})] \ . \qquad (1.5)$$

These integrals are divergent and are regulated by going to a Euclidean momentum space, with momentum cutoff Λ [Vo 91, Kl 92]. The equations of (1.3) can be solved for the scattering amplitudes T_S and T_P :

$$T_S(q^2) = \frac{-G_s}{1 - G_s J_S(q^2)} \ . \qquad (1.6a)$$

and

$$T_P(q^2) = \frac{-G_s}{1 - G_s J_P(q^2)} \ . \qquad (1.6b)$$

The mass of the mesons is determined by the pole position; for example, $1 - G_s J_P(m_\pi^2) = 0$ determines the pion mass. The pion mass is zero if $m_q^0 = 0$.

Using this model, we can also exhibit some results of current algebra, such as the Goldberg-Treiman and the Gell-Mann-Oakes-Renner relations. The model has two shortcomings. It is not a renormalizable field theory, so that a regularization scheme must be specified to define the divergent integrals. The second shortcoming is that quarks are not confined. This leads to a nonphysical imaginary part of $J_S(q^2)$ and $J_P(q^2)$, for $q^2 > 4m_q^2$, corresponding to both the quark and antiquark going on mass shell. In this work we want to eliminate this unphysical process (via a confining potential).

1.3 Models of Baryons

One may describe a meson as a two-body system. The Bethe-Salpeter equation can be solved and Lorentz-covariant meson wave functions can be obtained. However, the standard models of baryons generally lack Lorentz covariance. The first model of a baryon was the constituent quark model. It was based on the SU(3)-flavor group and was constructed in 1964 by Gell-Mann and Zweig. Nonrelativistic potential models were used in conjunction with the SU(3) model and the quarks were often taken to move in an oscillator potential.

In 1974 we saw the introduction of bag models of the nucleon. The bag model is based on the assumption that QCD ground state does not support chromoelectric current. The hadrons are represented as color singlet "bags" of perturbative vacuum occupied by quarks and gluons. The hadron wave function is obtained by solving the

Dirac equations derived from the lagrange density [Jo 78]

$$\mathcal{L}_{bag} = (\mathcal{L}_{QCD} - B)\,\theta(\bar{q}q) , \qquad (1.7)$$

where the θ-function (which is zero for negative arguments) defines the volume occupied by confined system. The "bag constant" B represents the difference in energy density between the QCD vacuum and the perturbative vacuum ($B \simeq 66$ MeV/fm^3).

Chiral lagrangians can be used to study baryons. One example is the Skyrme model. The skyrmion is the soliton solution derived from a specific form of a chiral Lagrangian. The physical solutions are projections of the skyrmion with appropriate quantum numbers [Ba 83].

Another model that has been studied is a chiral confining model. It is constructed by introduction of color dielectric function $\kappa(x)$. The expectation value of this function is zero in vacuum. The function $\kappa(x)$ modifies the quark-meson interaction terms in the Lagrangian and it prevents the existence of a colored object in the vacuum.

Here we consider the model of the nucleon based on the NJL model. [See Eq.(1.1).] For the study of baryons, it is useful to transform the lagrangian so that it describes the interaction between two quarks, rather than using the form given in Eq.(1.1), which is most appropriate for the study of meson properties [Is 93a, 93b]. One finds that the quark-quark interaction gives rise to bound states (diquarks). The quark-quark T-matrix can be written in terms of these diquarks. With that representation, the three-body equation for the nucleon can be reduced to an effective two-body equation.

The solution is Lorentz invariant and takes into account correlations between quarks. Chapter 5 of this work contains the details of this program.

Chapter 2

Coupled-Channel Dynamics in the Nambu-Jona-Lasinio Model

2.1 The Sigma Meson

A low-mass scalar-isoscalar meson (of mass of about 500-600 MeV) plays an important role in the boson-exchange model of the nucleon-nucleon interaction [Ma 89], in the Walecka model [Se 86] and in relativistic Brueckner-Hartee-Fock Theory [Ce 86]. For example, the nucleon-nucleon interaction can be described by a relativistic one-boson-exchange potential (OBEP) [Ma 89]. This potential can be used to obtain the NN scattering amplitude by solving a reduced (three-dimensional) form of the Bethe-Salpeter equation. The OBE potential is constructed by summing the contribution of the various mesons (π,σ,ϱ,ω) exchanged between the nucleons. The coupling constants of the mesons to nucleons can be obtained by fitting experimental data. Almost all of the mesons used correspond to physical particles and their masses are taken from the data tables. The (scalar-isoscalar) sigma meson used in the OPE potential has the mass of about 550 MeV. (This meson provides an important part of the potential – the intermediate range attraction.) However, the existence of such a particle is not supported by any experimental evidence. In the data tables one finds physical scalar-isoscalar states at 975 MeV and

1400 MeV. These are the $f_0(975)$ and $f_0(1400)$ resonances. We suggest that the $f_0(1400)$ is predominantly a $q\bar{q}$ state, while the $f_0(975)$ is likely to be a quasibound $K\bar{K}$ state. The fact that the width of the $f_0(1400)$ is about 200-400 MeV, while the width of the $f_0(975)$ is about 47 MeV, tends to support our identification.

Exchange of the sigma meson is usually interpreted as "correlated two-pion exchange". In contrast, in the NJL model the sigma meson is constructed as a quark-antiquark bound state. In this work, we consider the strong mixing between the quark-antiquark channel and two-pion channel, and consider the consequences of such coupling for our study of the nature of the sigma meson.

2.2 Coupling of the Sigma Meson to the Two-Pion Continuum

To better understand the dynamics in the scalar-isoscalar sector, it is useful to study the coupling of the $q\bar{q}$ channel to two-pion channel. This coupling can be evaluated in the NJL model. For the purposes of this calculation, the pion can be treated as elementary particle, with the mass calculated in the basic NJL model. Further, pion propagators can be used in the calculation of Feynman diagrams. For example, the coupling of a meson of $q\bar{q}$ character to the $\pi\pi$ channel can be calculated in a one-loop approximation, as shown in Fig. 2.1(a). That coupling gives rise to an effective interaction in the $q\bar{q}$ channel of type shown in Fig. 2.1(b). Since the three-loop calculation implied by Fig. 2.1(b) is difficult, we first consider the approximation presented in Fig. 2.1(d). That implies that the process shown in Fig. 2.1(b) is

approximated by the process in Fig. 2.1(c). The use of this approximation defines model A. The explicit calculation of the three-loop diagram, in some approximation, serves to define model B.

With our approximation, the coupled-channel problem can be solved algebraically. Pion rescattering can be also included by introduction of a four-pion vertex with coupling constant G_π. The equations for the T matrices have the form

$$T_{qq}(q^2) = K_{qq} + K_{qq}\,\hat{J}_s(q^2)\,T_{qq}(q^2) + K_{q\pi}\,\hat{J}_\pi(q^2)\,T_{\pi q}(q^2) \quad , \tag{2.1}$$

$$T_{\pi q}(q^2) = K_{\pi q} + K_{\pi\pi}\,\hat{J}_\pi(q^2)\,T_{\pi q}(q^2) + K_{\pi q}\,\hat{J}_S(q^2)\,T_{qq}(q^2) \quad . \tag{2.2}$$

(See Fig. 2.2) Here,

$$K_{qq} = -G_S\, I_B \cdot I_A \tag{2.3}$$

$$K_{\pi q} = G_{S\pi}\, I_B \cdot I_\pi \tag{2.4}$$

$$K_{\pi q} = G_{S\pi}\, I_\pi \cdot I_A \tag{2.5}$$

$$K_{\pi\pi} = G_\pi\, I_\pi \cdot I_\pi \tag{2.6}$$

and

$$T_{qq}(q^2) = f_{qq}(q^2)\, I_B \cdot I_A \quad , \tag{2.7}$$

$$T_{q\pi}(q^2) = f_{q\pi}(q^2)\, I_A \cdot I_\pi \quad , \tag{2.8}$$

with

$$I_A = 1^{\text{Dirac}}\, 1^{\text{isospin}}\, 1^{\text{color}} \tag{2.9}$$

denoting the product of unit matrices in Dirac, flavor, and color spaces. In Eq. (2.3), the two unit operators, I_A and I_B, refer to the initial and final $q\bar{q}$ pair . In Eq. (2.4) we define the transition matrix connecting the $q\bar{q}$ states to states of two pions.

The symbol I_π denotes a unit operator in the pion isospin space . (In Eq. (2.6), we define an interaction matrix for $\pi\pi\to\pi\pi$. However, in the following we will put $G_\pi=0$.) Equations (2.7) and (2.8) specify the structure of the T matrices, T_{qq} and $T_{q\pi}$, respectively. Finally, the quantities, $\hat{J}_S(q^2)$ and $\hat{J}_\pi(q^2)$ appearing in Eqs. (2.1) and (2.2) are defined to be

$$\hat{J}_S(q^2) = -i \int \frac{d^4k}{(2\pi)^4} S_F(q+k)\, S_F(k)\, 1^{\text{isospin}}\, 1^{\text{color}} \quad , \tag{2.10}$$

and

$$\hat{J}_\pi(q^2) = -i \int \frac{d^4k}{(2\pi)^4} G(q+k)\, G(k)\; I_\pi \cdot I_\pi \; . \tag{2.11}$$

Equations (2.1) and (2.2) can be simplified by summing the isospin and color indices. We obtain the equations for the amplitudes defined in Eqs. (2.7) and (2.8),

$$f_{qq}(q^2) = -G_S + G_S J_S(q^2) f_{qq}(q^2) + G_{S\pi} J_\pi(q^2) f_{\pi q}(q^2) \quad , \tag{2.12}$$

$$f_{\pi q}(q^2) = G_S + G_{\pi S} J_\pi(q^2) f_{\pi q}(q^2) - G_{S\pi} J_S(q^2) f_{qq}(q^2) \quad , \tag{2.13}$$

where, with $iS_F(k) = i[\not{k} - m_q^{const} + i\epsilon]^{-1}$ and $iG(k) = i[k^2 - m_\pi^2 + i\epsilon]^{-1}$, we have

$$J_S(q^2) = n_c n_f i \int \frac{d^4k}{(2\pi)^4} Tr[\, S_F(q+k)\, S_F(k)\,] \ , \tag{2.14}$$

and

$$J_\pi(q^2) = 3i \int \frac{d^4k}{(2\pi)^4} G(q+k)\, G(k) \quad . \tag{2.15}$$

The integrals in Eqs. (2.14) and (2.15) can be evaluated for $q^2 < (2m_q^{cons})^2$ by using a Euclidean momentum space, with cutoff Λ. The result is

$$J_S(q^2) = \frac{3}{2\pi^2} \int_0^1 dx \left[\Lambda^2 - 3A \ln \frac{\Lambda^2 + A}{A} + 2A \frac{\Lambda^2}{\Lambda^2 + A} \right] ; \quad q^2 < 4m_q^2 \tag{2.16}$$

and

$$J_\pi(q^2) = -\frac{3}{2\pi^2} P\int_0^1 \left[\ln\left|\frac{\Lambda^2+B}{B}\right| - \frac{\Lambda^2}{\Lambda^2+B}\right] dx - \frac{3i}{8\pi}\sqrt{1-\frac{4m_\pi^2}{q^2}}\,\theta(q^2-4m_\pi^2)\,, \qquad (2.17)$$

with $A = m_q^2 - q^2x(1-x)$ and $B = m_\pi^2 - q^2x(1-x)$. Here, we have written m_q^{cons} as m_q, for simplicity.

The solution of the coupled (algebraic) equations, Eqs. (2.12) and (2.13), for $f_{qq}(q^2)$ is [Ce 93d]

$$f_{qq}(q^2) = \frac{-G_S + \dfrac{G_{S\pi}J_\pi(q^2)G_{S\pi}}{1 - G_\pi J_\pi(q^2)}}{1 - G_S J_S(q^2) + \dfrac{G_{S\pi}J_\pi(q^2)G_{S\pi}J_S(q^2)}{1 - G_\pi J_\pi(q^2)}} \,. \qquad (2.18)$$

For $q^2 < (2m_q^{cons})^2$, $J_S(q^2)$ is real, while $J_\pi(q^2)$ has an imaginary part for $q^2 > (2m_\pi)^2$. The values of $J_S(q^2)$ are presented in the upper part of Fig. 2.3, while the lower part of that figure shows Re $J_\pi(q^2)$ and Im $J_\pi(q^2)$. Note that Re $J_\pi(q^2)$ and Im $J_\pi(q^2)$ are related through a dispersion relation. Thus, the peak in Re $J_\pi(q^2)$ is associated with the opening of the two-pion channel at $q^2=(2m_\pi)^2$. In this figure, the heavy line on horizontal axis denotes the region $q^2 > (2m_q^{cons})^2$. (This region starts at $q^2=0.365$ GeV^2 for the parameters considered here.) Predictions of the model in this region are not useful, since the two-quark continuum represents an unphysical aspect of the NJL model, if we are to use that model to represent some aspects of QCD.

In a similar fashion, we can obtain $T_{\pi\pi}$. The relevant equations are

$$T_{\pi\pi}(q^2) = K_{\pi\pi} + K_{\pi q}\, \hat{J}_s(q^2)\, T_{\pi\pi}(q^2) + K_{\pi\pi}\, \hat{J}_\pi(q^2)\, T_{\pi\pi}(q^2) \quad , \tag{2.19}$$

and

$$T_{q\pi}(q^2) = K_{q\pi} + K_{q\pi}\, \hat{J}_\pi(q^2)\, T_{\pi\pi}(q^2) + K_{qq}\, \hat{J}_S(q^2)\, T_{q\pi}(q^2) \quad . \tag{2.20}$$

The solution for the amplitude $f_{\pi\pi}(q^2)$ is then [Ce 93d]

$$f_{\pi\pi}(q^2) = \frac{G_\pi - \dfrac{G_{S\pi} J_S(q^2) G_{S\pi}}{1 - G_S J_S(q^2)}}{1 - G_\pi J_\pi(q^2) + \dfrac{G_{S\pi} J_S(q^2) G_{S\pi} J_\pi(q^2)}{1 - G_S J_S(q^2)}} \quad . \tag{2.21}$$

If $G_\pi = 0$, we have

$$f_{\pi\pi}(q^2) = -\frac{G_{\pi S} J_S(q^2) G_{S\pi}}{1 - G_S J_S(q^2) + G_{\pi S}^2 J_S(q^2) J_\pi(q^2)} \quad , \tag{2.22}$$

$$= -\frac{G_{\pi S} J_S(q^2)\, G_{S\pi}}{D(q^2)} \quad , \tag{2.23}$$

where the last two equations serve to define $D(q^2)$. The denominator, $D(q^2)$, may be used to obtain a value for the phase shift, δ_0^0, describing elastic π-π scattering. We have

$$\tan\delta_0^0 = - \frac{\mathrm{Im}\, D(q^2)}{\mathrm{Re}\, D(q^2)} \qquad (2.24)$$

in the case $G_\pi=0$.

2.3 Calculation of Pion-Pion Scattering in the Extended NJL Model

First, we discuss model A, where the coupling of the $q\bar{q}$ channel to two-pion channel is approximated as in Fig. 2.1(d). (As noted above, in all our calculations we have put $G_\pi=0$.) We consider $G_{S\pi}$ to be an adjustable parameter at this point. Increasing $G_{S\pi}$ leads to broader resonance in the scattering amplitude. There is also a downward shift in the resonance energy that becomes larger as $G_{S\pi}$ is increased. These features may be seen in Fig. 2.4, where we plot δ_0^0 for several values of $G_{S\pi}$. The other parameters are $m_q^{cons} = 302$ MeV, $G_S = 7.91$ GeV^{-2} and $\Lambda = 1.0$ GeV. For $G_{S\pi} = 1.0$ GeV^{-1}, we have indicated a quite narrow resonance at $E_R \simeq 2m_q^{cons}$. For $G_{S\pi} = 2.0$ GeV^{-1}, the resonance is broadened somewhat. When $G_{S\pi} = 3.0$ GeV^{-1}, one can see the point where phase shift passes through 90 degrees ($\sqrt{s} = E_R$). We find $E_R = 0.590$ GeV. The width is found to be $\Gamma = 0.113$ GeV in this case. When $G_{S\pi} = 4.0$ GeV^{-1}, we have $E_R = 0.542$ GeV, which corresponds to a downward shift of about 60 MeV relative to $2m_q^{cons}$.

In this case, we find $\Gamma = 0.248$ GeV. (As we will see, we have reason to adopt the value $G_{S\pi} = 3.8$ GeV^{-1}.)

In Fig. 2.4, we have also represented the experimental data, in a schematic fashion, by the dashed line. It should be clear that the resonant behavior seen in various curves in Fig. 2.4 is inconsistent with the experimental data. Note that, even though the resonance is quite broad, the phase shift passes through 90 degrees for $\sqrt{s} = E_R$. In order to clarify the dynamics of the model, we have made an arbitrary change of Λ from 1.0 GeV to $\Lambda = 1.1$ GeV. That effectively makes the $q\bar{q}$ interaction stronger. We keep the original value of $m_q^{cons} = 302$ MeV, however. The result of this modification may be seen in Fig. 2.5, where curves a, b, and c are the results for $G_{S\pi} = 1.0$ GeV^{-1}, 2.0 GeV^{-1} and 2.5 GeV^{-1}, respectively. In this figure, we more clearly see the increase of both the downward shift of the resonance and the resonance width with increasing $G_{S\pi}$.

2.4 Effective Mass of the Sigma Meson

In Fig. 2.6, we present results for Re $D(q^2)$ for $G_{S\pi} = 1.0$ GeV^{-1} (dashed line) and $G_{S\pi} = 4.0$ GeV^{-1} (solid line). We also show Im $D(q^2)$ for $G_{S\pi} = 4.0$ GeV^{-1} (dotted line). The two-quark continuum starts at $q_{th}^2 = 0.365$ GeV^2, when $m_q^{cons} = 0.302$ GeV. When $G_{S\pi} = 4.0$ GeV^{-1}, we have $E_R = 0.542$ MeV or $q_{th}^2 = 0.294$ GeV^2, which is below the two-quark continuum. With reference to Fig. 2.6, it is also of interest to note that the slopes of the dashed and solid lines differ at $q^2 \simeq 0$. If we consider this model to be useful for $q^2 \simeq 0$, we see that the inclusion of the two-pion

continuum makes a significant change in the mass, $m_\sigma(0)$, that is to be used to parametrize the quark-antiquark scattering amplitudes for $q^2 \simeq 0$. For example, for $G_{S\pi}$ = 1.0 GeV^{-1}, $m_\sigma(0) \simeq 0.775$ GeV, while for $G_{S\pi}$ = 4.0 GeV^{-1}, we would have $m_\sigma(0)$ $\simeq$ 0.500 GeV. In Fig. 2.6, we also see that, for the dashed curve, the value of $m_\sigma(0)$ is significantly different from the physical mass that corresponds to a zero of $D(q^2)$.

We now turn to a discussion of model B. If we perform a more complex calculation, as represented by Fig. 2.1(b), for example, we can provide a value of the effective coupling, $G_{S\pi}$, in terms of the parameters of the NJL model: Λ, $g_{\pi qq}$, m_q^{cons}, G_S, and m_π. This can be done, if we adjust the value of the imaginary parts of the diagrams of Fig. 2.1(b) and 2.1(c) to be equal for small values of q^2 , with $q^2 > 4m_\pi^2$. A description of the evaluation of the diagram of Fig. 2.1(b) is given in the Appendix A. We proceed by calculating the imaginary part of the diagram and obtain the real part by means of a dispersion relation. This procedure requires some extrapolation of the imaginary part of the diagram, Im $M(q^2)$, into the region $q^2 > (2m_q^{const})^2$, where we do not attempt to calculate $M(q^2)$. We choose to perform a linear extrapolation that is depicted in Fig. 2.7. In that figure, values of $ReG_{\pi S}^2 J_\pi(q^2)$ and $ImG_{\pi S}^2 J_\pi(q^2)$ are shown as dashed lines for the choice $G_{S\pi}$ = 3.8 GeV^{-1}. That value of $G_{S\pi}$ leads to the coincidence of the curves for $ImM(q^2)$ and $ImG_{\pi S}^2 J_\pi(q^2)$ for small $q^2 > 4m_\pi^2$. We note the different behavior seen for $ImM(q^2)$ and $ImG_{\pi S}^2 J_\pi(q^2)$ for $q^2 \geq 0.2 GeV^2$. We also see a different behavior for $ReM(q^2)$ and $ReG_{\pi S}^2 J_\pi(q^2)$ for $q^2 \geq 0.1 GeV^2$. This difference is such as to lead to an upward shift of the resonance, since $ReM(q^2) > 0$ for $q^2 \geq 0.28$ GeV^2, while

Re $G_{\pi S}^2 J_\pi(q^2)$ is negative in that region.

The fact that the resonance is shifted upward in model B is reflected in the values for $D(q^2)$ obtained in that model. (To obtain $D(q^2)$ in model B, we need only replace $G_{\pi S}{}^2 J_\pi(q^2)$ in our previous formula by $M(q^2)$.) Values of Re $D(q^2)$ and Im $D(q^2)$ are shown in Fig. 2.8, where we see that Re $D(q^2) \neq 0$ in the region $q^2 < (2m_q{}^{const})^2$. We also note a rapid variation of Re $D(q^2)$ with the opening of the two-pion channel.

Inspection of Fig. 2.8 also tells us that, for the region around $q^2 = 0$, $\mathrm{Re}D(q^2) \simeq (q^2 - m_\sigma{}^2)$ with $m_\sigma \simeq 0.55$ GeV. This represents a specific example of how the mass parameter m_σ could depend on the region of q^2 under consideration. We may call the appropriate value of $m_\sigma(q^2)$ for $q^2 \leq 0$, the effective mass. In this work, we denote the effective mass as $m_\sigma(0)$. From Fig. 2.8, we see that $m_\sigma(0) \simeq 550$ MeV. While we cannot study the behavior of $D(q^2)$ for $q^2 > (2m_q{}^{const})^2$, Fig. 2.8 does suggest that the zero of Re $D(q^2)$ is such that the physical mass is significantly larger than $m_\sigma(0)$.

We now wish to overcome some of the limitations of the analysis presented in this section. In particular, in the next chapter, we show how a model of confinement may be introduced that allows us to consider coupling to the two-pion channel when $q^2 > (2m_q)^2$. As we will see, our model of confinement eliminates the $q\bar{q}$ cut that appear in the coupled-channel T-matrix, for example [Ce 93c].

Chapter 3

Description of the Confinement

3.1 The Linear Confining Potential

There are a number of models of the confinement that may be considered. For example, one can study quark propagators that do not allow for on-mass shell propagation, or one may consider a bag model of confinement. We here will use a linear potential to describe confinement in the study of meson structure. We will see that, when the linear potential is included, the quark and antiquark are prevented from going on-mass-shell simultaneously. In our model, which is related to that of Gross and Milana [Gr 91, Gr 92], we will see that one particle can be on-mass-shell. The formalism is such as to prevent the other particle from going on-mass-shell. That is, the amplitude for decay has a zero when both quark and antiquark are on-mass-shell.

To confine quarks in a meson we used a coordinate-space linear potential of the form

$$V_L(\vec{r}) = \kappa|\vec{r}|\exp(-\mu|\vec{r}|) \quad . \tag{3.1}$$

We note that, if μ is small enough, Eq. (3.1) represents a linear potential over a range of several fermis. Usually, taking $\mu \simeq 0.050$ GeV is adequate. The advantage of using Eq. (3.1) is that finite values of μ regulate the strong singularities at $\vec{k} = 0$ of the Fourier transform of $V_L(\vec{k})$.

If we use the potential of Eq. (3.1), find that the Fourier transform is

$$K(\Delta^2) = 4\pi\kappa \left\{ - \frac{2}{(\Delta^2 + \mu^2)^2} + \frac{8\mu^2}{(\Delta^2 + \mu^2)^3} \right\} , \qquad (3.2)$$

with $\Delta^2 = (\vec{k} - \vec{k}')^2$.

Note that this form of Δ^2 does not describe energy transfer. If we had placed the quark on-mass-shell, rather then specifying $k^0 = 0$, we would have $\Delta^2 = -[E(\vec{k}) - E(\vec{k}')]^2 + (\vec{k} - \vec{k}')^2$. As discussed by Gross and Milana in [Gr 91] and [Gr 92], allowing for energy transfer worsens the convergence properties of the integral equation they study and requires the insertion of form factors. We have not considered that option here.

3.2 The Vertex Function for Confined Quarks in the Scalar-Isoscalar Channel

Consider the sum of diagrams in the upper-part of Fig. 3.1(b). These diagrams serve to define a vertex, the filled triangular shape in Fig. 3.1(b). In Fig. 3.1(c), we

show the equation satisfied by the vertex, where, for the scalar-isoscalar channel, the driving term is unity in the Dirac, flavor and color space. (Note that the Bethe-Salpeter equation for a bound state would be homogeneous. In that case there would be no driving term and we would have an engenvalue problem. That feature characterizes the bound-state problem considered by Gross and Milana.)

The notation we will adopt is shown in Fig. 3.2. In general, the scalar-isoscalar vertex is a Dirac matrix that depends on three variables:

$$\hat{\Gamma}(P^2, P\cdot k, k^2) = \Gamma_1(P^2, P\cdot k, k^2) + \not{P}\,\Gamma_2(P^2, P\cdot k, k^2) + \not{\hat{k}}\,\Gamma_3(P^2, P\cdot k, k^2) + \not{P}\not{\hat{k}}\,\Gamma_4(P^2, P\cdot k, k^2), \tag{3.3}$$

where

$$\hat{k}^\mu \equiv k^\mu - \frac{(k\cdot P)P^\mu}{P^2}\,. \tag{3.4}$$

In the general case, the equation satisfied by the vertex $\hat{\Gamma}(P^2,P\cdot k,k^2)$ is

$$\hat{\Gamma}(P,k) = 1 + i\int \frac{d^4k'}{(2\pi)^4} O^i(1)S(P/2+k')\Gamma(P,k')S(-p/2+k')O^i(2)V_i(k,k'), \tag{3.5}$$

where a sum over i is implied. Here, we have introduced a interaction of the form [Gr 91, Gr 92]

$$\hat{V}(k,k') = \sum_i O^i(1)O^i(2)V_i(k,k'), \tag{3.6}$$

where $O^i(1)$ and $O^i(2)$ are Dirac or isospin matrices associated with the sources of confining potential.

We have chosen to study the form

$$\hat{V}(k,k') = K(\Delta^2)\ \mathbf{1}(1)\ \mathbf{1}(2) \tag{3.7}$$

corresponding to a scalar confining potential.

Instead of using the basis defined by Eq. (3.1), we can use an equivalent basis constructed with the use of positive and negative-energy projection operators. For the scalar-isoscalar vertex, we define functions Γ^{++}, Γ^{+-}, etc.:

$$\Lambda^{(+)}(\vec{k})\hat{\Gamma}(P^2,P\cdot k,k^2)\Lambda^{(+)}(\vec{k}) = \Lambda^{(+)}(\vec{k})\Lambda^{(+)}(\vec{k})\Gamma^{++}(P^2,P\cdot k,k^2) \quad , \tag{3. 8}$$

$$\Lambda^{(+)}(\vec{k})\hat{\Gamma}(P^2,P\cdot k,k^2)\Lambda^{(-)}(-\vec{k}) = \Lambda^{(+)}(\vec{k})\Lambda^{(-)}(-\vec{k})\Gamma^{+-}(P^2,P\cdot k,k^2) \quad , \tag{3. 9}$$

$$\Lambda^{(-)}(-\vec{k})\hat{\Gamma}(P^2,P\cdot k,k^2)\Lambda^{(+)}(\vec{k}) = \Lambda^{(-)}(-\vec{k})\Lambda^{(+)}(\vec{k})\Gamma^{-+}(P^2,P\cdot k,k^2) \quad , \tag{3.10}$$

$$\Lambda^{(-)}(-\vec{k})\hat{\Gamma}(P^2,P\cdot k,k^2)\Lambda^{(-)}(-\vec{k}) = \Lambda^{(-)}(-\vec{k})\Lambda^{(-)}(-\vec{k})\Gamma^{--}(P^2,P\cdot k,k^2) \quad , \tag{3.11}$$

where

$$\Lambda^{(+)}(\vec{k}) = \frac{\not{k}_{on} + m_q}{2m_q} \quad , \tag{3.12}$$

and

$$\Lambda^{(-)}(-\vec{k}) = \frac{\not{\tilde{k}}_{on} + m_q}{2m_q} \quad , \tag{3.13}$$

with $k^{\mu}_{on} = (E(\vec{k}), \vec{k})$ and $\tilde{k}^{\mu}_{on} = (-E(\vec{k}), \vec{k})$.

We can use the fact that

$$S(p) = \frac{m_q}{E(\vec{p})}\left[\frac{\Lambda^{(+)}(\vec{p})}{p^0 - E(\vec{p}) + i\epsilon} + \frac{\Lambda^{(-)}(-\vec{p})}{p^0 + E(\vec{p}) - i\epsilon}\right] \quad , \tag{3.14}$$

and define

$$S^{(+)}(p) = \frac{m_q}{E(\vec{p})} \frac{\Lambda^{(+)}(\vec{p})}{p^0 - E(\vec{p}) + i\epsilon} , \tag{3.15}$$

and

$$S^{(-)}(p) = - \frac{m_q}{E(\vec{p})} \frac{\Lambda^{(-)}(-\vec{p})}{p^0 + E(\vec{p}) - i\epsilon} , \tag{3.16}$$

so that $S(p) = S^{(+)}(p) + S^{(-)}(p)$.

We also put $\vec{P} = 0$ and use the approximation of evaluating the k_0' integrals by closing the contour in the lower-half plane and picking up the residues at the Green's function poles. We find that Γ^{+-} is only coupled to Γ^{-+} and that Γ^{++} and Γ^{--} may be determined from the knowledge of Γ^{+-} and Γ^{-+}. We also find that the interaction potentials do not contain P^0, which now only appears in the energy denominators.

The equations obtained in the projection operator scheme, in the absence of retardation, are

$$\begin{bmatrix} \Gamma^{+-}(P^0, |\vec{k}|) \\ \Gamma^{-+}(P^0, |\vec{k}|) \end{bmatrix} = \begin{bmatrix} 1 \\ 1 \end{bmatrix} + \int \frac{d\vec{k}'}{(2\pi)^3} V(\vec{k}-\vec{k}') t(\vec{k}-\vec{k}') \begin{bmatrix} \Gamma^{+-}(P^0, |\vec{k}'|) \\ \Gamma^{-+}(P^0, |\vec{k}'|) \end{bmatrix} , \tag{3.17}$$

where the matrix $t(\vec{k},\vec{k}')$ is

$$t(\vec{k},\vec{k}') = \begin{bmatrix} \dfrac{A(\vec{k},\vec{k}')}{P^0-2E(\vec{k}')+i\epsilon} & \dfrac{B(\vec{k},\vec{k}')}{P^0+2E(\vec{k}')-i\epsilon} \\ \dfrac{-B(\vec{k},\vec{k}')}{P^0-2E(\vec{k}')+i\epsilon} & \dfrac{-A(\vec{k},\vec{k}')}{P^0+2E(\vec{k}')-i\epsilon} \end{bmatrix} . \tag{3.18}$$

Here,

$$A(\vec{k},\vec{k}') = \frac{1}{2E^2(\vec{k}')}\left[-\vec{k}'^2 + \frac{\vec{k}\cdot\vec{k}'}{\vec{k}^2}(E(\vec{k})E(\vec{k}') + m_q^2)\right] , \tag{3.19}$$

and

$$B(\vec{k},\vec{k}') = \frac{1}{2E^2(\vec{k}')}\left[\vec{k}'^2 + \frac{\vec{k}\cdot\vec{k}'}{\vec{k}^2}(E(\vec{k})E(\vec{k}') - m_q^2)\right] . \tag{3.20}$$

We now consider scalar confinement and make use of the interaction of Eqs. (3.1)-(3.2). We define

$$a_0(|\vec{k}|,|\vec{k}'|) = \int d\Omega_{k'} K(\Delta^2) \ , \tag{3.21}$$

$$= -32\pi^2\kappa\left\{\frac{1}{x^2-y^2} - \frac{4\mu^2 x}{(x^2-y^2)^2}\right\} \ , \tag{3.22}$$

where

$$x = \vec{k}^2 + \vec{k}'^2 + \mu^2, \tag{3.23}$$

and

$$y = 2|\vec{k}||\vec{k}'|. \tag{3.24}$$

We also need

$$a_1(|\vec{k}|,|\vec{k}'|) = \int d\Omega_{k'} K(\Delta^2)(\hat{k}\cdot\hat{k}'), \tag{3.25}$$

$$= \frac{1}{y}[x a_0 - b_1], \tag{3.26}$$

where

$$b_1 = 16\pi^2\kappa\left\{ \frac{1}{y}\ln\left[\frac{x-y}{x+y}\right] + \frac{8\mu^2}{x^2-y^2} \right\}. \tag{3.27}$$

Thus, Eq (3.17) may be written

$$\begin{bmatrix} \Gamma^{++}(P^0,|\vec{k}|) \\ \Gamma^{-+}(P^0,|\vec{k}|) \end{bmatrix} = \begin{bmatrix} 1 \\ 1 \end{bmatrix} + \int d|\vec{k}'|h(\vec{k},\vec{k}') \begin{bmatrix} \Gamma^{++}(P^0,|\vec{k}'|) \\ \Gamma^{-+}(P^0,|\vec{k}'|) \end{bmatrix}, \tag{3.28}$$

where the matrix $h(\vec{k},\vec{k}')$ is

$$h(\vec{k},\vec{k}') = \begin{bmatrix} \dfrac{\alpha(\vec{k},\vec{k}')}{P^0-2E(\vec{k}')+i\epsilon} & \dfrac{\beta(\vec{k},\vec{k}')}{P^0+2E(\vec{k}')-i\epsilon} \\ \dfrac{-\beta(\vec{k},\vec{k}')}{P^0-2E(\vec{k}')+i\epsilon} & \dfrac{-\alpha(\vec{k},\vec{k}')}{P^0+2E(\vec{k}')-i\epsilon} \end{bmatrix}. \tag{3.29}$$

Here, $\alpha(\vec{k},\vec{k}')$ and $\beta(\vec{k},\vec{k}')$ only depend upon the magnitudes of $\vec{k}$ and $\vec{k}'$. We have,

$$\alpha(\vec{k},\vec{k}') = \frac{1}{(2\pi)^3}\frac{\vec{k}'^2}{2E^2(\vec{k}')}\left\{ -\vec{k}'^2 a_0 + \frac{|\vec{k}'|}{|\vec{k}|}[E(\vec{k})E(\vec{k}') + m_q^2]a_1 \right\}$$

(3. 30)

and

$$\beta(\vec{k},\vec{k}') = \frac{1}{(2\pi)^3}\frac{\vec{k}'^2}{2E^2(\vec{k}')}\left\{ \vec{k}'^2 a_0 + \frac{|\vec{k}'|}{|\vec{k}|}[E(\vec{k})E(\vec{k}') - m_q^2]a_1 \right\}.$$

(3. 31)

We note that our equations take on a relatively simple form, in part, due to neglect of retardation of the interaction.

3.3 Calculations of Quark-Loop Integrals with Vertex Functions of a Confining Potential.

Results obtained for $\Gamma^{+-}(P^0,|\vec{k}|)$ and $\Gamma^{-+}(P^0,|\vec{k}|)$ are shown in Figs. 3.3 and 3.4. It is important to note that the value of vertex function, $\Gamma(P^0,|\vec{k}|)$, corresponds to the case where both quark and antiquark go on their positive mass shells. That occurs when $|\vec{k}| = k_{on} \equiv \sqrt{P_0^2/4 - m_q^2}$. For confining potentials, we have $\Gamma^{+-}(P^0, k_{on}) = 0$.

We may use our vertex functions in the calculation of the quark-loop integrals that appear in the NJL model. This procedure will remove the imaginary part of these quark-loop integrals that is related to the (unphysical) decay of a meson into a quark and an

antiquark. We wish to calculate the diagrams shown on Figs 3.1(a) and 3.1(b). Calculation of $J'(q^2)$ - the "confined" analog of $J(q^2)$ is straightforward. The only vertex functions which contribute to the integral are $\Gamma^{+-}(P^0, |\vec{k}|)$ and $\Gamma^{-+}(P^0, |\vec{k}|)$, if we again assume that the only relevant poles are those of the Green's functions in the lower-half k_0 plane. In this case, Eq.(2.14) is replaced by

$$J_S'(P^2) = in_c n_f \mathrm{Tr} \int \frac{d^4k}{(2\pi)^4} [S^{(+)}(p/2+k)\Gamma^{+-}(P^0, |\vec{k}|)S^{(-)}(-p/2+k) + S^{(-)}(P/2+k)\Gamma^{-+}(P^0, |\vec{k}|)S^{(+)}(-P/2+k)] , \quad (3.32)$$

in the case where $\vec{P} = 0$. The result obtained, when using the values of Γ^{+-} and Γ^{-+} shown in Figs. 3.3 and 3.4 in the calculation of $J_S'(P^2)$, is shown in Fig. 3.5 as a solid line. For this figure we have $\kappa = 0.2$ GeV^2. The imaginary part of $J_S'(P^2)$ is zero, as expected.

Now consider the calculation of $M'(P^2)$, the function obtained from $M(P^2)$ by introduction of vertex functions of the confining potential. (See Figs 3.6(a)-3.6(b)). In discussing the passage from $M(P^2)$ to $M'(P^2)$, it is useful to define the "form factor" $F(P^2, P \cdot k, k^2)$ shown in Fig 3.6(c). If we include a vertex correction due to confinement, we will call this function $F'(P^2, P \cdot k, k^2)$. We define (see Appendix A)

$$F(P^2, P\cdot k, k^2) = i\int \frac{d^4k'}{(2\pi)^4} Tr[S(P/2+k')S(-P/2+k')\gamma_5 S(k'-k)\gamma_5].$$

(3. 33)

We note that, if the pions are on-mass-shell, $(P/2+k)^2 = m_\pi^2$ and $(-P/2+k)^2 = m_\pi^2$, so that $P\cdot k = 0$. Including vertex functions for the confining field, we have

$$\begin{aligned} F'(P^2, P\cdot k, k^2) = i\int \frac{d^4k'}{(2\pi)^4} Tr[&S^{(+)}(P/2+k')S^{(+)}(-P/2+k')\gamma_5 S(k'-k)\gamma_5 \\ &+ S^{(+)}(P/2+k')\Gamma^{+-}(P,k')S^{(-)}(-P/2+k')\gamma_5 S(k'-k)\gamma_5 \\ &+ S^{(-)}(P/2+k')\Gamma^{-+}(P,k')S^{(+)}(-P/2+k')\gamma_5 S(k'-k)\gamma_5 \\ &+ S^{(-)}(P/2+k')S^{(-)}(-P/2+k')\gamma_5 S(k'-k)\gamma_5]. \end{aligned}$$

(3. 34)

In Eq. (3.34), we have not included vertices such as Γ^{++} and Γ^{--} that would appear between $S^{(+)}(P/2+k')$ and $S^{(+)}(-P/2+k')$, or between $S^{(-)}(P/2+k')$ and $S^{(-)}(-P/2+k')$. These vertices are difficult to calculate, since they involve Z-graphs generated by the confining field. As long as we use a linear potential for the confining field, we believe it is best not to introduce the vertex functions Γ^{++} and Γ^{--}.

In Eq. (3.34), all integrals are evaluated by first performing the k_0'-integral in the

complex k_0' plane and picking up the residues at the poles of the propagators $S^{(-)}(P/2+k')$ and $S^{(-)}(-P/2+k')$. The insertion of $\Gamma^{+-}(P,k')$ and $\Gamma^{-+}(P,k')$ is sufficient to remove unphysical cuts for $P^2<4m_q^2$, so that only the physical two-pion cut contributes to Im $M'(P^2)$.

In Fig. 3.7, we show values obtained for $M'(P^2)$ as a dashed line. In the calculation all three-momenta in the loop integral for the form factor, F', are cut off at $\Lambda_3 = 0.702$ GeV. (That value corresponds to an Euclidean-momentum cutoff of 1.0 GeV and was chosen to reproduce results calculated previously for $P^2 < 4m_q^2$, where a Wick rotation could be made).

In Fig. 3.7, we show, as a solid line, the result of a calculation made without a model of confinement. In that case, only the principal value of the integral defining the form factor $F(P^2, P\cdot k, k^2)$ was kept. Thus, only the two-pion cut contributed to $\mathrm{Im}M(P^2)$. It may be seen that such an approximation, although without justification, does provide a reasonable approximation to Im $M'(P^2)$ (dashed curve).

Once we have values for Im $M'(P^2)$, we can use a dispersion relation to obtain $\mathrm{Re}\,M'(P^2)$:

$$\mathrm{Re}\,M'(P^2) = -\frac{\mathcal{P}}{\pi}\int_{4m_\pi^2}\frac{\mathrm{Im}\,M'(P'^2)dP'^2}{P^2-P'^2}. \tag{3.35}$$

The result obtained for $\mathrm{Re}M'(P^2)$ is shown in Fig. 3.8 as a solid line, while $\mathrm{Im}M'(P^2)$, is shown as a dashed line.

In Fig. 3.9, we exhibit the denominator of the scalar-isoscalar T-matrix calculated

in various approximations. The dot-dashed curve shows the function $1\text{-}G_S J_S(P^2)$ and we see a zero at $P^2 = m_\sigma^2$, where $m_\sigma \simeq 0.62$ GeV. The dashed line shows the value of $1\text{-}G_S J_S'(P^2)$. The zero of this quantity is at $P^2 \simeq (0.79 \text{ GeV})^2$. Finally, the solid line shows the quantity $1\text{-}G_S J_S'(P^2)\text{-}M'(P^2)J_S'(P^2)$. There, we see that the pole in the T-matrix has been moved up to about $P^2 \simeq (0.84 \text{ GeV})^2$.

Although the pole in the T-matrix is at a fairly large energy, we will still have an unsatisfactory situation given our understanding of experimental data. Therefore, we define $D'(P^2) = 1\text{-}G_S(P^2)J_S'(P^2)\text{-}M'(P^2)J_S'(P^2)$, using a momentum-dependent coupling constant $G_S(P^2)$ to weaken the interaction at the larger values of P^2. In Fig. 3.10 we exhibit $G_S(P^2)$. (Note that $G_S(0)=7.91$ GeV^{-1}). The solid line in the upper part of Fig. 3.10 shows $D'(P^2)$, while the dashed line is $1\text{-}G_S(P^2)J_S'(P^2)$. These values of $D'(P^2)$ (solid line) yield a rather featureless scalar-isoscalar T-matrix in accord with our understanding of the experimental data.

Chapter 4

The Scalar-Isoscalar Current Correlator

4.1 The Scalar-Isoscalar Current Correlator in the NJL Model

We define the scalar current $j_S(x) = \bar{q}(x)q(x)$ and consider the correlation function [Ce 93a]

$$-iC_T(P^2) = \int d^4x\ e^{iP\cdot x} \langle 0|T[j_S(x)j_S(0)]|0\rangle \ . \tag{4.1}$$

We write

$$C_T(P^2) = J_S'(P^2) + C_S(P^2), \tag{4.2}$$

where $J_S'(P^2)$ is the quark-loop integral of Eq. (3.32), modified to include a vertex, $\hat{\Gamma}(P,k)$, for the confining field. The function $C_S(P^2)$ satisfies an unsubtracted dispersion relation

$$\mathrm{Re}\, C_S(P^2) = -\frac{\mathcal{P}}{\pi}\int_{4m_\pi^2} dP' \frac{\mathrm{Im}\, C_S(P'^2)}{P^2 - P'^2}\ , \tag{4.3}$$

and has a cut starting at $4m_\pi^2$. That function describes the coupling of the $q\bar{q}$ states to the two-pion continuum. To obtain Im $C_S'(P^2)$, we calculate the discontinuity across the two-pion cut. In Fig 4.1(a), we show the basic physical process. There we see that the $q\bar{q}$ pair is created at a point. The wave-matrix Ω takes this $q\bar{q}$ pair into two on-mass-shell pions. The wave matrix may be written in terms of a T-matrix, $t_{\pi q}$, describing the transition: $q\bar{q} \rightarrow \pi\pi$. If we use our coupled-channel quark-hadron model, we obtain the diagrams of Fig. 4.1, where crosses denote on-mass-shell pions and t_{qq} is the $q\bar{q}$ T-matrix of our model. Thus, we see that we have model for $t_{\pi q}(P^2)$ based on knowledge of $t_{qq}(P^2)$. (See Eq. (2.13)). Recall that, given our interpretation of experimental data, $t_{qq}(P^2)$ has only a relatively weak dependence over the entire range of P^2 in our model. (See Fig. 3.10 and Eq.(3.1)).

We now define

$$-\mathrm{Im}C_S(P^2) = \mathrm{Im}C^{(0)}(P^2) + \mathrm{Im}C^{(1)}(P^2) + \mathrm{Im}C^{(2)}(P^2), \tag{4.4}$$

where $\mathrm{Im}C^{(0)}(P^2)$, $\mathrm{Im}C^{(1)}(P^2)$ and $\mathrm{Im}C^{(2)}(P^2)$ corresponds to Fig. 4.2(a), Fig. 4.2(b) and Fig. 4.2(c), respectively. (The crosses on the wavy lines denote on-mass-shell pions). We constructed $\mathrm{Im}C^{(2)}(P^2)$ in terms of the discontinuity of the $q\bar{q}$ T-matrix. We find that

$$\text{Im } t_{qq}(P^2) = \frac{\text{Im } M'(P^2)}{|D'(P^2)|^2} , \tag{4.5}$$

where

$$D'(P^2) = 1 - G_s(P^2)J'(P^2) + M'(P^2)J'(P^2). \tag{4.6}$$

Thus, we see that Fig. 4.2(c) gives

$$\text{Im } C^{(2)}(P^2) = \frac{J_s'(P^2)\ \text{Im } M'(P^2)\ J_s'(P^2)}{|D'(P^2)|^2} . \tag{4.7}$$

From inspection of Fig. 4.2(a), we find

$$\text{Im} C^{(0)}(P^2) = \frac{\text{Im } M'(P^2)}{G_s(P^2)^2} . \tag{4.8}$$

(This term is very small and neglected). Further, from Fig. 4.2(b), we have

$$\text{Im} C^{(1)}(P^2) = \frac{2\text{Re} D'(P^2)}{|D'(P^2)|^2} \frac{J_s'(P^2)}{G_s(P^2)} \text{Im} M'(P^2) . \tag{4.9}$$

In Fig. 4.3, we show values obtained for $\text{Im}C^{(2)}(P^2)$ (solid line) and $-\text{Im}C(P^2) \simeq \text{Im}C^{(1)}(P^2) + \text{Im}C^{(2)}(P^2)$ (dashed line). We proceed to calculate $\text{Re}C(P^2)$ by use of the

dispersion relation of Eq. (4.3). The solid line in Fig. 4.4 shows the value obtained for $ReC(P^2)$ when $ImC(P^2)$ of Fig. 4.4 is used [Ce 93a].

4.2 Interpolation Between the Low-Energy and the High-Energy Behavior of the Hadronic Current Correlator

To maintain a close analogy to the description of a vector meson, we define

$$P^2\bar{\Pi}_S(P^2) = C_T(P^2) - C_T(0) , \tag{4.10}$$

$$P^2\Pi_S^{cont}(P^2) = J_S'(P^2) - J_S'(0) , \tag{4.11}$$

$$P^2\Pi_S^{Res}(P^2) = C_S(P^2) - C_S(0) . \tag{4.12}$$

We have found values of $J_S'(P^2)$ for relatively small P^2, say $P^2 < 1GeV^2$. To obtain values of $J_S'(P^2)$ for all P^2 we can use dispersion relation and the imaginary part of quark loop diagram $Im\Pi_S^{cont}(s)$ [Sh 93b]. The function $Im\Pi_S^{cont}(s)$ represents the imaginary part of the quark-loop integral calculated in perturbation theory. It can be parametrized as

$$\mathrm{Im}\,\Pi_S^{cont}(s) = \frac{3}{4\pi}\left[1 + \exp\left[\frac{\sqrt{s_0} - \sqrt{s}}{\delta}\right]\right]^{-1}, \tag{4.13}$$

where s_0 is a threshold factor. The form of this parametrization requires that we make a subtraction, if we are to write a dispersion relation. We have

$$\bar{J}_S(P^2) = J'_S(0) + \frac{P^2}{P_0^2}[J'_S(P_0^2) - J'_S(0)] + \frac{P^2(P^2 - P_0^2)}{\pi}\int ds \frac{\mathrm{Im}\Pi_S^{cont}(s)}{(P_0^2 - s)(P^2 - s)}. \tag{4.14}$$

We found $J'_S(0) = 0.088\ \mathrm{GeV}^2$ and, with $P_0^2 = 1\ \mathrm{GeV}^2$, we have $J'_S(P_0^2) = 0.157\,\mathrm{GeV}^2$. [Sh 93b]. In Fig. 4.5 we show $\mathrm{Im}\Pi_S^{cont}(s)$. The dashed curve was calculated using the generalized NJL model. It is seen that the dispersion relation yields a smooth curve that interpolates between the asymptotic behavior and the nonperturbative behavior described by the NJL model and is shown as a dashed line in Fig. 4.5.

It is not necessary to make a subtraction in $\Pi_S(P^2)$. However, we have made such a subtraction so that we may exhibit a function that is not singular for $P^2 = 0$. Thus, we have

$$\bar{\Pi}_S(P^2) = \frac{[\bar{J}_S(P^2) - J'_S(0)]}{P^2} + \frac{[C_S(P^2) - C_S(0)]}{P^2}. \tag{4.15}$$

This function is shown in Fig. 4.6 as a solid line, while the dashed line represents the second term on right-hand side of Eq. (4.10). We remark that the resonant-like behavior of $[C_s(P^2) - C_s(0)]/P^2$ dominates the values of $\bar{\Pi}_s(P^2)$ for $-4\,GeV^2 < P^2 < 4\,GeV^2$. For large, negative P^2, the values of $\bar{\Pi}_s(P^2)$ are given by $-(3/4\pi^2)\ln|P^2| + 0.064$, with P^2 in GeV^2 units. (That function provides a very good approximation to $\bar{J}_s(P^2)/P^2$ for $P^2 < 1\ GeV^2$.) As discussed earlier, the behavior seen in Fig. 4.6 does <u>not</u> imply that there is a <u>physical</u> sigma meson of mass of about 500 MeV. On the other hand, the behavior for $P^2 < 0$ is well approximated using a sigma-dominance model.

Chapter 5

The Properties of Diquarks

5.1 The Lagrangian in the Diquark Representation

The nucleon can be constructed as a mixture of a scalar diquark and a axialvector diquark, both bound to a quark. The constituent quark model suggests that the nucleon contains about equal amplitudes of the scalar diquark - quark state and the axialvector diquark - quark state. We will calculate the masses and vertex functions for these two kinds of diquarks.

The NJL lagrangian for the quark-quark channel is [Is 93a, Is93b]

$$\mathcal{L} = \bar{q}(i\,\partial_\mu\gamma^\mu - m_0)q - \frac{\bar{G}_S}{2}\sum_{c=1}^{3}(\bar{q}\gamma_5 C\tau_2 t^c\bar{q}^T)(q^T C^{-1}\gamma_5\tau_2 t^c q)$$

$$+ \frac{\bar{G}_V}{2}\sum_{c=1}^{3}(\bar{q}i\gamma_\mu C\vec{\tau}\tau_2 t^c\bar{q}^T)(q^T iC^{-1}\gamma^\mu\tau_2\vec{\tau}t^c q) + \ldots \quad . \tag{5.1}$$

Here, the SU(3)-color matrices are $(t^c)_{ab} = i\sqrt{\frac{3}{2}}\,\epsilon_{abc}$. The normalization is such that $\mathrm{tr}\ t^c t^{c'} = 3\,\delta^{cc'}$. The matrix C is the charge-conjugation transformation matrix. (In terms of Dirac matrices, we have $C = i\gamma_0\gamma_2$). The second term in the lagrangian of Eq. (5.1)

contributes to the two-body T-matrix in the scalar diquark channel, and the third term to the two-body T-matrix in the axialvector channel. This form of the lagrangian is obtained by use of a Fierz transformation. One can use the original form of the NJL lagrangian [see Eq.(1.1)] as the starting point of the Fierz transformation. In this case $\bar{G}_S = G_S/6$ and $\bar{G}_V = G_S/12$. If one uses the color-current lagrangian, with an interaction term of the form

$$\mathcal{L}_I(x) = -G_C(\bar{q}\gamma_\mu \frac{\lambda_c^i}{2} q)(\bar{q}\gamma^\mu \frac{\lambda_c^i}{2} q) \ , \tag{5.2}$$

the relation between the coupling constants is $\bar{G}_S = G_S/2$ and $\bar{G}_V = G_S/4$. We will not use these relations and we will treat $\bar{G}_S$ and $\bar{G}_V$ as parameters in our model.

The Bethe-Salpeter equation for a quark-quark T-matrix in the scalar channel is

$$T_S^d(q^2) = -2\bar{G}_S + \bar{G}_S J_S^d(q^2) T_S^d(q^2) \ . \tag{5.3}$$

This equation is similar to Eqs. (1.3a) and (1.3b). The function $J_S^d(q^2)$ is a quark-loop integral

$$J_S^d(q^2) = -i6 \int \frac{d^4k}{(2\pi)^4} Tr[\gamma_5 C S^T(q-k) C^{-1} \gamma_5 S(k)] , \tag{5.4}$$

$$= -i6 \int \frac{d^4k}{(2\pi)^4} Tr[\gamma_5 S(-q+k) \gamma_5 S(k)] \quad . \tag{5.5}$$

Note, that the function $J_S^d(q^2)$ is equal to the quark-loop integral in the pion channel, $J_P(q^2)$. (See. Eq. (1.5).) The solution of Eq. (5.3) is

$$T_S^d(q^2) = \frac{-2\bar{G}_S}{1 - \bar{G}_S J_S^d(q^2)} . \tag{5.6}$$

The equation $1 - \bar{G}_S J_S^d(m_S) = 0$ determines the scalar-diquark mass.

The Bethe-Salpeter equation for a quark-quark T-matrix in the transverse component of the axialvector channel is

$$T_V^{\mu\nu}(q^2) = -2\bar{G}_V \hat{g}^{\mu\nu} + \bar{G}_V J_{V\ \lambda}^{\mu}(q^2)\ T_V^{\lambda\nu}(q^2) , \tag{5.7}$$

with

$$T_V^{\mu\nu}(q^2) = T_V^d(q^2) \hat{g}^{\mu\nu} , \tag{5.8}$$

and

$$J_V^{\mu\nu}(q^2) = J_V^d(q^2)\,\hat{g}^{\mu\nu}. \tag{5.9}$$

Here $\hat{g}^{\mu\nu} = g^{\mu\nu} - \frac{q^\mu q^\nu}{q^2}$.

The quark-loop integral $J_V^{\mu\nu}(q^2)$ is

$$J_V^{\mu\nu}(q^2) = -i6\int \frac{d^4k}{(2\pi)^4}\,\mathrm{Tr}[\hat{\gamma}^\mu C S^T(q-k) C^{-1}\gamma^\nu S(k)], \tag{5.10}$$

$$= -i6\int \frac{d^4k}{(2\pi)^4}\,\mathrm{Tr}[\hat{\gamma}^\mu S(-q+k)\gamma^\nu S(k)]\ . \tag{5.11}$$

The function $J_V^d(q^2)$ can be found by multiplying Eq. (5.11) by $g_{\mu\nu}$,

$$J_V^d(q^2) = -i2\int \frac{d^4k}{(2\pi)^4}\,\mathrm{Tr}[\hat{\gamma}^\mu S(-q+k)\gamma_\mu S(k)]\ . \tag{5.12}$$

The solution of Eq. (5.7) can be written in terms of scalar functions defined by Eqs. (5.8) and (5.9),

$$T_V^d(q^2) = \frac{-2\bar{G}_V}{1 - \bar{G}_V J_V^d(q^2)}\ . \tag{5.13}$$

The equation $1 - \bar{G}_V J_V^d(m_V^2) = 0$ determines the axialvector-diquark mass.

We now wish to extend the model of diquarks by introducing a confinement potential in the quark-quark channel.

5.2 The Scalar Diquark and the Interaction V_L

We now introduce the vertex for a scalar diquark to go into two quarks in the presence of the confining potential V_L. The lineal potential V_L was introduced in Chapter 3. (See Eqs (3.1) and (3.1)). The "driving term" of our equation is $\gamma_5 C^{-1} \tau_2 t_c$, however, τ_2 and t_c may be factored out of the equation. Therefore, we define $\hat{\Gamma}_S(P,k)$ as the solution of the equation

$$\hat{\Gamma}_S(P,k)\gamma_5 C = \gamma_5 C + i\int \frac{d^4k'}{(2\pi)^4} S(P/2+k')\, \hat{\Gamma}_S(P,k')\gamma_5 C\, S^T(P/2-k')\, V_L(k-k') . \tag{5.14}$$

Using the fact that $C\, S^T(k)\, C^{-1} = S(-k)$, it is easy to see that Eq. (5.14) looks like the equation describing the pseudoscalar-meson vertex functions. We multiply Eq. (5.14) by iC^{-1} from the right and find

$$\hat{\Gamma}_S(P,k)\, i\gamma_5 = i\gamma_5 + i\int \frac{d^4k'}{(2\pi)^4} S(P/2+k')\hat{\Gamma}_S(P,k')\, i\gamma_5 S(-P/2+k')V_L(k-k'). \tag{5.15}$$

In order to solve Eq. (5.15), we will use the projection operator basis described in Chapter 3. In the scalar-diquark case, the introduction of four scalar functions Γ_S^{++}, Γ_S^{+-}, Γ_S^{-+} and Γ_S^{--} is useful. We define these functions by the relations,

$$\Lambda^{(+)}(\vec{k})\, \hat{\Gamma}_S(P,k)\, i\gamma_5\, \Lambda^{(+)}(-\vec{k}) = \Gamma_S^{++}(P,k)\, \Lambda^{(+)}(\vec{k})\, i\gamma_5 \Lambda^{(+)}(-\vec{k}), \tag{5.16}$$

$$\Lambda^{(+)}(\vec{k})\, \hat{\Gamma}_S(P,k)\, i\gamma_5\, \Lambda^{(-)}(-\vec{k}) = \Gamma_S^{+-}(P,k)\, \Lambda^{(+)}(\vec{k})\, i\gamma_5 \Lambda^{(-)}(-\vec{k}), \tag{5.17}$$

$$\Lambda^{(-)}(\vec{k})\, \hat{\Gamma}_S(P,k)\, i\gamma_5\, \Lambda^{(+)}(-\vec{k}) = \Gamma_S^{-+}(P,k)\, \Lambda^{(-)}(\vec{k})\, i\gamma_5 \Lambda^{(+)}(-\vec{k}), \tag{5.18}$$

and

$$\Lambda^{(-)}(\vec{k})\, \hat{\Gamma}_S(P,k)\, i\gamma_5\, \Lambda^{(-)}(-\vec{k}) = \Gamma_S^{--}(P,k)\, \Lambda^{(-)}(\vec{k})\, i\gamma_5 \Lambda^{(-)}(-\vec{k}). \tag{5.19}$$

As in our study of the scalar meson, only two of these functions appear in the equations for the vertex function. These functions are Γ^{+-} and Γ^{-+}, as was the case in our previous study. We will use an approximation in which the coupling between Γ^{+-} and Γ^{-+} is dropped. Then, the uncoupled equations describing the vertex function of the scalar diquark have the final form

$$\Gamma_S^{+-}(P_0,|\vec{k}|) = 1 + \int \frac{d^3k'}{(2\pi)^3} \frac{E(\vec{k})}{4m_q^2 E(\vec{k}')} (E(\vec{k})E(\vec{k}') - \vec{k}\vec{k}' + m_q^2) V_L(|\vec{k}-\vec{k}'|) \frac{\Gamma_S^{+-}(P_0,|\vec{k}'|)}{P_0 - 2E(\vec{k}) + i\epsilon},$$

(5.20)

and

$$\Gamma_S^{-+}(P_0,|\vec{k}|) = 1 + \int \frac{d^3k'}{(2\pi)^3} \frac{E(\vec{k})}{4m_q^2 E(\vec{k}')} (E(\vec{k})E(\vec{k}') - \vec{k}\vec{k}' + m_q^2) V_L(|\vec{k}-\vec{k}'|) \frac{-\Gamma_S^{+-}(P_0,|\vec{k}'|)}{P_0 + 2E(\vec{k}) - i\epsilon}.$$

(5.21)

The introduction of the potential V_L modifies the quark-antiquark T-matrix. It can be shown that the solution of the Bethe-Salpeter equation in the case that both the NJL interaction and potential V_L are present is

$$T'^{d}_S(P^2) = \frac{-2\bar{G}_S}{1 - \bar{G}_S J'^{d}_S(P^2)} . \qquad (5.22)$$

The quark-quark loop integral in the presence of the potential V_L is

$$J'^{d}_S(P^2) = -i6 \int \frac{d^4k}{(2\pi)^4} Tr[\hat{\Gamma}_S(P,k)\gamma_5 C S^T(P/2-k) C^{-1}\gamma_5 S(P/2+k)] , \qquad (5.23)$$

$$J'^{d}_{S}(P^2) = -6\int \frac{d^3k}{(2\pi)^3}\,\frac{1}{2}\left[\frac{\Gamma_S^{+-}(P_0,|\vec{k}|)}{P_0 - 2E(\vec{k}) + i\epsilon} - \frac{\Gamma_S^{-+}(P_0,|\vec{k}|)}{P_0 + 2E(\vec{k}) - i\epsilon}\right] . \qquad (5.24)$$

The functions $\Gamma_S^{+-}(P,k)$ and $\Gamma_S^{-+}(P,k)$ are presented in Fig. 5.1 and function $J'^{d}_{S}(P^2)$ is presented in Fig. 5.2. The choice of parameters that was made and results of our calculations are presented in Table 5.1.

5.3 The Axialvector Diquark and the Interaction V_L

In case of the axialvector-isovector diquark the equation for the vertex that sums the effects of the confining field is

$$\hat{\Gamma}^{\mu}_{V}(P,k)C = \hat{\gamma}^{\mu}C + i\int \frac{d^4k'}{(2\pi)^4} S(P/2+k')\,\hat{\Gamma}^{\mu}_{V}(P,k')C\,S^{T}(P/2-k')V_L(|\vec{k}-\vec{k}'|) , \qquad (5.25)$$

with $\hat{\gamma}^{\mu} \equiv \gamma^{\mu} - \not{P}P^{\mu}/P^2$. Equation (5.25) can be reduced to the equation that appears in the study of the vector meson. (We saw a similar reduction when we studied the scalar diquark.)

The vertex function in case of the axialvector diquark is described by eight scalar functions. These functions can be defined by the following decomposition :

$$S(P/2+k)\hat{\Gamma}^{\mu}_{V}(P,k)\,C\,S^{T}(P/2-k)\,C^{-1} = S(P/2+k)\hat{\Gamma}^{\mu}_{V}(P,k)\,S(-P/2+k) \tag{5.26}$$

$$= \sum_{i,j\,\in\,(+-)} \left[O^{\mu}_{[i,j]}(1,\vec{k})\,\Gamma^{[i,j]}_{V1}(P_0,|\vec{k}|) + O^{\mu}_{[i,j]}(2,\vec{k})\,\Gamma^{[i,j]}_{V2}(P_0,|\vec{k}|)\right] . \tag{5.27}$$

In Eq. (5.27) the indices i and j are either plus signs or minus signs. Therefore, we have $O^{\mu}_{[+,+]}(1,\vec{k})$, $O^{\mu}_{[+,-]}(1,\vec{k})$, etc. The $O^{\mu}_{[i,j]}$ are defined as

$$O^{\mu}_{[i,j]}(1,\vec{k}) = \hat{k}^{\mu}\,\Lambda^{(i)}(\vec{k}_i)\,\Lambda^{(j)}(\vec{k}_j) , \tag{5.28}$$

and

$$O^{\mu}_{[i,j]}(2,\vec{k}) = \Lambda^{(i)}(\vec{k}_i)\,\gamma^{\mu}_{\perp}(P,k)\,\Lambda^{(j)}(\vec{k}_j) . \tag{5.29}$$

Here, $\hat{k}^{\mu} \equiv k^{\mu} - (k\cdot P)P^{\mu}/P^2$ and $\gamma^{\mu}_{\perp}(P,k) \equiv \hat{\gamma}^{\mu} - \hat{k}\,\hat{k}^{\mu}/\hat{k}^2$.

If we drop the terms which couple the $\Gamma^{[+-]}$ and $\Gamma^{[-+]}$ components, we may write equations for $\Gamma^{[+-]}_{V1}$ and $\Gamma^{[+-]}_{V2}$ that do not contain $\Gamma^{[-+]}_{V1}$ or $\Gamma^{[-+]}_{V2}$:

$$\Gamma^{[+-]}_{V\alpha}(P,k) = d^{+-}_{\alpha} + \sum_{\alpha'=1}^{2} \int \frac{d^3q}{(2\pi)^3} \left[\frac{m_q}{E(\vec{q})}\right]^2 V_L(|\vec{k}-\vec{q}|)\,\frac{t_{\alpha\alpha'}(\vec{k},\vec{q})}{P_0 - 2E(\vec{q}) + i\epsilon}\,\Gamma^{[+-]}_{V\alpha'}(P,q) . \tag{5.30}$$

Here, α and α' are either 1 or 2 and

$$d_1^{+-}(\vec{k}) = -\frac{m_q}{\vec{k}^2}\ , \tag{5.31}$$

$$d_2^{+-}(\vec{k}) = 1\ , \tag{5.32}$$

$$t_{11}(\vec{k},\vec{q}) = \frac{1}{m_q^2}\frac{(\vec{k}\cdot\vec{q})}{2\vec{k}^4}\left[\left(E(\vec{k})E(\vec{q})+m_q^2\right)(\vec{k}\cdot\vec{q}) - \vec{k}^2\vec{q}^2\right], \tag{5.33}$$

$$t_{22}(\vec{k},\vec{q}) = \frac{1}{m_q^2}\frac{E(\vec{q})}{4E(\vec{k})}\left[\left(E(\vec{k})E(\vec{q})+m_q^2\right)\left[1+\frac{(\vec{k}\cdot\vec{q})^2}{\vec{k}^2\vec{q}^2}\right] - 2(\vec{k}\cdot\vec{q})\right], \tag{5.34}$$

$$t_{12}(\vec{k},\vec{q}) = \frac{1}{2m_q}\frac{E(\vec{q})[E(\vec{k})-E(\vec{q})]}{\vec{k}^2}\left[1-\frac{(\vec{k}\cdot\vec{q})^2}{\vec{k}^2\vec{q}^2}\right], \tag{5.35}$$

and

$$t_{21}(\vec{k},\vec{q}) = \frac{1}{4m_q}\frac{[E(\vec{q})-E(\vec{k})]}{E(\vec{k})}\vec{q}^2\left[1-\frac{(\vec{k}\cdot\vec{q})^2}{\vec{k}^2\vec{q}^2}\right]. \tag{5.36}$$

The quark-quark T-matrix in the axialvector channel in the presence of the interaction V_L is

$$T'^{d}_{V}(P^2) = \frac{-2\bar{G}_V}{1-\bar{G}_V J'^{d}_{V}(P^2)}\ . \tag{5.22}$$

The quark-loop integral modified by the confinement interaction is

$$J'^{d}_{A}(P^2) = -i2\int \frac{d^4k}{(2\pi)^4} Tr[\, S(P/2+k)\, \hat{\Gamma}^{\mu}_{A}(P,k)\, C S^{T}(P/2-k)\, C^{-1} \hat{\gamma}_{\mu}\,] \,. \qquad (5.19)$$

The vertex functions $\Gamma^{[+-]}_{A1}(P,k)$ and $\Gamma^{[+-]}_{A2}(P,k)$ are presented in Fig. 5.3 and the function $J'^{d}_{V}(P^2)$ is presented in Fig. 5.4. Our choice of parameters and our results are summarized in Table 5.1.

Chapter 6

The Nucleon in a Generalized NJL Model

6.1 Scalar Diquark Channel

We define the nucleon wave function to be the sum of a scalar (T = 0) diquark part and an axialvector (T = 1) diquark part [Re 90, Eb 86, Ce 89, Bu 92, Is 93a, Is 93b],

$$\Psi_N(P,k,s,t) = \Psi_S(P,k,s,t) + \Psi_V(P,k,s,t). \tag{6.1}$$

As a first step, we solve the reduced Faddeev equation for a nucleon containing only a scalar diquark. In this case, we can write the baryon wave function in two alternate representations:

$$\Psi_S(P,k,s,t) = \psi_{(1)}(P,k)\ u_N(\vec{P},s)\chi_t + \psi_{(2)}(P,k)\frac{\hat{k}}{\sqrt{-\hat{k}^2}}u_N(\vec{P},s)\chi_t. \tag{6.2}$$

and

$$\tilde{\Psi}_S(P,k,s,t) = \tilde{\psi}_{(1)}(P,k)\ \frac{2m_q\Lambda^{(+)}(\vec{k})}{\sqrt{2\,E(\vec{k})\,(E(\vec{k})+m_q)}}u_N(\vec{P},s)\chi_t$$

$$+\ \tilde{\psi}_{(2)}(P,k)\frac{-2m_q\Lambda^{(-)}(-\vec{k})}{\sqrt{2\,E(\vec{k})\,(E(\vec{k})-m_q)}}u_N(\vec{P},s)\chi_t\ . \tag{6.3}$$

These equations serve to define the wavefunctions, $\psi_{(1)}$, $\psi_{(2)}$, $\bar{\psi}_{(1)}$ and $\bar{\psi}_{(2)}$. Here $\Lambda^{(+)}(\vec{k})$ and $\Lambda^{(-)}(-\vec{k})$ are positive and negative-energy projection operators for the quark, χ_t is an isospinor for the nucleon, and $u_N(\vec{P},s)$ is a positive-energy Dirac spinor. The bound-state equation for $\Psi_S(P,k,s,t)$ of Eq. (6.2) is

$$[(P-k)^2 - m_S^2]\,(\not{k} - m_q)\,\Psi_S(P,k,s,t) = \\ i\int \frac{d^4k'}{(2\pi)^4}\,[\,N_C N_I\,(k|V^E(P)|k') + (k|V^C(P)|k')]\,\Psi_S(P,k',s,t)\ , \tag{6.4}$$

with $N_C = 3$, and the isospin factor $N_I = 1$ for the scalar-diquark model. (See Fig. 6.1.) The potential in the last equation is a sum of an exchange potential and a confinement potential. The exchange potential is given in terms of the scalar diquark-quark coupling constant g_S. When $\vec{P} = 0$, we have

$$(k|V^E(P)|k') = 2g_S^2\,\gamma_5 C^{-1} S^T_{(+)}(P-k-k')C\gamma_5\ , \tag{6.5}$$

$$= 2g_S^2\,\frac{m_q}{E(\vec{k}+\vec{k}')}\,\frac{\Lambda^{(+)}(\vec{k}+\vec{k}')}{P_0-k_0-k_0'-E(\vec{k}+\vec{k}')}\ , \tag{6.6}$$

where, in Eq. (6.5), we have used

$$S_{(+)}(k) = \frac{m_q}{E(\vec{k})}\,\frac{\Lambda^{(+)}(\vec{k})}{k_0-E(\vec{k})}\ . \tag{6.7}$$

Note also that $C^{-1}\,S^T(k)\,C = S(-k)$. In Eq.(6.4) we have kept only the part of the quark

propagator that is expressed in terms of positive-energy spinors. As we will see, our work leads us to believe that this represents a good approximation in the study of nucleon structure.

The linear confinement potential is

$$(k|V^C(P)|k') = -8\kappa\pi\left\{\frac{1}{[(\vec{k}'-\vec{k})^2+\mu^2]^2} - \frac{4\mu^2}{[(\vec{k}'-\vec{k})^2+\mu^2]^3}\right\}, \tag{6.8}$$

in momentum space. In coordinate space this potential takes the form

$$V^C(r) = \kappa r e^{-\mu r}, \tag{6.9}$$

where κ can be different for scalar and for axialvector diquarks.

We now multiply Eq. (6.4) by $\bar{u}_N(\vec{P},s)$ from the right and sum over s. The result of this procedure is the matrix wave function $\bar{\Psi}(P,k,t)$, that is now independent of s, but still depends on the isospin index t. This matrix wave function, in the baryon rest frame ($\vec{P} = 0$), is

$$\bar{\Psi}(P,k,t) = \sum_{i=1}^{2} \psi_{(i)}(P\cdot k, k^2)\, O_{(i)}(P,k)\chi_t, \tag{6.10}$$

where $\psi_{(1)}(P\cdot k,k^2)$ and $\psi_{(2)}(P\cdot k,k^2)$ were defined in Eq. (6.2). (Note that $P^2 = m_N^2$.)

Here, we define two matrices in the nucleon rest frame:

$$O_{(1)}(P,k) = \Lambda^{(+)}(\vec{P}=0) \ , \tag{6.11}$$

$$= \begin{bmatrix} 1 & 0 \\ 0 & 0 \end{bmatrix} , \tag{6.12}$$

and

$$O_{(2)}(P,k) = \frac{\hat{k}}{\sqrt{-\hat{k}^2}} \Lambda^{(+)}(\vec{P}=0) \ , \tag{6.13}$$

$$= \begin{bmatrix} 0 & 0 \\ -\vec{\sigma}\cdot\vec{k} & 0 \end{bmatrix} . \tag{6.14}$$

We can see that the wave functions $\psi_{(1)}(P\cdot k, k^2)$ and $\psi_{(2)}(P\cdot k, k^2)$ of Eq.(6.10) represent the upper and lower components of the baryon wave function, respectively.

Operators $O_{(1)}(P,k)$ and $O_{(2)}(P,k)$ produce a basis such that $Tr[O_{(i)}(P,k)\ O_{(j)}(P,k)] = 0$ for $i \neq j$. The bound-state equation, in the basis created by $O_{(1)}(P,k)$ and $O_{(2)}(P,k)$, has a matrix form

$$[(P-k)^2 - m_S^2] \sum_{j=1}^{2} K_{(ij)}\psi_{(j)}(P\cdot k, k^2) = i\int \frac{d^4k'}{(2\pi)^4} \sum_{j=1}^{2} V_{(ij)}\ \psi_{(j)}(P\cdot k', k'^2), \tag{6.15}$$

where i is either 1 or 2. (Recall that $\psi_{(j)}(P\cdot k, k^2)$ was first introduced in Eq.(6.2).) In Eq.(6.15),

$$K_{(ij)} = \frac{Tr[\tilde{O}_{(i)}(P,k)(\not{k} - m_q)O_{(j)}(P,k)]}{|Tr[\tilde{O}_{(i)}(P,k)\,O_{(i)}(P,k)]|}\,, \tag{6.16}$$

$$= \begin{pmatrix} k_0 - m_q & -|\vec{k}| \\ -|\vec{k}| & k_0 + m_q \end{pmatrix}, \tag{6.17}$$

$$V_{(ij)} = \frac{g_S^2 N_C N_I E_{(ij)}}{E(\vec{k}+\vec{k}')[P_0 - k_0 - k_0' - E(\vec{k}+\vec{k}')]} + C_{(ij)} V_L(|\vec{k}' - \vec{k}|)\,, \tag{6.18}$$

$$E_{(ij)} = \frac{Tr[\tilde{O}_{(i)}(P,k)[2m_q \Lambda^{(+)}(\vec{k}+\vec{k}')]O_{(j)}(P,k)]}{|Tr[\tilde{O}_{(i)}(P,k)\,O_{(i)}(P,k)]|}\,, \tag{6.19}$$

$$= \begin{pmatrix} E(\vec{k}+\vec{k}') + m_q & |\vec{k}'| + |\vec{k}|z \\ |\vec{k}| + |\vec{k}'|z & (E(\vec{k}+\vec{k}') - m_q)z \end{pmatrix}, \tag{6.20}$$

and

$$C_{(i,j)} = \frac{\mathrm{Tr}[\tilde{O}_{(i)}(P,k)\ 1\ O_{(j)}(P,k')]}{|\mathrm{Tr}[\tilde{O}_{(i)}(P,k)O_{(i)}(P,k)]|}\ , \tag{6.21}$$

$$= \begin{bmatrix} 1 & 0 \\ 0 & -z \end{bmatrix}\ , \tag{6.22}$$

where z is the cosine of the angle between $\vec{k}$ and $\vec{k}'$. (These various matrices are symmetric.)

We can now perform the integration over the angle between the vectors $\vec{k}$ and $\vec{k}'$ to define

$$(k|\bar{V}(P)|k') = \int_{-1}^{1} dz\ (k|V(P)|k'). \tag{6.23}$$

(Note that $(k|\bar{V}|k')$ depends only on the magnitudes of $\vec{k}$ and $\vec{k}'$ and on $P_0 = m_N$.)

The potential $\bar{V}(P)$ has the matrix form

$$\bar{V}_{(ij)} = \begin{pmatrix} C_1 & 0 \\ 0 & -C_2 \end{pmatrix} + g_s^2 N_C N_I \begin{pmatrix} I_1+m_q I_2 & |\vec{k}'|I_2+|\vec{k}|I_4 \\ |\vec{k}|I_2+|\vec{k}'|I_4 & I_3-m_q I_4 \end{pmatrix} , \tag{6.24}$$

where we can recognize the confinement and exchange parts. The various terms in Eq. (6.24) are

$$C_n = \int_{-1}^{1} dz\ z^n\ V_L(|\vec{k}'-\vec{k}|) , \tag{6.25}$$

$$I_{2n+1} = \int_{-1}^{1} dz\ z^n\ [P_0-k_o-k_0'-E(\vec{k}+\vec{k}')]^{-1} , \tag{6.26}$$

and

$$I_{2n+2} = \int_{-1}^{1} z^n \left\{E(\vec{k}+\vec{k}')[P_0-k_0-k_0'-E(\vec{k}+\vec{k}')]\right\}^{-1} ; \qquad n = 0,1,\ldots . \tag{6.27}$$

The analytic forms for these integrals are given in Appendix B.

It is useful to perform a unitary transformation in order to diagonalize the kinetic-energy matrix K of Eq.(6.17),

$$U^{-1}(\vec{k})\ K\ U(\vec{k}) = \mathrm{Diag}(\lambda_1,\lambda_2)\ , \tag{6.28}$$

where

$$U(\vec{k}) = \begin{bmatrix} \dfrac{|\vec{k}|}{\sqrt{2E(\vec{k})(E(\vec{k})-m_q)}} & \dfrac{-|\vec{k}|}{\sqrt{2E(\vec{k})(E(\vec{k})+m_q)}} \\ \dfrac{E(\vec{k})-m_q}{\sqrt{2E(\vec{k})(E(\vec{k})-m_q)}} & \dfrac{E(\vec{k})+m_q}{\sqrt{2E(\vec{k})(E(\vec{k})+m_q)}} \end{bmatrix} . \tag{6.29}$$

Note that $U(\vec{k})$ depends only on the magnitude of $\vec{k}$. The eigenvalues, λ_1 and λ_2, are

$$\lambda_1 = k_0 - E(\vec{k})\ , \tag{6.30}$$

and

$$\lambda_2 = k_0 + E(\vec{k})\ . \tag{6.31}$$

Let us define the two-component object

$$\Psi(P,k) = \begin{bmatrix} \psi_{(1)}(P,k) \\ \psi_{(2)}(P,k) \end{bmatrix} , \tag{6.32}$$

where $\psi_{(1)}(P,k)$ and $\psi_{(2)}(P,k)$ were first introduced in Eq.(6.2). We also define the wave function and the potential in the transformed basis as

$$\tilde{\Psi}(P,k) = U^{-1}(\vec{k})\,\Psi(P,k)\ , \tag{6.33}$$

and

$$\tilde{V} = U^{-1}(\vec{k})\,\bar{V}\,U(\vec{k}')\ , \tag{6.34a}$$

or

$$(k|\tilde{V}(P)|k') = U^{-1}(\vec{k})\,(k|\bar{V}(P)|k')\,U(\vec{k}')\ , \tag{6.34b}$$

where $U(\vec{k})$ was introduced in Eq. (6.29). We note that the interaction matrix $\tilde{V}$ remains symmetric in the new basis. We also note that

$$\tilde{\Psi}(P,k) = \begin{bmatrix} \tilde{\psi}_{(1)}(P,k) \\ \tilde{\psi}_{(2)}(P,k) \end{bmatrix}\ , \tag{6.35}$$

where $\tilde{\psi}_{(1)}(P,k)$ and $\tilde{\psi}_{(2)}(P,k)$ are the functions defined in Eq.(6.3).
We also define the kinetic term in the new basis,

$$\tilde{K} = \begin{bmatrix} k_0 - E(\vec{k}) & 0 \\ 0 & k_0 + E(\vec{k}) \end{bmatrix}\ . \tag{6.36}$$

Note that

$$\tilde{K}^{-1} = \frac{1}{k^2 - m_q^2} \begin{bmatrix} k_0 + E(\vec{k}) & 0 \\ 0 & k_0 - E(\vec{k}) \end{bmatrix} . \tag{6.37}$$

We define a baryon vertex function

$$\tilde{\Gamma}(P,k) = \begin{bmatrix} \tilde{\Gamma}_{(1)}(P,k) \\ \tilde{\Gamma}_{(2)}(P,k) \end{bmatrix} , \tag{6.38}$$

such that

$$\tilde{\Gamma}(P,k) = [(P-k)^2 - m_S^2]\, \tilde{K}\, \tilde{\Psi}(P,k) . \tag{6.39}$$

The array $\tilde{\Psi}(P,k)$ was defined in Eq.(6.35), and $\tilde{K}$ was defined in Eq.(6.36). The bound-state equation for this vertex function is

$$\begin{pmatrix} \tilde{\Gamma}_{(1)}(P,k) \\ \tilde{\Gamma}_{(2)}(P,k) \end{pmatrix} = i \int \frac{dk_0' \vec{k}'^2 d|\vec{k}'|}{(2\pi)^3}\, \tilde{V}\, \frac{1}{(P-k')^2 - m_S^2} \frac{1}{k'^2 - m_q^2} \begin{pmatrix} k_0' + E(\vec{k}') & 0 \\ 0 & k_0' - E(\vec{k}') \end{pmatrix} \begin{pmatrix} \tilde{\Gamma}_{(1)}(P,k') \\ \tilde{\Gamma}_{(2)}(P,k') \end{pmatrix} , \tag{6.40}$$

where $\tilde{V}$ denotes $(k|\tilde{V}(P)|k')$. Here, the integration over the azimuthal angle has been performed.

In order to obtain equations in a single variable, we make a number of

approximations. We assume that the most significant singularities in the complex k_0' plane are those due to the quark and diquark going on mass shell. That is, we neglect the singularities of the exchange potential. Then, if the quark goes on its positive mass shell, we see that the exchange potential of Eq.(6.6) is not singular, if $m_N > 3m_q$.

We have the choice of closing the contour in the upper-half or lower-half of the k_0' plane. We close the contour in the lower-half plane and evaluate the integral as the sum of two residues. The pole at $k_0 = E_q(\vec{k}) - i\epsilon$ represents the quark on its positive mass shell and the pole at $k_0 = P_0 + E_S(\vec{k}) - i\epsilon$ represents the diquark on its negative mass shell. We define the wave functions

$$\Psi_q(P,k) = \begin{bmatrix} \psi_{(1)}(P,k) \\ \psi_{(2)}(P,k) \end{bmatrix}_{k_0 = E_q(\vec{k})} , \tag{6.41}$$

and

$$\Psi_d(P,k) = \begin{bmatrix} \psi_{(1)}(P,k) \\ \psi_{(2)}(P,k) \end{bmatrix}_{k_0 = P_0 + E_S(\vec{k})} . \tag{6.42}$$

Similarly we have

$$\bar{\Psi}_q(P,k) = \begin{bmatrix} \bar{\psi}_{(1)}(P,k) \\ \bar{\psi}_{(2)}(P,k) \end{bmatrix}_{k_0 = E_q(\vec{k})} , \tag{6.43}$$

and

$$\tilde{\Psi}_d(P,k) = \begin{bmatrix} \tilde{\psi}_{(1)}(P,k) \\ \tilde{\psi}_{(2)}(P,k) \end{bmatrix}_{k_0 = P_0 + E_s(\vec{k})} . \tag{6.44}$$

As we will see, the wave functions of Eqs. (6.42) and (6.44) are rather small and may be dropped in a first approximation. We will use the notation

$$\tilde{\psi}^q_{(i)}(P,k) = \tilde{\psi}_{(i)}(P,k)_{k_0 = E_q(\vec{k})} , \qquad i = 1, 2 \tag{6.45}$$

and

$$\tilde{\psi}^d_{(i)}(P,k) = \tilde{\psi}_{(i)}(P,k)_{k_0 = P_0 + E_s(\vec{k})} , \qquad i = 1, 2. \tag{6.46}$$

We also define

$$\tilde{\Gamma}_q(P,k) = \begin{bmatrix} \tilde{\Gamma}_{(1)}(P,k) \\ \tilde{\Gamma}_{(2)}(P,k) \end{bmatrix}_{k_0 = E_q(\vec{k})} , \tag{6.47}$$

and

$$\tilde{\Gamma}_d(P,k) = \begin{bmatrix} \tilde{\Gamma}_{(1)}(P,k) \\ \tilde{\Gamma}_{(2)}(P,k) \end{bmatrix}_{k_0 = P_0 + E_s(\vec{k})} . \tag{6.48}$$

We will use the notation

$$\tilde{\Gamma}^q_{(i)}(P,k) = \tilde{\Gamma}_{(i)}(P,k)_{k_0 = E_q(\vec{k})} , \qquad i = 1, 2 , \tag{6.49}$$

and

$$\tilde{\Gamma}^d_{(i)}(P,k) = \tilde{\Gamma}_{(i)}(P,k)_{k_0 = P_0 + E_s(\vec{k})} , \qquad i = 1, 2. \tag{6.50}$$

Evaluation of the $\tilde{\Gamma}(P,k)$ at the poles essentially doubles the number of functions we need to consider. Therefore, it is useful to introduce a 4×4 matrix, $\hat{V}$ defined in terms of four potentials:

$$\hat{V} = \begin{bmatrix} \tilde{V}_{qq} & \tilde{V}_{qd} \\ \tilde{V}_{dq} & \tilde{V}_{dd} \end{bmatrix} . \tag{6.51}$$

Each potential, $\tilde{V}_{qq}$, $\tilde{V}_{qd}$, $\tilde{V}_{dq}$, and $\tilde{V}_{dd}$ is a 2×2 matrix in the two dimensional space used before the k_0' integral was completed. Here, when $\alpha = q$, k_0 is $E_q(\vec{k})$, and when $\alpha = d$, k_0 is $P_0 + E_S(\vec{k})$. Further, when $\beta = q$, k_0' is $E_q(\vec{k}')$, and when $\beta = d$, k_0' is $P_0 + E_S(\vec{k}')$.

The system of equations is, with α either d or q,

$$\tilde{\Gamma}_{\alpha}(P_0,|\vec{k}|) = \int \frac{\vec{k}'^2\, d|\vec{k}'|}{(2\pi)^2} \quad \frac{\tilde{V}_{\alpha q}\begin{bmatrix} 2E_q(\vec{k}') & 0 \\ 0 & 0 \end{bmatrix} \tilde{\Gamma}_q(P_0,|\vec{k}'|)}{2E_q(\vec{k}')[(P_0-E_q(\vec{k}'))^2-E_d(\vec{k}')^2]}$$

$$+ \frac{\tilde{V}_{\alpha d}\begin{bmatrix} P_0+E_d(\vec{k}')+E_q(\vec{k}') & 0 \\ 0 & P_0+E_d(\vec{k}')-E_q(\vec{k}') \end{bmatrix} \tilde{\Gamma}_d(P_0,|\vec{k}'|)}{2E_d(\vec{k}')[(P_0+E_d(\vec{k}'))^2-E_q(\vec{k}')^2]} \,. \tag{6.52}$$

The vertices $\tilde{\Gamma}_q(P_0,|\vec{k}|)$ and $\tilde{\Gamma}_d(P_0,|\vec{k}|)$ have upper and lower components. The lower component of $\tilde{\Gamma}_q(P_0,|\vec{k}|)$ decouples from the system of equations. We can then define a <u>three-component</u> vector, $\bar{\Gamma}(P_0,|\vec{k}|)$, with the first component equal to upper component of $\tilde{\Gamma}_q(P_0,|\vec{k}|)$ and the two remaining components equal to the upper and lower components of $\tilde{\Gamma}_d(P_0,|\vec{k}|)$. Thus

$$\bar{\Gamma}(P_0,|\vec{k}|) = \begin{bmatrix} \tilde{\Gamma}^q_{(1)}(P_0,|\vec{k}|) \\ \tilde{\Gamma}^d_{(1)}(P_0,|\vec{k}|) \\ \tilde{\Gamma}^d_{(2)}(P_0,|\vec{k}|) \end{bmatrix} . \tag{6.53}$$

Further, let us define a three-component amplitude

$$\Phi(P_0,|\vec{k}|) = D(\vec{k})\sqrt{N(\vec{k})}\ \bar{\Gamma}(P_0,|\vec{k}|)\ , \tag{6.54}$$

with

$$D(\vec{k}) = \begin{pmatrix} [P_0-E_q(\vec{k})-E_d(\vec{k})]^{-1} & 0 & 0 \\ 0 & 1 & 0 \\ 0 & 0 & 1 \end{pmatrix}\ , \tag{6.55}$$

and

$$N(\vec{k}) = \begin{pmatrix} \dfrac{1}{P_0-E_q(\vec{k})+E_d(\vec{k})} & 0 & 0 \\ 0 & \dfrac{1}{2E_d(\vec{k})[P_0-E_q(\vec{k})+E_d(\vec{k})]} & 0 \\ 0 & 0 & \dfrac{1}{2E_d(\vec{k})[P_0+E_q(\vec{k})+E_d(\vec{k})]} \end{pmatrix}. \tag{6.56}$$

The final bound-state equation has a symmetric form

$$D^{-1}(\vec{k})\Phi(P_0,|\vec{k}|) = \int \frac{\vec{k}'^2 d|\vec{k}'|}{(2\pi)^2}\sqrt{N(\vec{k})}\ V_R\ \sqrt{N(\vec{k}')}\ \Phi(P_0,|\vec{k}'|)\ .$$

(6.57)

Here, the potential V_R is a 3 x 3 matrix acting in the three-dimensional space defined above and may be obtained from $\hat{V}$ by deleting the second row and second column.

The solution of Eq.(6.57) for $\Phi(P_0, |\vec{k}|)$ has been obtained. However, it is more useful to present the various functions that make up $\Psi(P,k)$ and $\tilde{\Psi}(P,k)$ of Eq. (6.32) and (6.35). These functions are shown in Figs 6.2 - 6.3. Note that only one of four components of $\tilde{\Psi}(P,k)$ is large. That component is the wave function that corresponds to the quark being on its positive mass shell. (See Eq.(6.3).)

6.2 Coupled Equations: Scalar and Axialvector Diquarks

In general, one needs eight functions of two variables to describe the situation in which we have both scalar (T = 0) and axialvector (T = 1) diquarks in the nucleon. Evaluation of integrals at the poles of the Green's functions double this number to sixteen. We will argue that the functions with either the scalar or the axialvector diquark on their negative mass shell are small. Neglecting such functions reduces the number of wave functions we need to consider to eight. As we will see, four of these eight functions can be expressed in terms of the other four. Therefore, we will be solving coupled equations for four functions of a single variable.

We may write the axialvector-diquark wave function, in analogy to Eq. (6.2), as

$$\Psi_V^\mu(P,k,s,t) = \gamma_5 \left[\psi_{(3)}(P,k) \frac{P^\mu}{m_N} + \psi_{(5)}(P,k) \frac{\hat{k}^\mu}{\sqrt{-\hat{k}^2}} + \psi_{(7)}(P,k) \frac{\tilde{\gamma}^\mu(P,k)}{\sqrt{2}} \right] u_N(\vec{P},s)\chi_t$$

$$+ \gamma_5 \left[\psi_{(4)}(P,k) \frac{P^\mu}{m_N} + \psi_{(6)}(P,k) \frac{\hat{k}^\mu}{\sqrt{-\hat{k}^2}} + \psi_{(8)}(P,k) \frac{\tilde{\gamma}^\mu(P,k)}{\sqrt{2}} \right] \frac{\hat{k}}{\sqrt{-\hat{k}^2}} u_N(\vec{P},s)\chi_t \ , \tag{6.58}$$

where we have defined six functions of two variables, $\psi_{(i)}(P,k)$, with $i = 3,\ldots,8$. Here,

$$\hat{k}^\mu = k^\mu - \frac{(k \cdot P)P^\mu}{P^2} , \tag{6.59}$$

and

$$\tilde{\gamma}^\mu(P,k) = \gamma^\mu - \frac{P^\mu \not{P}}{P^2} - \frac{\hat{k}^\mu \not{\hat{k}}}{\hat{k}^2} . \tag{6.60}$$

Note that $P^\mu \tilde{\gamma}_\mu(P,k) = P^\mu \hat{k}_\mu = \hat{k}^\mu \tilde{\gamma}_\mu(P,k)$.

One can be seen that $\Psi_S(P,k,s,t)$ of Eq. (6.2) and $\Psi_V^\mu(P,k,s,t)$ of Eq.(6.58) satisfy coupled equations of the form

$$[(P-k)^2 - m_S^2](\not{k} - m_q)\ \Psi_S(P,k,s,t) =$$

$$i\int \frac{d^4k'}{(2\pi)^4}\Big[N_c^{SS}N_i^{SS}(k|V_{SS}^E(P)|k')\Psi_S(P,k',s,t) + N_c^{SV}N_i^{SV}(k|V_{SV}^{E\mu}(P)|k')\Psi_{V\mu}(P,k',s,t)\Big]$$

$$+ i\int \frac{d^4k'}{(2\pi)^4}(k|V_S^C(P)|k')\Psi_S(P,k',s,t) \qquad (6.61)$$

and

$$[(P-k)^2 - m_V^2](\not{k} - m_q)\ \Psi_V^\mu(P,k,s,t) =$$

$$i\int \frac{d^4k'}{(2\pi)^4}\Big[N_c^{VS}N_i^{VS}(k|V_{VS}^{E\mu}(P)|k')\Psi_S(P,k',s,t) + N_c^{VV}N_i^{VV}(k|V_{VV}^{E\mu'\mu}(P)|k')\Psi_{V\mu'}(P,k',s,t)\Big]$$

$$+ i\int \frac{d^4k'}{(2\pi)^4}(k|V_V^C(P)|k')\Psi_V^\mu(P,k',s,t)\ . \qquad (6.62)$$

Here, the contributions of the quark-exchange interaction are

$$(k|V_{SS}^E(P)|k') = 2g_S^2\ \gamma_5 C^{-1}S_{(+)}^T(P-k-k')C\ \gamma_5\ , \qquad (6.63)$$

$$(k|V_{SV}^{E\mu}(P)|k') = 2g_S g_V\ \gamma_5 C^{-1}\ S_{(+)}^T(P-k-k')\ C\gamma^\mu\ , \qquad (6.64)$$

$$(k|V_{VS}^{E\,\mu}(P)|k') = 2g_V g_S\ \gamma^\mu C^{-1} S_{(+)}^T(P-k-k')C\ \gamma_5\ , \tag{6.65}$$

$$(k|V_{VV}^{E\,\mu'\mu}(P)|k') = 2g_V^2\ \gamma^{\mu'} C^{-1}\ S_{(+)}^T(P-k-k')\ C\gamma^\mu\ . \tag{6.66}$$

The confinement potential does not couple the scalar and axialvector diquark components. We have

$$(k|V_{S,V}^C(P)|k') = -8\,\kappa_{S,V}\,\pi \left\{ \frac{1}{[(\vec{k}'-\vec{k})^2+\mu^2]^2} - \frac{4\mu^2}{[(\vec{k}'-\vec{k})^2+\mu^2]^3} \right\}, \tag{6.67}$$

where κ_S and κ_V may be different.

The color and isospin factors appearing in Eqs. (6.61)-(6.62) are

$$\begin{aligned} N_c^{SS} &= N_c^{SV} = N_c^{VS} = N_c^{VV} = 3\ , \\ N_i^{SS} &= 1\ , \\ N_i^{SV} &= 3\ , \\ N_i^{VS} &= 1\ , \end{aligned} \tag{6.68}$$

and

$$N_i^{VV} = -2\ .$$

As in the case of the scalar diquark, we multiply the Eqs. (6.61) and (6.62) by $\bar{u}_N(\vec{P},s)$ from the right and sum over the spin index s.

For the complete two-channel problem, with both scalar and axialvector diquarks, we consider following two forms of the wave function

$$\Psi(P,k) = \sum_{i=1}^{8} \psi_{(i)}(P,k)\, O_{(i)}(P,k)\chi_t \ , \tag{6.69}$$

and

$$\tilde{\Psi}(P,k) = \sum_{i=1}^{8} \tilde{\psi}_{(i)}(P,k)\, \tilde{O}_{(i)}(P,k)\chi_t \ . \tag{6.70}$$

These equations serve to extend the expansions made in Eqs. (6.2) and (6.3). The wave functions $\psi_{(i)}$ and $\tilde{\psi}_{(i)}$ are related by a transformation that will be given at a later point. [See Eq.(6.102).] The first two basis vectors represent the scalar channel and the six remaining vectors represent the axialvector channel. We define the basis functions for Eq. (6.69):

$$O_{(1)}(P,k) = \Lambda^{(+)}(\overline{P}) \ , \tag{6.71}$$

$$O_{(2)}(P,k) = \frac{\hat{k}}{\sqrt{-\hat{k}^2}}\, \Lambda^{(+)}(\overline{P}) \ , \tag{6.72}$$

$$O_{(3)}(P,k) = \gamma_5 \frac{P^\mu}{m_N} \Lambda^{(+)}(\vec{P}) \ , \tag{6.73}$$

$$O_{(4)}(P,k) = \gamma_5 \frac{\hat{k}}{\sqrt{-\hat{k}^2}} \frac{P^\mu}{m_N} \Lambda^{(+)}(\vec{P}) \ , \tag{6.74}$$

$$O_{(5)}(P,k) = \gamma_5 \frac{\hat{k}^\mu}{\sqrt{-\hat{k}^2}} \Lambda^{(+)}(\vec{P}) \ , \tag{6.75}$$

$$O_{(6)}(P,k) = \gamma_5 \frac{\hat{k}^\mu}{\sqrt{-\hat{k}^2}} \frac{\hat{k}}{\sqrt{-\hat{k}^2}} \Lambda^{(+)}(\vec{P}) \ , \tag{6.76}$$

$$O_{(7)}(P,k) = \gamma_5 \frac{\tilde{\gamma}^\mu(P,k)}{\sqrt{2}} \Lambda^{(+)}(\vec{P}) \ , \tag{6.77}$$

and

$$O_{(8)}(P,k) = \gamma_5 \frac{\tilde{\gamma}^\mu(P,k)}{\sqrt{2}} \frac{\hat{k}}{\sqrt{-\hat{k}^2}} \Lambda^{(+)}(\vec{P}). \tag{6.78}$$

Also,

$$\tilde{O}_{(1)}(P,k) = \xi_{+}\Lambda^{(+)}(\vec{k})\,\Lambda^{(+)}(\vec{P}) \ , \tag{6.79}$$

$$\tilde{O}_{(2)}(P,k) = -\xi_{-}\Lambda^{(-)}(-\vec{k})\,\Lambda^{(+)}(\vec{P}) \ , \tag{6.80}$$

$$\tilde{O}_{(3)}(P,k) = -\xi_{-}\Lambda^{(+)}(\vec{k})\gamma_5\frac{P^{\mu}}{m_N}\Lambda^{(+)}(\vec{P}) \ , \tag{6.81}$$

$$\tilde{O}_{(4)}(P,k) = \xi_{+}\Lambda^{(-)}(-\vec{k})\gamma_5\frac{P^{\mu}}{m_N}\Lambda^{(+)}(\vec{P}) \ , \tag{6.82}$$

$$\tilde{O}_{(5)}(P,k) = \xi_{-}\Lambda^{(+)}(\vec{k})\gamma_5\frac{\hat{k}^{\mu}}{\sqrt{-\hat{k}^2}}\Lambda^{(+)}(\vec{P}) \ , \tag{6.83}$$

$$\tilde{O}_{(6)}(P,k) = -\xi_{-}\Lambda^{(-)}(-\vec{k})\gamma_5\frac{\hat{k}^{\mu}}{\sqrt{-\hat{k}^2}}\Lambda^{(+)}(\vec{P}) \ , \tag{6.84}$$

$$\tilde{O}_{(7)}(P,k) = \xi_{+}\Lambda^{(+)}(\vec{k})\gamma_5\frac{\tilde{\gamma}^{\mu}(P,k)}{\sqrt{2}}\Lambda^{(+)}(\vec{P}) \ , \tag{6.85}$$

and

$$\tilde{O}_{(8)}(P,k) = -\xi_{-}\Lambda^{(-)}(-\vec{k})\gamma_5 \frac{\tilde{\gamma}^{\mu}(P,k)}{\sqrt{2}} \Lambda^{(+)}(\vec{P}). \qquad (6.86)$$

Here $\xi_{+} = 2m_q/\sqrt{2E_q(\vec{k})[E(\vec{k})+m_q]}$ and $\xi_{-} = 2m_q/\sqrt{2E_q(\vec{k})[E(\vec{k})-m_q]}$. As we will see, only $\tilde{\psi}_{(1)}(P,k)$, $\tilde{\psi}_{(3)}(P,k)$, $\tilde{\psi}_{(5)}(P,k)$ and $\tilde{\psi}_{(7)}(P,k)$ of Eq. (6.70) will be important in our solution.

Using the basis defined by Eqs. (6.71)-(6.78), we can write Eqs.(6.61) and (6.62) in the matrix form,

$$[(P-k)^2 - m^2_{d(i)}] \sum_{j=1}^{8} K_{(ij)}\psi_{(j)}(P,k) = i\int \frac{d^4k'}{(2\pi)^4} \sum_{j=1}^{8} V_{(ij)}\psi_{(j)}(P,k) \ . \qquad (6.87)$$

In Eq. (6.87), $m_{d(1),(2)} = m_S$, $m_{d(3),\ldots,(8)} = m_v$ and

$$K_{(ij)} = \frac{Tr[\tilde{O}_{(i)}(P,k)(\not{k} - m_q)O_{(j)}(P,k)]}{|Tr[\tilde{O}_{(i)}(P,k)O_{(i)}(P,k)]|} =$$

$$\begin{pmatrix}
k_0 - m_q & -|\vec{k}| & 0 & 0 & 0 & 0 & 0 & 0 \\
-|\vec{k}| & k_0 + m_q & 0 & 0 & 0 & 0 & 0 & 0 \\
0 & 0 & -k_0 - m_q & |\vec{k}| & 0 & 0 & 0 & 0 \\
0 & 0 & |\vec{k}| & -k_0 + m_q & 0 & 0 & 0 & 0 \\
0 & 0 & 0 & 0 & k_0 + m_q & -|\vec{k}| & 0 & 0 \\
0 & 0 & 0 & 0 & -|\vec{k}| & k_0 - m_q & 0 & 0 \\
0 & 0 & 0 & 0 & 0 & 0 & k_0 - m_q & -|\vec{k}| \\
0 & 0 & 0 & 0 & 0 & 0 & -|\vec{k}| & k_0 + m_q
\end{pmatrix}.$$

Eq. (6.88)

Also,

$$V_{(ij)} = \frac{F_{(ij)}\, E_{(ij)}}{E(\vec{k}+\vec{k}')[P_0 - k_0 - k_0' - E(\vec{k}+\vec{k}')]} + C_{(ij)}\, V_L(|\vec{k}' - \vec{k}|) \ , \qquad (6.89)$$

$$\begin{aligned} F_{(ij)} &= N_C^{SS}\, N_I^{SS}\, g_S^2 \ , && \text{if (i) and (j)} \le 2, \\ F_{(ij)} &= N_C^{SV}\, N_I^{SV}\, g_S g_V \ , && \text{if (i)} \le 2, \ \text{(j)} \ge 3, \\ F_{(ij)} &= N_C^{VS}\, N_I^{VS}\, g_V g_S \ , && \text{if (i)} \ge 3, \ \text{(j)} \le 2, \\ F_{(ij)} &= N_C^{VV}\, N_I^{VV}\, g_V^2 \ , && \text{if (i) and (j)} \ge 3, \end{aligned} \qquad (6.90)$$

and

$$E_{(ij)} = \frac{Tr[\tilde{O}_{(i)}(P,k)\ 2\, m_q\ \Gamma^d_{(j)}\, \Lambda^{(-)}(\vec{k}+\vec{k}')\, \Gamma^d_{(i)}\ O_{(j)}(P,k)]}{|Tr[\tilde{O}_{(i)}(P,k)\, O_{(i)}(P,k)]|} \ , \qquad (6.91)$$

with diquark vertices $\Gamma^d_{(i)} = \gamma_5$ for i = 1,2 and $\Gamma^d_{(i)} = \gamma^\mu$ for i = 3,...,8.

Further,

$$C_{(ij)} = \frac{Tr[\tilde{O}_{(i)}(P,k)\ 1\ O_{(j)}(P,k')]}{|Tr[\tilde{O}_{(i)}(P,k)\,O_{(i)}(P,k)]|} =$$

$$\begin{pmatrix}
1 & 0 & 0 & 0 & 0 & 0 & 0 & 0 \\
0 & -z & 0 & 0 & 0 & 0 & 0 & 0 \\
0 & 0 & 1 & 0 & 0 & 0 & 0 & 0 \\
0 & 0 & 0 & -z & 0 & 0 & 0 & 0 \\
0 & 0 & 0 & 0 & -z & 0 & 0 & 0 \\
0 & 0 & 0 & 0 & 0 & z^2 & \frac{-(1-z^2)}{\sqrt{2}} & 0 \\
0 & 0 & 0 & 0 & 0 & \frac{-(1-z^2)}{\sqrt{2}} & \frac{1+z^2}{2} & 0 \\
0 & 0 & 0 & 0 & 0 & 0 & 0 & -z
\end{pmatrix}$$

Eq. (6.92)

$$
\begin{pmatrix}
\tilde{E}+m_q & k'+kz & -\tilde{E}+m_q & -k-k'z & -k'-kz & -\tilde{E}-m_q & \tilde{E}+m_q & k'+kz \\
k+k'z & (\tilde{E}-m_q)z & \tilde{E}-m_q & k+k'z & (\tilde{E}-m_q)z & k(2z^2-1)+k'z & (k'+kz)z & (\tilde{E}-m_q)z \\
-\tilde{E}+m_q & \tilde{E}-m_q & \tilde{E}+m_q & -k'-kz & k'+kz & -\tilde{E}+m_q & \sqrt{2}(\tilde{E}+m_q) & -\sqrt{2}(k'+kz) \\
-k'-kz & k'+kz & -k-k'z & (\tilde{E}-m_q)z & -(\tilde{E}+m_q)z & k'(1+z)(2z-1) & \sqrt{2}(k'+kz)z & -\sqrt{2}(\tilde{E}+m_q)z \\
-k-k'z & (\tilde{E}-m_q)z & k+k'z & -(\tilde{E}+m_q)z & (\tilde{E}-m_q)z & -k'-kz & \sqrt{2}(k+k'z) & \sqrt{2}(\tilde{E}+m_q)z \\
-\tilde{E}-m_q & k'(2z^2-1)+kz & -\tilde{E}+m_q & k(1+z)(2z-1) & -k-k'z & (\tilde{E}+m_q)(2z^2-1) & (\tilde{E}+m_q)z^2 & \sqrt{2}(-k-k'z)z \\
\tilde{E}+m_q & (k+k'z)z & \sqrt{2}(\tilde{E}+m_q) & \sqrt{2}(k+k'z)z & \sqrt{2}(k'+kz) & (\tilde{E}+m_q)z^2 & (\tilde{E}+m_q)(1-z^2) & k'(z-1) \\
k+k'z & (\tilde{E}-m_q)z & -\sqrt{2}(k+k'z) & -\sqrt{2}(\tilde{E}+m_q)z & \sqrt{2}(\tilde{E}+m_q)z & \sqrt{2}(-k'-kz)z & k(z-1) & 0
\end{pmatrix}
$$

Eq.(6.93). The exchange potential matrix, $E_{(ij)}$. Here $k = |\vec{k}|$, $k' = |\vec{k}'|$ and $\tilde{E} = E(\vec{k}+\vec{k}')$.

As in the case of the scalar diquark, z is the cosine of the angle between $\vec{k}$ and $\vec{k}'$. We can now perform the integration over z to define

$$(k|\bar{V}(P)|k') = \int_{-1}^{1} dz\,(k|V(P)|k'). \tag{6.94}$$

The potential $\bar{V}(P)$ has the matrix form

$$\bar{V}_{(ij)} = F_{(ij)}\bar{V}^{E}_{(ij)} + \bar{V}^{C}_{(ij)}\,, \tag{6.95}$$

where $F_{(ij)}$ was defined in Eq. (6.90). Here the confinement part is

$$\bar{V}^{C}_{(ij)} = \begin{Bmatrix} C_0 & 0 & 0 & 0 & 0 & 0 & 0 & 0 \\ 0 & -C_1 & 0 & 0 & 0 & 0 & 0 & 0 \\ 0 & 0 & C_0 & 0 & 0 & 0 & 0 & 0 \\ 0 & 0 & 0 & -C_1 & 0 & 0 & 0 & 0 \\ 0 & 0 & 0 & 0 & -C_1 & 0 & 0 & 0 \\ 0 & 0 & 0 & 0 & 0 & C_2 & \frac{C_2-C_0}{\sqrt{2}} & 0 \\ 0 & 0 & 0 & 0 & 0 & \frac{C_2-C_0}{\sqrt{2}} & \frac{C_2+C_0}{2} & 0 \\ 0 & 0 & 0 & 0 & 0 & 0 & 0 & -C_1 \end{Bmatrix}$$

Eq.(6.96)

$$
\begin{pmatrix}
I_1+m_qI_2 & k'I_2+kI_4 & -I_1+m_qI_2 & -kI_2-k'I_4 & -k'I_2-kI_4 & -I_1-m_qI_2 & I_1+m_qI_2 & k'I_2+kI_4 \\
k'I_4+kI_2 & I_3-m_qI_4 & I_1-m_qI_4 & kI_2+k'I_4 & I_3-m_qI_4 & 2kI_6-kI_2+k'I_4 & k'I_4+kI_6 & I_3-m_qI_4 \\
-I_1+m_qI_2 & I_2-m_qI_4 & I_1+m_qI_2 & -kI_4-k'I_2 & kI_4+k'I_2 & -I_1+m_qI_2 & \sqrt{2}(I_1+m_qI_2) & -\sqrt{2}(kI_4+k'I_2) \\
-k'I_2-kI_4 & k'I_2+kI_4 & -k'I_4-kI_2 & I_3-m_qI_4 & -I_3-m_qI_4 & k'(I_4-I_2+2I_6) & \sqrt{2}(k'I_4+kI_6) & -\sqrt{2}(I_3+m_qI_4) \\
-kI_2-k'I_4 & I_3-m_qI_4 & k'I_4+kI_2 & -I_3-m_qI_4 & I_3-m_qI_4 & -k'I_2-kI_4 & \sqrt{2}(kI_2+k'I_4) & \sqrt{2}(I_3+m_qI_4) \\
-I_1-m_qI_2 & 2k'I_6-k'I_2+kI_4 & -I_1+m_qI_2 & k(I_4-I_2+2I_6) & -kI_2-k'I_4 & \begin{matrix}2I_5-I_1\\+2m_qI_6-m_qI_2\end{matrix} & I_5+m_qI_6 & -\sqrt{2}(kI_4+k'I_6) \\
I_1+m_qI_2 & kI_4+k'I_6 & \sqrt{2}(I_1+m_qI_2) & \sqrt{2}(kI_4+k'I_6) & \sqrt{2}(k'I_2+kI_4) & I_5+m_qI_6 & I_1-I_5+m_q(I_2-I_6) & -k'I_2-k'I_6 \\
kI_2+k'I_4 & I_3-m_qI_4 & -\sqrt{2}(k'I_4+kI_2) & -\sqrt{2}(I_3+m_qI_4) & \sqrt{2}(I_3+m_qI_4) & -\sqrt{2}(k'I_4+kI_6) & -kI_2-kI_6 & 0
\end{pmatrix}
$$

Eq.(6.97). The matrix $\bar{V}^{I:}_{(i)(j)}$.

The functions C_i and I_i were defined previously. (See Eqs. (6.25)-(6.27).)

Following the procedure described in case of the scalar-diquark model, we perform a unitary transformation in order to diagonalize the kinetic-energy matrix K,

$$U^{-1}(\vec{k})\, K\, U(\vec{k}) = \mathrm{Diag}(\lambda_1,\ldots,\lambda_8)\ , \tag{6.98}$$

where

$$U(\vec{k}) = \begin{pmatrix} \frac{|\vec{k}|}{D_-} & \frac{-|\vec{k}|}{D_+} & 0 & 0 & 0 & 0 & 0 & 0 \\ \frac{E_q-m_q}{D_-} & \frac{E_q+m_q}{D_+} & 0 & 0 & 0 & 0 & 0 & 0 \\ 0 & 0 & \frac{|\vec{k}|}{D_+} & \frac{-|\vec{k}|}{D_-} & 0 & 0 & 0 & 0 \\ 0 & 0 & \frac{E_q+m_q}{D_+} & \frac{E_q-m_q}{D_-} & 0 & 0 & 0 & 0 \\ 0 & 0 & 0 & 0 & \frac{|\vec{k}|}{D_+} & \frac{-|\vec{k}|}{D_-} & 0 & 0 \\ 0 & 0 & 0 & 0 & \frac{E_q+m_q}{D_+} & \frac{E_q-m_q}{D_-} & 0 & 0 \\ 0 & 0 & 0 & 0 & 0 & 0 & \frac{|\vec{k}|}{D_-} & \frac{-|\vec{k}|}{D_+} \\ 0 & 0 & 0 & 0 & 0 & 0 & \frac{E_q-m_q}{D_-} & \frac{E_q+m_q}{D_+} \end{pmatrix}$$

Eq. (6.99)

Here $D_+ = \sqrt{2E_q(E_q + m_q)}$, $D_- = \sqrt{2E_q(E_q - m_q)}$ and $E_q = E_q(\vec{k})$.

The eigenvalues are

$$\lambda_{(i)} = \begin{bmatrix} k_0 - E_q(\vec{k}) \\ k_0 + E_q(\vec{k}) \\ -k_0 + E_q(\vec{k}) \\ -k_0 - E_q(\vec{k}) \\ k_0 - E_q(\vec{k}) \\ k_0 + E_q(\vec{k}) \\ k_0 - E_q(\vec{k}) \\ k_0 + E_q(\vec{k}) \end{bmatrix} . \tag{6.100}$$

We now define the analog of $\Psi(P,k)$ that was introduced previously,

$$\Psi(P,k) = \begin{bmatrix} \psi_{(1)}(P,k) \\ \psi_{(2)}(P,k) \\ \vdots \\ \psi_{(8)}(P,k) \end{bmatrix} . \tag{6.101}$$

As before, we also define the wave function and potential in the transformed basis

$$\tilde{\Psi}(P,k) = U^{-1}(\vec{k})\, \Psi(P,k) , \tag{6.102}$$

where

$$\tilde{\Psi}(P,k) = \begin{bmatrix} \tilde{\psi}_{(1)}(P,k) \\ \tilde{\psi}_{(2)}(P,k) \\ \vdots \\ \tilde{\psi}_{(8)}(P,k) \end{bmatrix} , \tag{6.103}$$

and

$$\tilde{V} = U^{-1}(\vec{k})\, \vec{V}\, U(\vec{k}') . \tag{6.104}$$

Recall that the various $\tilde{\psi}_{(i)}(P,k)$ have been defined previously in Eq.(6.70). The interaction matrix $\tilde{V}$ remains symmetric in the new basis. We define

$$\tilde{K} = \mathrm{Diag}(\lambda_{(1)},\ldots,\lambda_{(8)}) , \tag{6.105}$$

and a baryon vertex function

$$\tilde{\Gamma}(P,k) = [(P-k)^2 - \bar{m}_d^2]\, \tilde{K}\, \tilde{\Psi}(P,k) . \tag{6.106}$$

Here $\bar{m}_d = \mathrm{Diag}(m_{d(1)},\ldots,m_{d(8)})$. The bound state equation for vertex function is

$$\tilde{\Gamma}(P,k) = i \int \frac{dk_0' \vec{k}'^2 d|\vec{k}'|}{(2\pi)^3}\, \tilde{V}\, \frac{1}{(P-k')^2 - \bar{m}_d^2} \tilde{K}^{-1}\, \tilde{\Gamma}(P,k') , \tag{6.107}$$

where $\tilde{V}$ denotes $(k|\tilde{V}(P)|k')$. Here the integration over the azimuthal angle has been

performed. Note that $\tilde{\Gamma}(P,k)$ has <u>eight</u> elements and $\tilde{V}$ and $\tilde{K}^{-1}$ are 8×8 matrices.

In order to complete the integration over k_0', we close the contour in the lower-half plane. The integral can be evaluated as the sum of two residues. The pole at $k_0 = E_q(\vec{k}) - i\epsilon$ represents the quark on its positive mass shell and the pole at $k_0 = P_0 + E_d(\vec{k}) - i\epsilon$ represents the diquark on its negative mass shell. We found that the contribution from the diquark pole to the wave function was negligible in the case of the scalar diquark. We expect that a similar contribution from the axialvector diquark would be even smaller, since the axialvector diquark has a larger mass. We will neglect that contributions in our equations. In this approximation, the wave function is described by only <u>four</u> functions that represent quarks on their positive mass shells.

Since we have eliminated four functions, we modify our notation. We now define the four vertex functions $\bar{\Gamma}_{(i)} = \tilde{\Gamma}_{(2i-1)}$, $i=1,\ldots,4$. In order to make the potential symmetric, we define the amplitude

$$\Phi_{(i)}(P_0, |\vec{k}|) = N_{(i)} \frac{\bar{\Gamma}_{(i)}(P,k)}{[P_0 - E_q(\vec{k})]^2 - E_{(i)}^2(\vec{k})} , \tag{6.108}$$

were $i = 1,\ldots,4$ and

$$N_{(i)} = \begin{bmatrix} 1 \\ -\sqrt{3} \\ \sqrt{3} \\ \sqrt{3} \end{bmatrix} . \tag{6.109}$$

The symmetric bound-state equation has a final form

$$n_{(i)}[(P_0-E_q(\vec{k}))^2 - E^2_{d(i)}(\vec{k})]\Phi_{(i)}(P_0,|\vec{k}|) = \int \frac{d|\vec{k}'|}{(2\pi)^2}\,[\,f_{(ij)}\tilde{V}^E_{(ij)} + \tilde{V}^C_{(ij)}]\,\Phi_{(j)}(P_0,|\vec{k}'|)\ , \tag{6.110}$$

where i = 1,2,3,4. In Eq. (6.110)

$$n_{(i)} = \begin{bmatrix} 1 \\ -1 \\ 1 \\ 1 \end{bmatrix}\ , \tag{6.111}$$

and

$$\begin{aligned} f_{(ij)} &= N_C^{SS} N_I^{SS} g_S^2\ , && \text{if (i) and (j)} \le 2, \\ f_{(ij)} &= N_C^{SV} \sqrt{3}\, g_S g_V\ , && \text{if (i)} \le 2,\ \text{(j)} \ge 3, \\ f_{(ij)} &= N_C^{VS} \sqrt{3}\, g_V g_S\ , && \text{if (i)} \ge 3,\ \text{(j)} \le 2, \\ f_{(ij)} &= N_C^{VV} N_I^{VV} g_V^2\ , && \text{if (i) and (j)} \ge 3. \end{aligned} \tag{6.112}$$

6.3 Results of Calculation

It useful to present the solution of the coupled equations for the four important functions $\bar{\psi}_{(1)}(P,k)$, $\bar{\psi}_{(3)}(P,k)$, $\bar{\psi}_{(5)}(P,k)$ and $\bar{\psi}_{(7)}(P,k)$. (See Eq. (6.70).) We exhibit such results in Fig. 6.6 and 6.7. The various parameters are given in the figure captions. For example, if we use $\bar{G}_S$ = 7.9 GeV^2 and $\bar{G}_V$ = =9.5 GeV^2, we obtain a scalar diquark

of mass $m_S = 400$ MeV, and an axialvector diquark of mass $m_V = 750$ MeV. The value of κ was taken such that the nucleon mass was found to be $m_N = 938$ MeV.

One can assess the relative importance of the four wave functions by calculating their individual contributions to the charge form factor of the proton at $q^2 = 0$. (Note that $F_p(0)=1$.) We write these contributions as $F^p_{(i)}(0)$, so that

$$F_p(0) = F^p_{(1)}(0) + F^p_{(3)}(0) + F^p_{(5)}(0) + F^p_{(7)}(0) \; . \; . \qquad (6.113)$$

We found $F^p_{(1)}(0) = 0.42$, $F^p_{(3)}(0) = 0.08$, $F^p_{(5)}(0) = 0.10$ and $F^p_{(7)}(0) = 0.40$. Recall that $F^p_{(1)}(0)$ denotes the scalar-diquark contribution, while $F^p_{(3)}(0)$, $F^p_{(5)}(0)$ and $F^p_{(7)}(0)$ are axialvector-diquark contributions. We also consider a small variation of our parameters and give the results in Fig. 6.7 for the case $\bar{G}_S = 7.9$ GeV^2 and $\bar{G}_V = 8.45$ GeV^2. Here $m_S = 400$ MeV, $m_V = 850$ MeV and $\kappa = 0.096$. In this case $F_p(0) = 1$ with $F^p_{(1)}(0) = 0.49$, $F^p_{(3)}(0) = 0.08$, $F^p_{(5)}(0) = 0.09$ and $F^p_{(7)}(0) = 0.34$. Again, we see about equal weight for the scalar and axialvector-diquark components. That is in general accord with what would be expected from the SU(6) constituent quark model.

It is interesting to note that, since the wave function $\psi_{(1)}(|\vec{k}|)$ has a larger extent in momentum than $\psi_{(7)}(|\vec{k}|)$, it corresponds to a smaller object in coordinate space. That is, the quark plus scalar-diquark system is more strongly bound than the quark plus axialvector-diquark system. This feature, that depends on the spin dependence of the quark-quark interaction, is often used to understand the experimental values of the ratio $F_2^n(x)$ / $F_2^p(x)$, where $F_2^n(x)$ are $F_2^p(x)$ are neutron and proton structure functions [We 94].

of mass $m_S = 400$ MeV, and an axialvector diquark of mass $m_V = 750$ MeV. The value of $\kappa = 0.13$ GeV^2 was taken such that the nucleon mass was found to be $m_N = 938$ MeV.

One can assess the relative importance of the four wave functions by calculating their individual contributions to the charge form factor of the proton at $q^2 = 0$. (Note that $F_p(0)=1$.) We write these contributions as $F^p_{(i)}(0)$, so that

$$F_p(0) = F^p_{(1)}(0) + F^p_{(3)}(0) + F^p_{(5)}(0) + F^p_{(7)}(0) \ . \qquad (6.113)$$

We found $F^p_{(1)}(0) = 0.42$, $F^p_{(3)}(0) = 0.08$, $F^p_{(5)}(0) = 0.10$ and $F^p_{(7)}(0) = 0.40$. Recall that $F^p_{(1)}(0)$ denotes the scalar-diquark contribution, while $F^p_{(3)}(0)$, $F^p_{(5)}(0)$ and $F^p_{(7)}(0)$ are axialvector-diquark contributions. We also consider a small variation of our parameters and give the results in Fig. 6.7 for the case $\bar{G}_S = 7.9$ GeV^2 and $\bar{G}_V = 8.45$ GeV^2. Here $m_S = 400$ MeV, $m_V = 850$ MeV and $\kappa = 0.11$ GeV^2. In this case $F_p(0) = 1$ with $F^p_{(1)}(0) = 0.49$, $F^p_{(3)}(0) = 0.08$, $F^p_{(5)}(0) = 0.09$ and $F^p_{(7)}(0) = 0.34$. Again, we see about equal weight for the scalar and axialvector-diquark components. That is in general accord with what would be expected from the SU(6) constituent quark model.

It is interesting to note that, since the wave function $\psi_{(1)}(|\vec{k}|)$ has a <u>larger</u> extent in momentum than $\psi_{(7)}(|\vec{k}|)$, it corresponds to a <u>smaller</u> object in coordinate space. That is, the quark plus scalar-diquark system is more strongly bound than the quark plus axialvector-diquark system. This feature, that depends on the spin dependence of the quark-quark interaction, is often used to understand the experimental values of the ratio $F_2^n(x) / F_2^p(x)$, where $F_2^n(x)$ are $F_2^p(x)$ are neutron and proton structure functions [We 94].

functions the Lorentz index was written explicitly on the left hand side of Eq. (7.2). Note also that the $\tilde{O}_{(i)}$ (i = 3,5,7) have the same Lorentz index, but that index has not been written.

The electromagnetic vertex of the nucleon can be expressed by two form factors,

$$<\vec{P}+\vec{q},s'|J^{\mu}_{em}(0)|\vec{P},s> = \bar{u}_N(\vec{P}+\vec{q},s')\left[\gamma^{\mu}F_1(q^2) + i\sigma^{\mu\nu}q_{\nu}\frac{F_2(q^2)}{2m_N}\right]u_N(\vec{P},s). \tag{7.4}$$

For example, for the proton, we have $F_1^p(q^2)$ and $F_2^p(q^2)$, with $F_1^p(q^2) = 1$. In order to determine the form factors, we introduce the Dirac matrix

$$\Gamma^{\mu}_{em}(P,k) = \sum_{ss'} u(\vec{P}+\vec{q},s')<\vec{P}+\vec{q},s'|J^{\mu}_{em}(0)|\vec{P},s>\bar{u}(\vec{P},s) \ . \tag{7.5}$$

There are four contributions to $\Gamma^{\mu}_{em}(P,k)$:

$$\Gamma^{\mu}_{em}(P,k) = \Gamma^{\mu}_{em}(P,k)_{q,S} + \Gamma^{\mu}_{em}(P,k)_{d,S} + \Gamma^{\mu}_{em}(P,k)_{q,V} + \Gamma^{\mu}_{em}(P,k)_{d,V} \ . \tag{7.6}$$

The contributions from the scalar-diquark channels to Figs. 7.1(a) and 7.1(b) are

$$\Gamma^{\mu}_{em}(P,k)_{q,S} =$$

$$i\int \frac{d^4k}{(2\pi)^4}\ \hat{\Gamma}^{(1)}_N(P+q,k+q)\,S_{(+)}(k+q)\,Q_q\gamma^{\mu}S_{(+)}(k)\,\hat{\Gamma}^{(1)}_N(P,k)\,\frac{1}{(P-k)^2-m_S^2}\ , \tag{7.7}$$

and

$$\Gamma^{\mu}_{em}(P,q)_{d,S} =$$

$$i\int \frac{d^4k}{(2\pi)^4}\ \hat{\Gamma}^{(1)}_N(P+q,k)\,S_{(+)}(k)\,\hat{\Gamma}^{(1)}_N(P,k)\,\frac{1}{(P-k)^2-m_S^2}\,Q_d F^{\mu}_d\,\frac{1}{(P-k+q)^2-m_S^2}. \tag{7.8}$$

[See Figs 7.1(a) and 7.1(b). In Eq. (7.7), the photon is coupled to the quark and in Eq. (7.8), the photon is coupled to diquark.]

Here Q_q and Q_d are charge operators of the quark and the scalar diquark respectively and F^{μ}_d is the photon-diquark vertex. The vertex, F^{μ}_d, for a scalar pointlike diquark is

$$F^{\mu}_d = 2P^{\mu} - 2k^{\mu} + q^{\mu}\ . \tag{7.9}$$

Similar contributions from the axialvector diquark to Figs. 7.1(a) and 7.1(b) are

$$\Gamma^{\mu}_{em}(P,k)_{q,V} =$$

$$\sum_{j=2}^{4} i \int \frac{d^4k}{(2\pi)^4} \hat{\Gamma}_N^{(j)\alpha}(P+q,k+q) S_{(+)}(k+q) Q_q \gamma^{\mu} S_{(+)}(k) \hat{\Gamma}_N^{(j)\beta}(P,k) \frac{g_{\alpha\beta}}{(P-k)^2 - m_V^2} \ , \tag{7.10}$$

and

$$\Gamma^{\mu}_{em}(P,q)_{q,V} =$$

$$\sum_{j=2}^{4} i \int \frac{d^4k}{(2\pi)^4} \hat{\Gamma}_N^{(j)\alpha}(P+q,k) S_{(+)}(k) \hat{\Gamma}_N^{(j)\beta}(P,k) \frac{g_{\alpha\lambda}}{(P-k+q)^2 - m_V^2} Q_d F_d^{\mu\lambda\nu} \frac{g_{\beta\nu}}{(P-k)^2 - m_V^2} . \tag{7.11}$$

[See Figs. 7.1(a) and 7.1(b).] Here Q_q and Q_d are charge operators of the quark and the axialvector diquark and $F_d^{\mu\lambda\nu}$ is the photon-diquark vertex. The vertex, $F_d^{\mu\lambda\nu}$, for an axialvector pointlike diquark is

$$F_d^{\mu\lambda\nu} = (2P^{\mu} - 2k^{\mu} + q^{\mu}) g^{\lambda\nu} + (-P^{\lambda} + k^{\lambda} + q^{\lambda}) g^{\mu\nu} + (-P^{\nu} + k^{\nu} - 2q^{\nu}) g^{\mu\lambda} . \tag{7.12}$$

We can calculate the nucleon form factors by taking the trace of both sides of Eq. (7.5) after multiplying by γ_{μ} or by P_{μ}.

Under the assumption that the nucleon wave function is dominated by the amplitude with the quark on its positive mass shell, we have, for a pointlike diquark and for $q^2 \to 0$,

$$F_1(0)_q = \sum_i \int \frac{d^3k}{(2\pi)^3} Q_{q(i)} \frac{E_q(\vec{k}) + m_q}{2E_q(\vec{k})} \left\{ \frac{d}{dk_0} \left[\frac{[\Gamma_N^{(i)}(P,k)]^2}{(P_0 - k_0)^2 - [E_d^{(i)}(\vec{k})]^2} \right] \right\}_{k_0 = E_q(\vec{k})}$$

$$= \sum_i \int \frac{d^3k}{(2\pi)^3} Q_{q(i)} \frac{E_q(\vec{k}) + m_q}{2E_q(\vec{k})} \left[\frac{[\Gamma_N^{(i)}(P,k)]^2}{[(P_0 - k_0)^2 - [E_d^{(i)}(\vec{k})]^2]^2} 2(P_0 - k_0) \right]_{k_0 = E_q(\vec{k})}$$

$$+ \sum_i \int \frac{d^3k}{(2\pi)^3} Q_{q(i)} \frac{E_q(\vec{k}) + m_q}{2E_q(\vec{k})} \left[\frac{2\Gamma_N^{(i)}(P,k) \frac{d}{dk_0} \Gamma_N^{(i)}(P,k)}{(P_0 - k_0)^2 - [E_d^{(i)}(\vec{k})]^2} \right]_{k_0 = E_q(\vec{k})}, \tag{7.13}$$

and

$$F_1(0)_d = \sum_i \int \frac{d^3k}{(2\pi)^3} Q_{d(i)} \frac{E_q(\vec{k}) + m_q}{2E_q(\vec{k})} \left[\frac{[\Gamma_N^{(i)}(P,k)]^2}{[(P_0 - k_0)^2 - [E_d^{(i)}(\vec{k})]^2]^2} 2(P_0 - k_0) \right]_{k_0 = E_q(\vec{k})}, \tag{7.14}$$

where the various sums run over i = 1,3,5,7. Here ,

$$Q_{q(1)} = \frac{1}{6} + I_3, \qquad Q_{q(2)..(4)} = \frac{7}{30} - \frac{11}{15} I_3,$$

$$Q_{d(1)} = \frac{1}{3}, \qquad Q_{d(2)..(4)} = \frac{4}{15} + \frac{26}{15} I_3, \tag{7.15}$$

where I_3 = 1/2 for a proton and -1/2 for neutron.

It can be shown that the last term in Eq. (7.13) is proportional to the diagram of

Fig. 7.1(c). We will drop this term for the case of small q^2. In terms of the wave function, the form factor is

$$F_1(0) = F_1(0)_q + F_1(0)_d \tag{7.16}$$

$$\approx \sum_i \int \frac{d^3k}{(2\pi)^3}(Q_{q(i)} + Q_{d(i)})\bar{\psi}^2_{(i)}(P,k)2[P_0 - E_q(\vec{k})] \tag{7.17}$$

This yields the normalization condition

$$1 = \sum_i \int \frac{d^3k}{(2\pi)^3}\bar{\psi}^2_{(i)}(P,k)2[P_0 - E_q(\vec{k})]\,. \tag{7.18}$$

(Again, in Eqs. (7.17) and (7.18), the sum runs over i = 1,3,5,7.) If Eq.(7.18) is satisfied, we obtain the correct charge of the proton. (The charge of the neutron is zero.)

We can also calculate the magnetic moments. We write the nucleon form factors in terms of their isoscalar and isovector parts

$$\begin{aligned} F_1(q^2) &= F_{10}(q^2) + 2F_{11}(q^2)I_3\,, \\ F_2(q^2) &= F_{20}(q^2) + 2F_{21}(q^2)I_3\,. \end{aligned} \tag{7.19}$$

In terms of these values, the nucleon magnetic moments, μ_p and μ_n, are given by

$$\mu_p - 1 = F_{20}(0) + F_{21}(0), \tag{7.20}$$

and

$$\mu_n = F_{20}(0) - F_{21}(0). \tag{7.21}$$

The results obtained for the form factors, when the mass of axialvector diquark is 850 MeV, are presented in Table 7.1. In Table 7.2 we show the magnetic moments obtained for different choices of the axialvector diquark mass. The calculated values of magnetic moments are compared to experimental values in Fig. 7.2.

Chapter 8

Discussion and Conclusions

In our work on the scalar-isoscalar correlator [Ce 93a] and on coupled equations for the $q\bar{q}$ and $\pi\pi$ systems [Ce 93d] we obtained some interesting insight into the nature of the sigma meson that plays an important role in nuclear structure studies. Our basic results is that, when the momentum of the sigma is timelike ($p^2 \approx m_\sigma^2$), the sigma is very strongly coupled to the two-pion continuum and there is no physical sigma meson. That is, there is no pole in the T matrix for $\pi\pi$ scattering, for example. On the other hand, if the sigma momentum is timelike ($p^2 \leq 0$), the $q\bar{q}$ excitation is sufficiently well separated from two-pion continuum so as to appear as a distinct degree of freedom. Alternately, we can say that, if one inspects the scalar-isoscalar correlator in the spacelike regime, one sees a dependence on p^2 that is identical to what one would find if there were a pole at $p^2 \approx m_\sigma^2$ [Ce 93a]. Since the sigma meson one uses in nuclear physics is spacelike, we find that "meson" is a useful degree of freedom. Other studies show that the sigma meson is closely related to the field in nuclear matter that describes the partial restoration of chiral symmetry at a finite density [Ce 92, Ce 93e]. In our studies of the nucleon, we found that both the scalar-isoscalar diquark and the axialvector diquark play an important role in nucleon structure. The wave function we calculate is somewhat like that obtained from study of the SU(6) constituent-quark model.

It would appear that a model in which the quark wave function is expressed in terms of positive-energy spinors represents a good approximation. We have also isolated two major components of the nucleon wave function, expressed in terms of $\bar{\psi}_{(1)}(P,k)$ and $\bar{\psi}_{(7)}(P,k)$ in the nucleon rest frame. An interesting feature of our wave function is that it is sensitive to the spin dependence of the quark-quark interaction. It is seen that the

scalar-isoscalar diquark represents a smaller object that the axialvector-isovector diquark. This feature has consequences for study of deep-inelastic scattering from the nucleon [We 94].

Tables

Table 5.1. Values of the diquark masses, m_S and m_V, and the diquark-quark coupling constants are given for various $\bar{G}_S$ and $\bar{G}_V$. These calculations were made with $m_q = 0.350$ GeV, $\kappa = 0.2$ GeV^2, $\Lambda_3 = 0.702$ GeV and $\mu = 0.050$ GeV. Note that the axialvector diquarks are stable for large values of m_V due to our use of a model of confinement.

$\bar{G}_S$ (GeV^{-2})	m_S (GeV)	g_S	$\bar{G}_V$ (GeV^{-2})	m_V (GeV)	g_V
			11.0	0.558	4.89
			10.5	0.635	4.34
			10.0	0.697	3.98
			9.5	0.750	3.72
			9.0	0.799	3.50
8.5	0.255	3.80	8.5	0.845	3.32
8.0	0.380	3.11	8.0	0.890	3.16
7.5	0.470	2.75	7.5	0.933	3.01
7.0	0.535	2.51	7.0	0.976	2.89
6.5	0.592	2.38	6.5	1.020	2.76
6.0	0.644	2.18	6.0	1.065	2.65

Table 7.1. Contributions of the diagrams of Figs. 7(a) and 7(b) to the calculation of the form factors. The T = 0 form factors are F_{10} and F_{20} and the T = 1 form factors are F_{11} and F_{21}. (In this case μ_P = 2.87, μ_N = - 1.27 and m_V = 850 MeV.)

		$F_{10}(0)$	$F_{11}(0)$	$F_{20}(0)$	$F_{21}(0)$
Scalar Diquark	Quark Contribution (See Fig. 7.1a)	0.098	0.295	0.107	0.320
	Diquark Contribution (See Fig. 7.1b)	0.197	0.00	-0.066	0.000
Axialvector Diquark	Quark Contribution (See Fig. 7.1a)	0.096	-0.150	-0.085	0.133
	Diquark Contribution (See Fig. 7.1b)	0.109	0.355	0.344	1.119
Sum		0.50	0.50	0.300	1.572
Experiment		–	–	-0.06	1.85

Table 7.2. Dependence of the magnetic moments of the neutron and proton on the axialvector diquark mass.

Axialvector Diquark Mass	650 MeV	750 MeV	850 MeV	950 MeV
μ_P	3.28	3.10	2.87	2.63
μ_N	-1.52	-1.41	-1.27	-1.12

Figure Captions

Fig. 2.1 (a) Representation of a one-loop perturbative calculation of the sigma width in the case the sigma is assumed to be stable, in first approximation.

(b) Representation of the coupling of the $q\bar{q}$ channel to 2-pion channel. The diagram shows the effective interaction in the $q\bar{q}$ channel due to the excitation of the 2-pion channel. Here, the wavy line denotes a pion and the heavy dots represent the pion-quark coupling, $g_{\pi qq}$.

(c) An approximation to the process shown in Fig. 2.2(b), where $G_{\pi S}$ is an effective coupling constant for $q + \bar{q} \rightarrow \pi + \pi$.

(d) Schematic representation of the approximation used to replace the three-loop calculation of Fig. 2.1(b) by that of Fig. 2.1(c).

Fig. 2.2 Schematic representation of Eqs. (2.1) and (2.2). Here, T = iM, where M is the invariant amplitude as defined by Bjorken and Drell.

Fig. 2.3 The real part of $J_S(q^2)$ is shown as a solid line. The dotted line represents $\mathrm{Re}J_\pi(q^2)$, while the dashed line represents Im $J_\pi(q^2)$. Here, the parameters of the NJL model are $G_S = 7.91\ \mathrm{GeV}^{-2}$, $m_q = 0.302$ MeV and $\Lambda = 1.0$ GeV. (The same cutoff is used for $J_S(q^2)$ and for $J_\pi(q^2)$.)

Fig. 2.4 The phase shift, δ_0^0, is shown for the parameters $\Lambda = 1.0$ GeV, $G_\pi = 0$, $G_S = 7.91\ \mathrm{GeV}^{-2}$, $m_q = 302$ MeV and $m_\pi = 139$ MeV.

a) $G_{\pi S} = 1.0\ \mathrm{GeV}^{-1}$,

b) $G_{\pi S} = 2.0\ GeV^{-1}$,

c) $G_{\pi S} = 3.0\ GeV^{-1}$,

d) $G_{\pi S} = 4.0\ GeV^{-1}$.

For $G_{\pi S} = 3.0\ GeV^{-1}$, we have $E_R = 0.590$ GeV and $\Gamma = 0.113$ GeV, while for $G_{\pi S} = 4.0\ GeV^{-1}$, $E_R = 0.542$ GeV and $\Gamma = 0.248$ GeV. The energy, E_R, denotes the point when the phase shift is equal to 90 degrees. The short-dash lines represent a suggested extrapolation of curves a and b into the region of the two-quark continuum. The long-dash line is a schematic representation of the experimental data for δ_0^0.

Fig. 2.5 Similar caption as that of Fig. 2.4, except that the use of $\Lambda = 1.1$ GeV, yields a stronger attraction than that seen in Fig. 2.4.

a) $G_{\pi S} = 1.0\ GeV^{-1}$,

b) $G_{\pi S} = 2.0\ GeV^{-1}$,

c) $G_{\pi S} = 2.5\ GeV^{-1}$.

Fig. 2.6 Values of $D(q^2)$ obtained in model A are shown. [See Eqs. (2.22) and (2.23).] Re $D(q^2)$ for $G_{\pi S} = 1.0\ GeV^{-1}$ is shown as a dashed line, while for $G_{\pi S} = 4.0\ GeV^{-1}$, Re $D(q^2)$ is shown as a solid line. The dotted line shows Im $D(q^2)$ for $G_{\pi S} = 4.0\ GeV^{-1}$. (The value of Im $D(q^2)$ for $G_{\pi S} = 1.0\ GeV^{-1}$ is too small to be easily shown in this figure.) Note the downward shift in the resonance position with the increase of $G_{\pi S}$. (When $G_{\pi S} = 4.0\ GeV^{-1}$, the resonance is at $E_R = 0.542$ GeV and has a width $\Gamma = 0.248$ GeV - see Fig. 2.5).The heavy line on the horizontal axis denotes the region of the quark-antiquark continuum.

Fig. 2.7 Values of Re $G_{\pi S}^2 J_\pi(q^2)$ are shown as a dot-dash line and Im $G_{\pi S}^2 J_\pi(q^2)$ is shown as a dotted line. Here, $G_{\pi S} = 3.8\ GeV^{-1}$. The solid line shows Im $M(q^2)$, while the dashed line is a phenomeenological extension of that quantity for $q^2 > (2m_q^{const})^2$. The double-dot-dash line denotes Re $M(q^2)$. The parameters used are $\Lambda = 1.0$ GeV, $G_S = 7.91\ GeV^{-2}$, $m_q = 302$ MeV, $m_\pi = 139$ MeV and $g_{\pi qq} = 2.68$.

Fig. 2.8 Real and imaginary parts of $D(q^2)$ for model B are shown as a solid and a dotted line, respectively. (The parameters are those listed in the caption to Fig 2.7.)The dashed line is tangent to Re $D(q^2)$ at $q^2 = 0$ and intersects the horizontal axis at about $q^2 = 0.3\ GeV^2$, giving rise to an effective mass, $m_\sigma(0) \simeq 0.55$ GeV. Here, $D(q^2) = 1 - G_S J_S(q^2) + M(q^2) J_S(q^2)$.

Fig. 3.1 (a) The quark-loop integral that arises in the analysis of the NJL model. A four-dimensional integral over k is implied.

(b) Inclusion of a long-range potential (wavy line) in the calculation of the quark-loop integral. The filled triangular region represents a vertex function.

(c) An integral equation for the vertex function is represented in schematic fashion. [See Fig 2.2.]

Fig. 3.2 (a) Representation of the four-dimensional integral equation for the scalar-isoscalar vertex $\hat{\Gamma}(P^2, P\cdot k, k^2)$. The wavy line denotes the interaction and the filled triangle is the vertex.

(b)-(c) Integral equations for the vertex with either the quark on its

positive mass-shell, or with the antiquark on its negative mass shell. In Fig. 2.2(b), we have $k_0 = -P_0/2 + E(\vec{k})$, and in Fig. 2.2(c), we have $k_0 = P_0/2 + E(\vec{k})$.

Fig. 3.3 Lorentz-scalar confinement. Values of $\Gamma^{+-}(P^0, |\vec{k}|)$ obtained from the solution of the coupled equations for Γ^{+-} and Γ^{-+}, are shown. Here $m_q = 0.33$ GeV, $\mu = 0.05$ GeV and $\kappa = 0.3$ GeV^2. (A cutoff on the magnitude of the various momenta of 1.0 GeV was used.) Note that $\Gamma^{+-}(P^0, |\vec{k}|) \to 1$ for large $|\vec{k}|$ and that $\Gamma^{+-}(P^0, k_{on}) = 0$. Values of P^0 and k_{on} are given starting with the uppermost curve:

a) $P^0 = 0.69$ GeV; $k_{on} = 0.10$ GeV,

b) $P^0 = 0.76$ GeV; $k_{on} = 0.18$ GeV,

c) $P^0 = 0.80$ GeV; $k_{on} = 0.22$ GeV,

d) $P^0 = 0.90$ GeV; $k_{on} = 0.30$ GeV.

Fig. 3.4 Lorentz-scalar confinement. Values of $\Gamma^{-+}(P^0, |\vec{k}|)$ obtained from the solution of the coupled equations for Γ^{+-} and Γ^{-+} are shown. (See caption to Fig. 3.3.) Note that the $\Gamma^{-+}(P^0, |\vec{k}|)$ decrease for large $|\vec{k}|$, and are close to unity for $|\vec{k}| = 1$ GeV. Starting with the lowest curve and moving upward we have $P^0 = 0.69$ GeV, $P^0 = 0.76$ GeV, $P^0 = 0.80$ GeV and $P^0 = 0.90$ GeV. (Corresponding values of k_{on} are given in the caption to Fig. 3.3.)

Fig. 3.5 The dashed line shows the value of $\mathrm{Re}J_S(q^2)$, while the dotted line is $\mathrm{Im}J_S(q^2)$. The solid line represents the value of $J_S'(P^2)$, calculated using the functions Γ^{+-} and Γ^{-+}. Here $m_q = 0.302$ GeV, $\mu = 0.05$ GeV, $\kappa = 0.2$

GeV^2 and $\Lambda_3 = 0.702$ GeV.

Fig. 3.6 (a) A diagrammatic representation of $-iM(P^2)$ is shown. Here, the wavy lines are pions. The small filled circles are either pion-quark vertices or factors of iG_S.

(b) The function $M'(P^2)$ is obtained by inserting vertex functions (filled triangular areas) at the $q\bar{q}$ vertices.

(c) A form factor, $F(P^2, P\cdot k, k^2)$ defined in the evaluation of $M(P^2)$. If a vertex operator is included, the function is denoted as $F'(P^2, P\cdot k, k^2)$.

Fig. 3.7 Values of $\mathrm{Im}\,M'(P^2)$ are shown as a dashed line. The solid line is the result of an approximation where one calculates the form factor $F(P^2, P\cdot k, k^2)$ by keeping only the principal value of the loop integral.

Fig. 3.8 Values of $\mathrm{Re}\,M'(P^2)$ (solid line) obtained from a dispersion relation using $\mathrm{Im}\,M'(P^2)$ (dashed line) from Fig. 3.7.

Fig. 3.9 Values of the denominator of the scalar-isoscalar $q\bar{q}$ T-matrix are shown. The dot-dashed curve is $1 - G_S J_S(P^2)$. The dashed curve is $1 - G_S J'_S(P^2)$ and the solid curve is $D(P^2) = 1 - G_S J'_S(P^2) + M'(P^2) J'_S(P^2)$.

Fig 3.10 Values of $1 - G_S J'_S(P^2)$ (dashed line) and $D(P^2) = 1 - G_S J'_S(P^2) + M'(P^2) J'_S(P^2)$ (solid line) are shown. Here we have replaced the constant G_S by $G_S(P^2)$, shown in the lower part of the figure, when calculating $D(P^2)$.

Fig. 4.1 (a) The figure shows the discontinuity of the correlator, $C(P^2)$, across the two-pion cut. The wave operators, Ω and Ω^+, take the quark-antiquark pair created at point into two on-mass-shell pions.

(b) The wave operator may be expressed in terms of the T-matrices, $t_{\pi q}$ and $t_{q\pi}$ giving rise to the figures shown here.

Fig. 4.2 Model for $ImC(P^2)$ obtained from our coupled-channel quark-hadron model,

(a) $ImC^{(0)}(P^2)$ (See Eq. (4.8)),

(b) $ImC^{(1)}(P^2)$ (See Eq. (4.9)),

(c) $ImC^{(2)}(P^2)$ (See Eq. (4.7)).

Fig. 4.3 The figure shows $ImC^{(1)}(P^2)$ (solid line) and $ImC(P^2) \simeq ImC^{(1)}(P^2) + ImC^{(2)}(P^2)$ (dashed line).

Fig. 4.4 Values of Re $C(P^2)$ obtained from $ImC(P^2)$ by means of a dispersion relation are show. The dotted line denotes an approximation with $C(P^2) = a^4/(P^2 - m_\sigma^2)$. Here $a = 0.0424$ GeV^4 and $m_\sigma^2 = 0.502$ GeV.

Fig. 5.1 The vertex amplitude for the scalar diquark to go into two quarks is shown. The parameters used are $m_q = 0.350$ GeV, $\mu = 0.050$ GeV and $\kappa = 0.2$ GeV^2.

(a) The function $\Gamma^{-+}(P_0, |\vec{k}|)$ is given for several values of P_0^2

a) $P_0^2 = 0.1$ GeV^2,

b) $P_0^2 = 0.4$ GeV^2,

c) $P_0^2 = 0.5$ GeV^2,

d) $P_0^2 = 0.6$ GeV^2.

(b) The function $\Gamma^{-+}(P_0, |\vec{k}|)$ is presented for values of P_0^2 listed in part (a). The function is very insensitive to the change of the energy of the scalar diquark.

Fig. 5.2 The value of the quark-quark loop integral in the scalar-diquark channel (in the presence of the potential V_L) is shown. The integral, $J'^{d}_{S}(P^2)$, was calculated using the vertex functions presented in Figs 5.1(a) and 5.1(b). In addition to the parameters given in the caption of Fig 5.1, a cutoff of $\Lambda_3 = 0.702$ GeV for the quark momenta was used.

Fig. 5.3 The figure shows the axialvector vertex for the diquark to go into a quark and diquark. Here, as in the case of scalar diquark, the parameters used are $m_q = 0.350$ GeV, $\mu = 0.050$ GeV and $\kappa = 0.2$ GeV^2.

(a) The function $-\frac{\vec{k}^2}{m_q}\Gamma^{[+-]}_{1V}(P,k)$ is presented for

a) $P_0^2 = 0.1$ GeV^2,

b) $P_0^2 = 0.4$ GeV^2,

c) $P_0^2 = 0.6$ GeV^2,

d) $P_0^2 = 0.8$ GeV^2.

(b) The function $\Gamma^{[+-]}_{2V}(P,k)$ is shown for the values of P_0^2 given in part (a).

Fig. 5.4 The quark-quark loop integral in the axialvector channel in the presence of the linear potential, $J'^{d}_{V}(P^2)$ is shown. This function was calculated using the vertex functions from Fig. 5.3. The cutoff $\Lambda_3 = 0.702$ GeV on the quark momenta was used.

Fig. 6.1 The vertex function on the quark-diquark model is represented by the shaded area. The heavy line denotes the nucleon of momentum P. The first term on the right-hand side represents the exchange potential and the second term represents the confining interaction. The double line denotes a diquark that may be either scalar-isoscalar or axialvector-isovector. If both kinds of diquarks appear in the formalism, the figure represents a set of coupled equations.

Fig. 6.2 The wave functions describing the scalar diquark-quark system are shown.

(a) The diagram shows the function $\tilde{\psi}^{q}_{(1)}(P,k)$. The parameters used here are $m_q = 0.350$ GeV, $m_S = 0.400$ GeV, $m_N = 0.938$ GeV, $\mu = 0.050$ GeV and $\kappa = 0.032$ GeV^2.

(b) The functions $\tilde{\psi}^{q}_{(2)}(P,k)$, $\tilde{\psi}^{d}_{(1)}(P,k)$ and $\tilde{\psi}^{d}_{(2)}(P,k)$ are shown.

Fig. 6.3 The wave functions of the scalar diquark-quark system defined by Eq. (6.2) are shown. The parameters given in the caption to Fig. 6.1 were used. The functions $\psi^{q}_{(1)}(P,k)$ and $\psi^{q}_{(2)}(P,k)$ are shown. The functions $\psi^{d}_{(1)}(P,k)$ and $\psi^{d}_{(2)}(P,k)$ are significantly smaller and are not shown.

Fig. 6.4 The functions $\tilde{\psi}_{(i)}(|\vec{k}|)$ are shown for i = 1,3,5,7. The parameters used are $m_q = 0.350$ GeV, $m_S = 0.400$ GeV, $m_V = 0.750$ GeV, $m_N = 0.938$ GeV, $\mu = 0.050$ GeV and $\kappa = 0.13$ GeV^2. The quark-diquark coupling constants were $g_{Sqq} = 3.05$ and $g_{Vqq} = 3.72$. These wave functions gave the magnetic moments $\mu_p = 3.10$ and $\mu_n = -1.41$.

Fig. 6.5 The functions $\tilde{\psi}_{(i)}(|\vec{k}|)$ are shown for i = 1,3,5,7 and for different values

of the axialvector-diquark mass. The parameters used are m_q = 0.350 GeV, m_S = 0.400 GeV, m_V = 0.850 GeV, m_N = 0.938 GeV, μ = 0.050 GeV and κ = 0.11 GeV^2. The quark-diquark coupling constants were g_{Sqq} = 3.05 and g_{Vqq} = 3.30. These wave functions gave the magnetic moments μ_p = 2.87 and μ_n = -1.27.

Fig. 7.1 Diagrams for calculation of nucleon form factors are shown.

(a) The contribution of the quark is shown.

(b) The contribution of the diquark is shown.

(c) The contribution of the exchange diagram is shown.

The wavy line denotes a photon of momentum q. The nucleon (heavy line) has momentum P initially and momentum P+q finally.

Fig. 7.2 The calculated values (dotted lines) of the magnetic moments of the proton and neutron are compared to the experimental values (μ_p = 2.79 and μ_n = -1.91) for various values of the axialvector diquark mass, m_V.

Figures

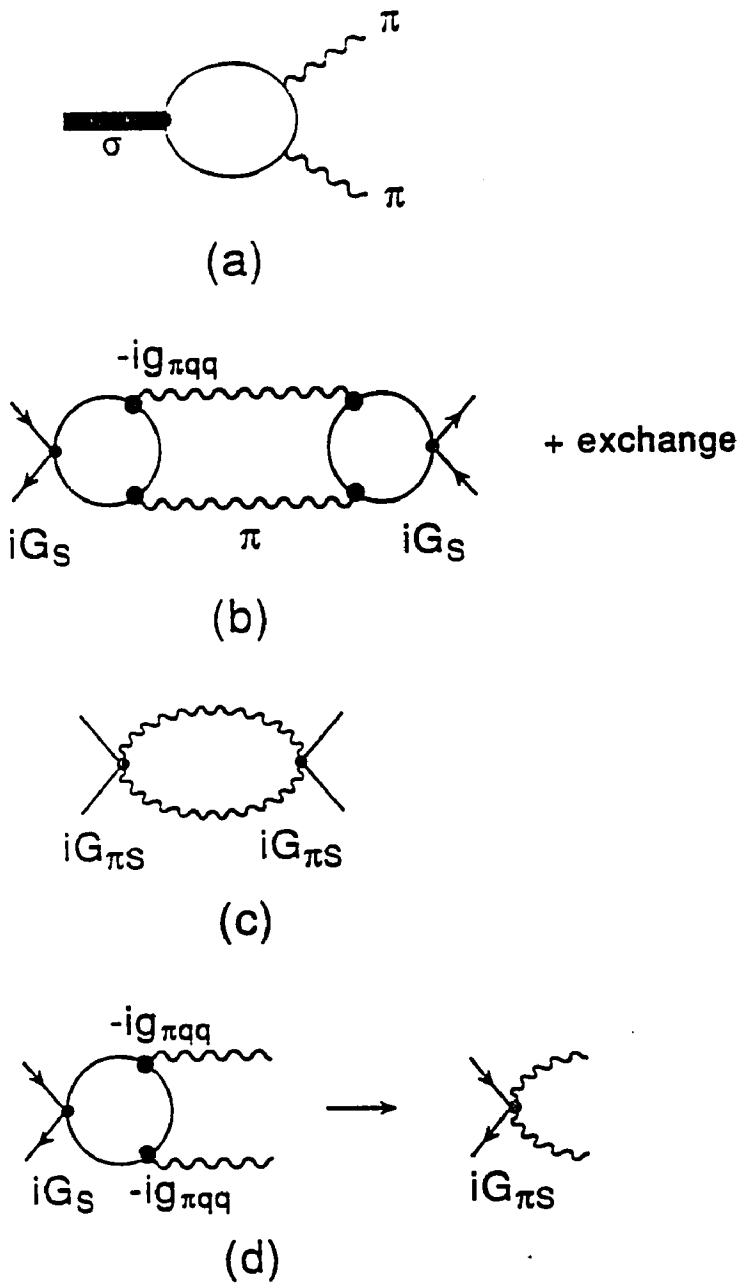

Fig. 2.1

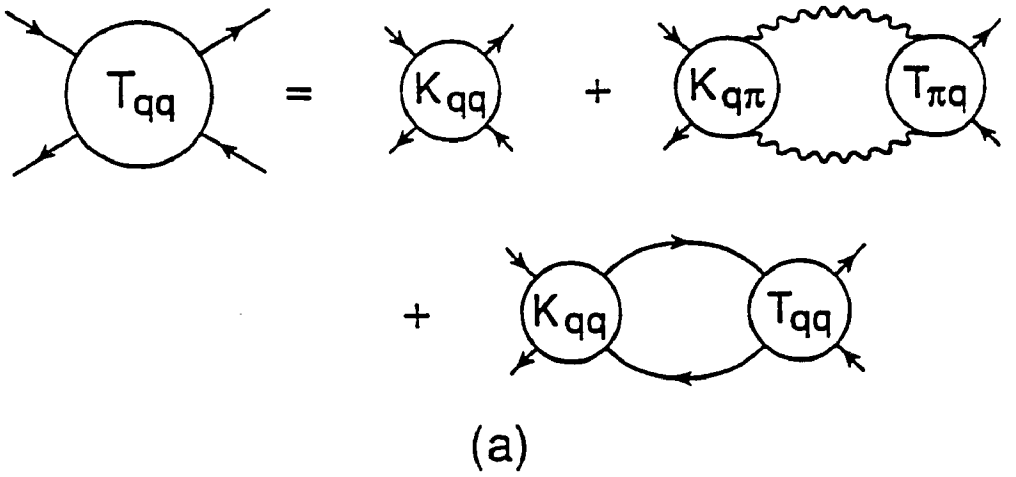

(a)

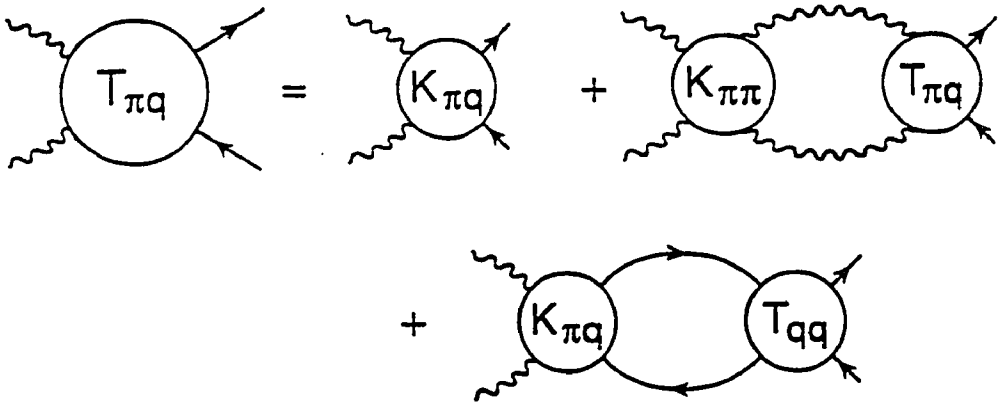

(b)

Fig. 2.2

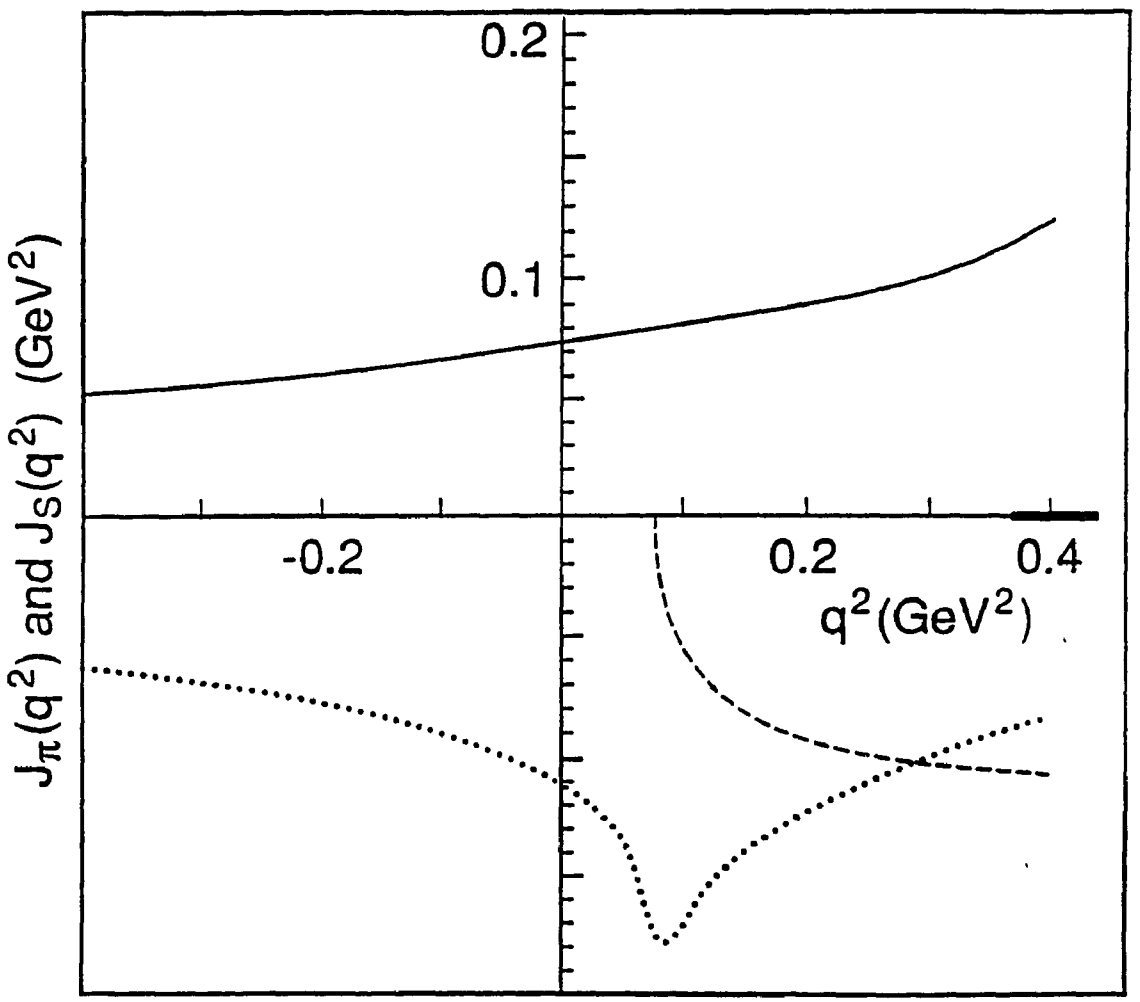

Fig. 2.3

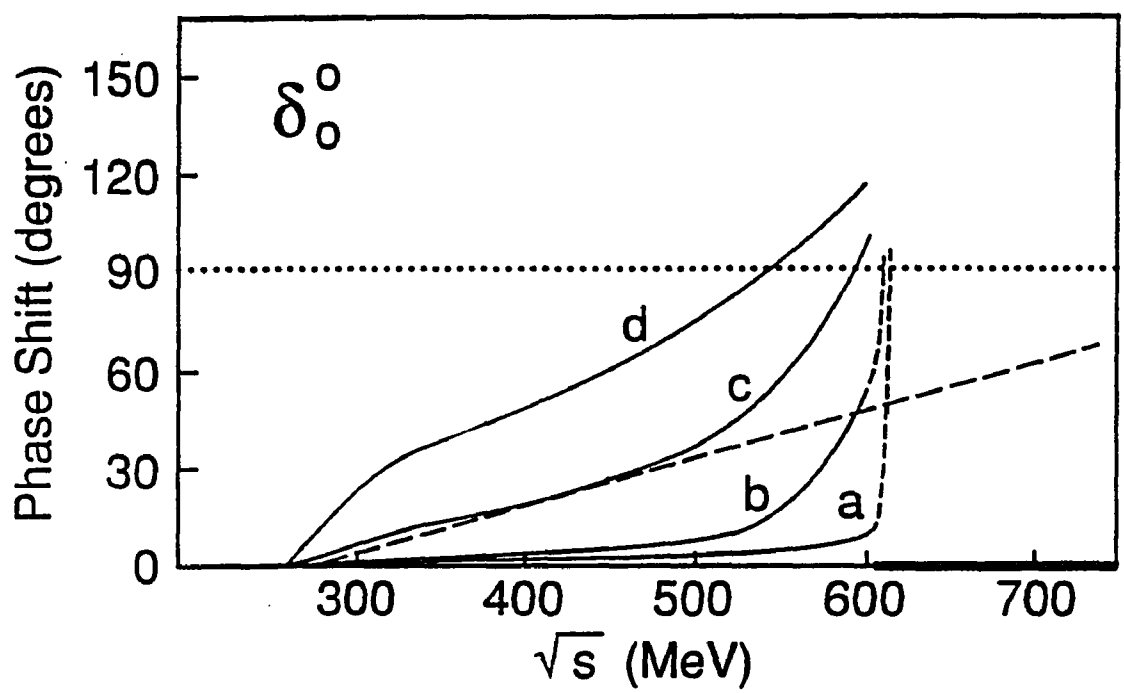
δ_o^o
Phase Shift (degrees)
150
120
90
60
30
0
300
400
500
600
700
$\sqrt{s}$ (MeV)
d
c
b
a

Fig. 2.4

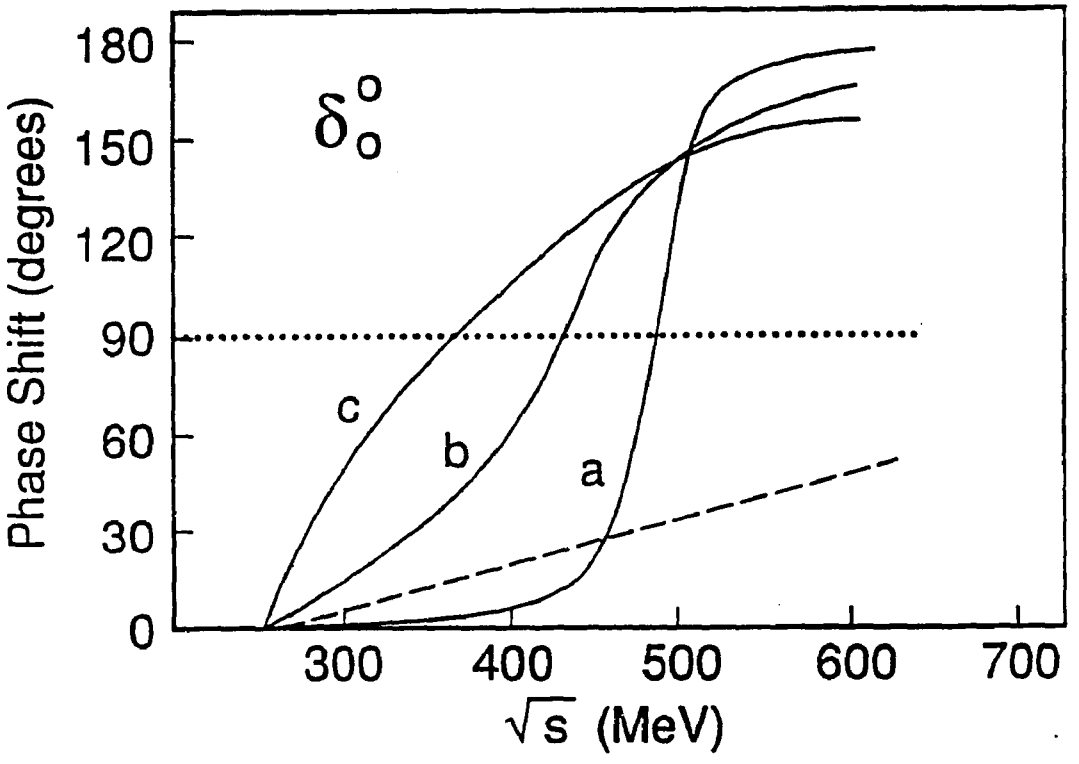
180
150
120
90
60
30
0
Phase Shift (degrees)
δ_o^o
c
b
a
300
400
500
600
700
$\sqrt{s}$ (MeV)

Fig. 2.5

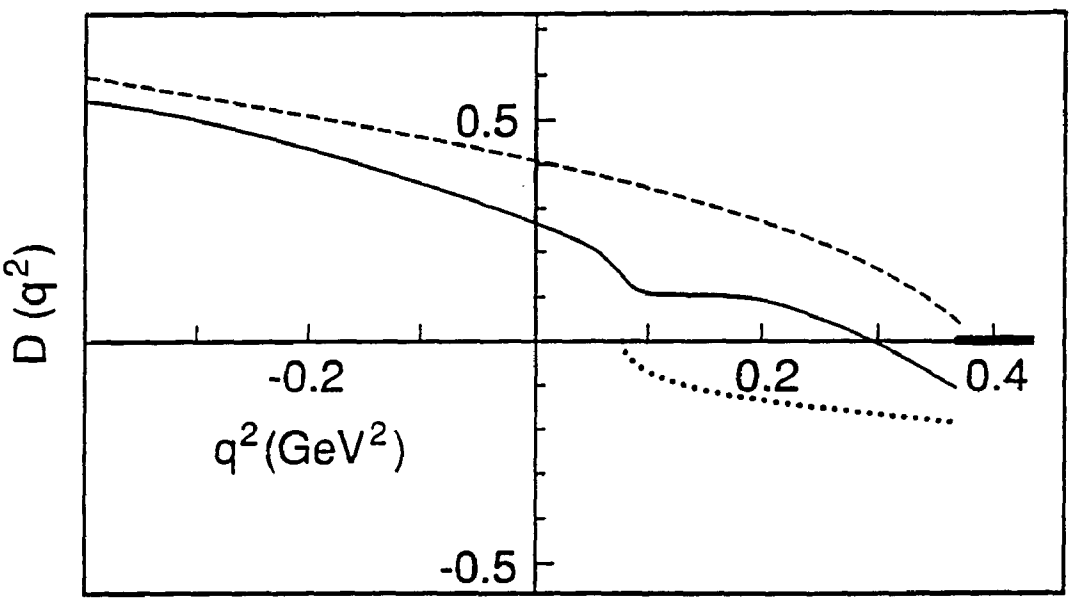

Fig. 2.6

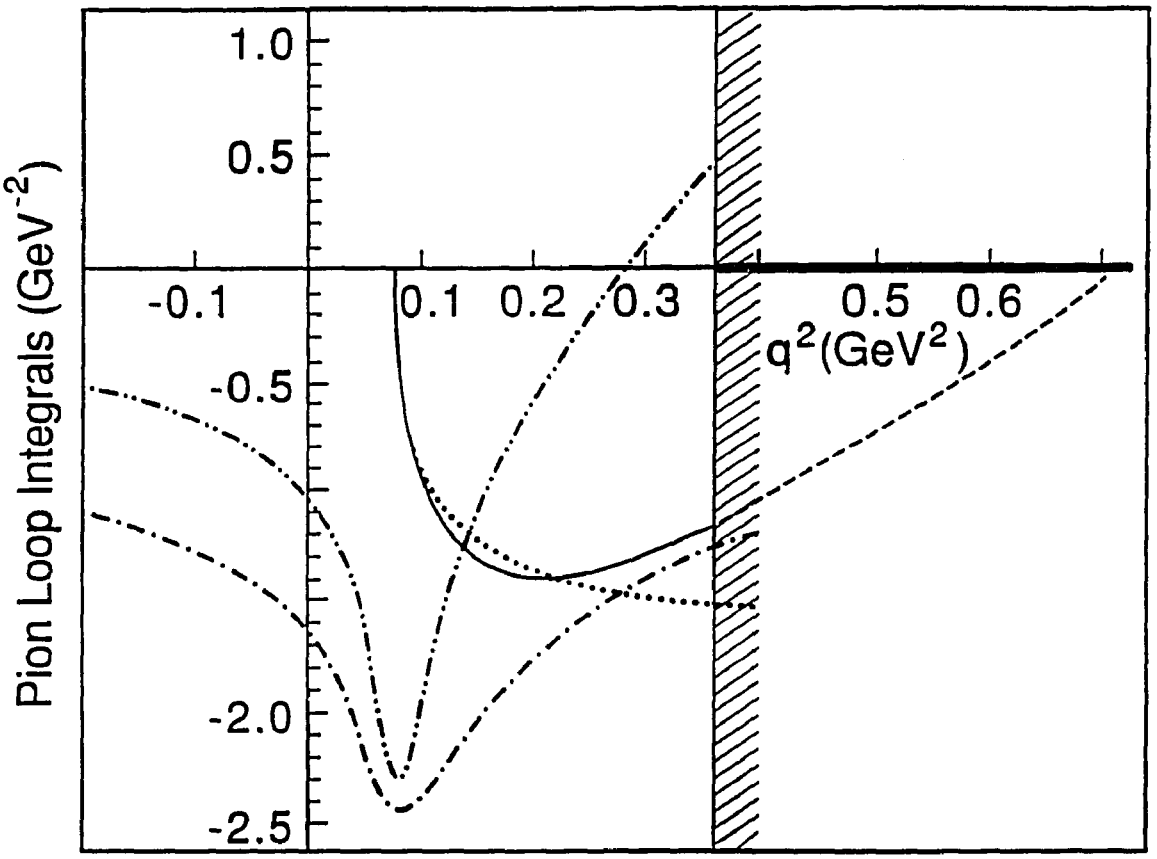

Fig. 2.7

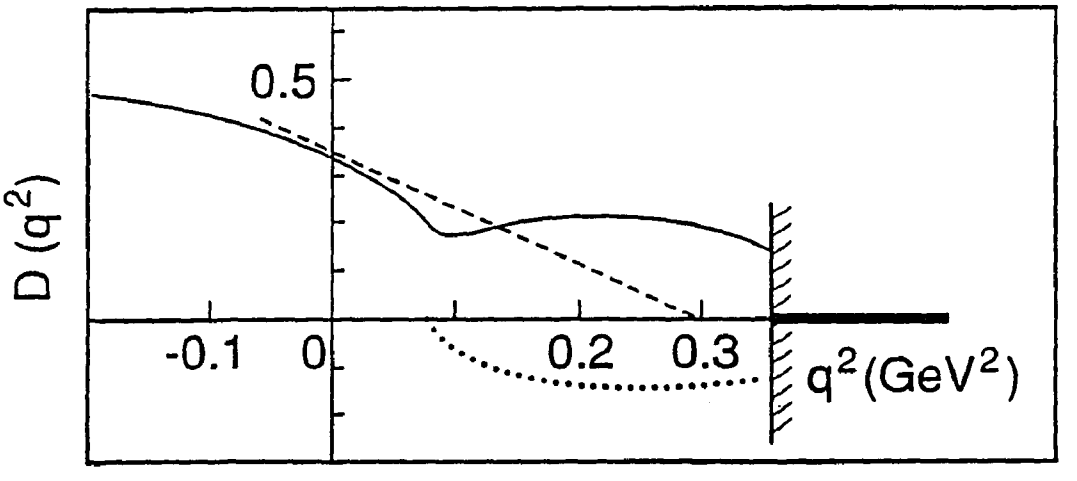

Fig. 2.8

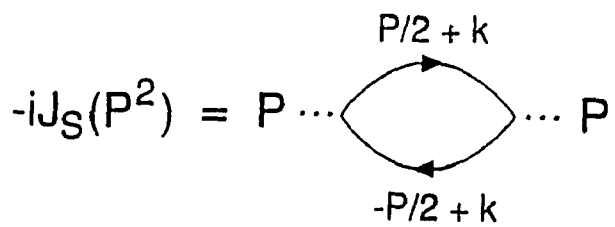

(a)

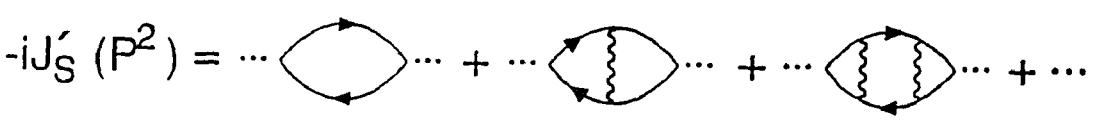

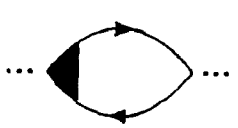

(b)

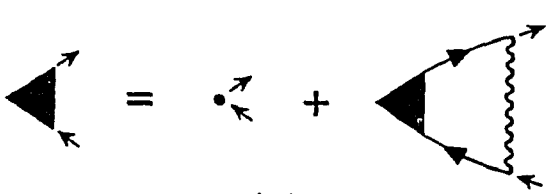

(c)

Fig. 3.1

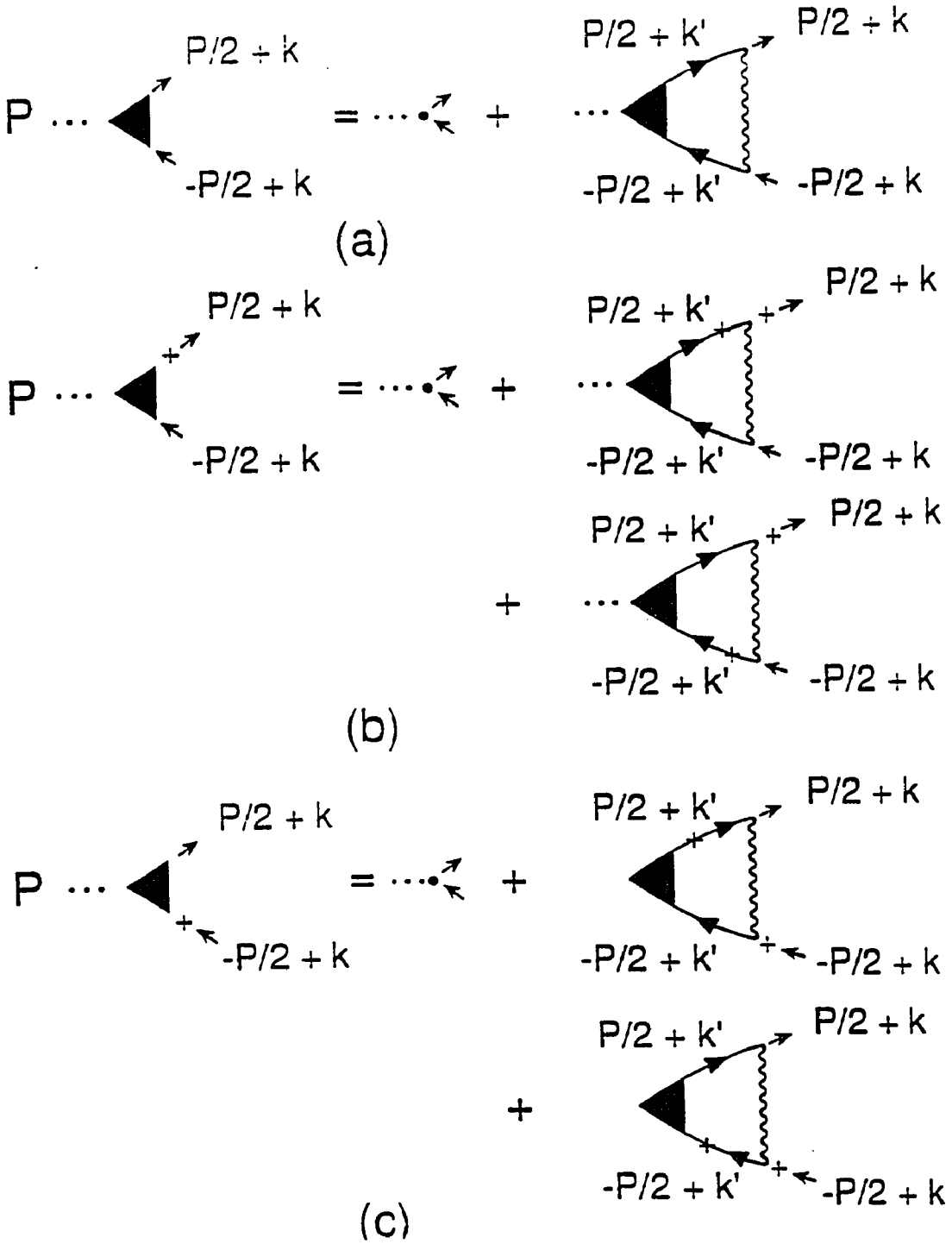

Fig. 3.2

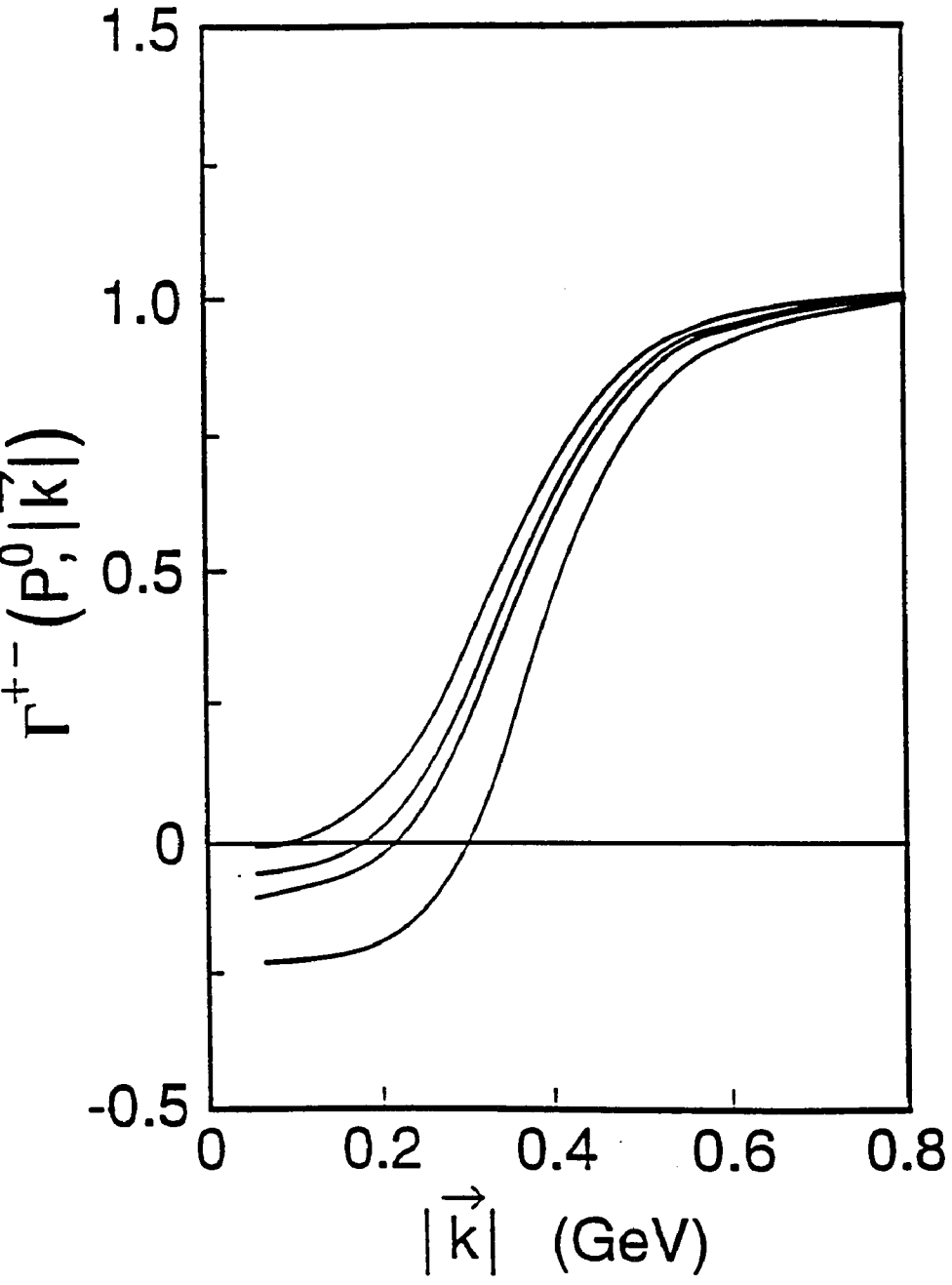

Fig. 3.3

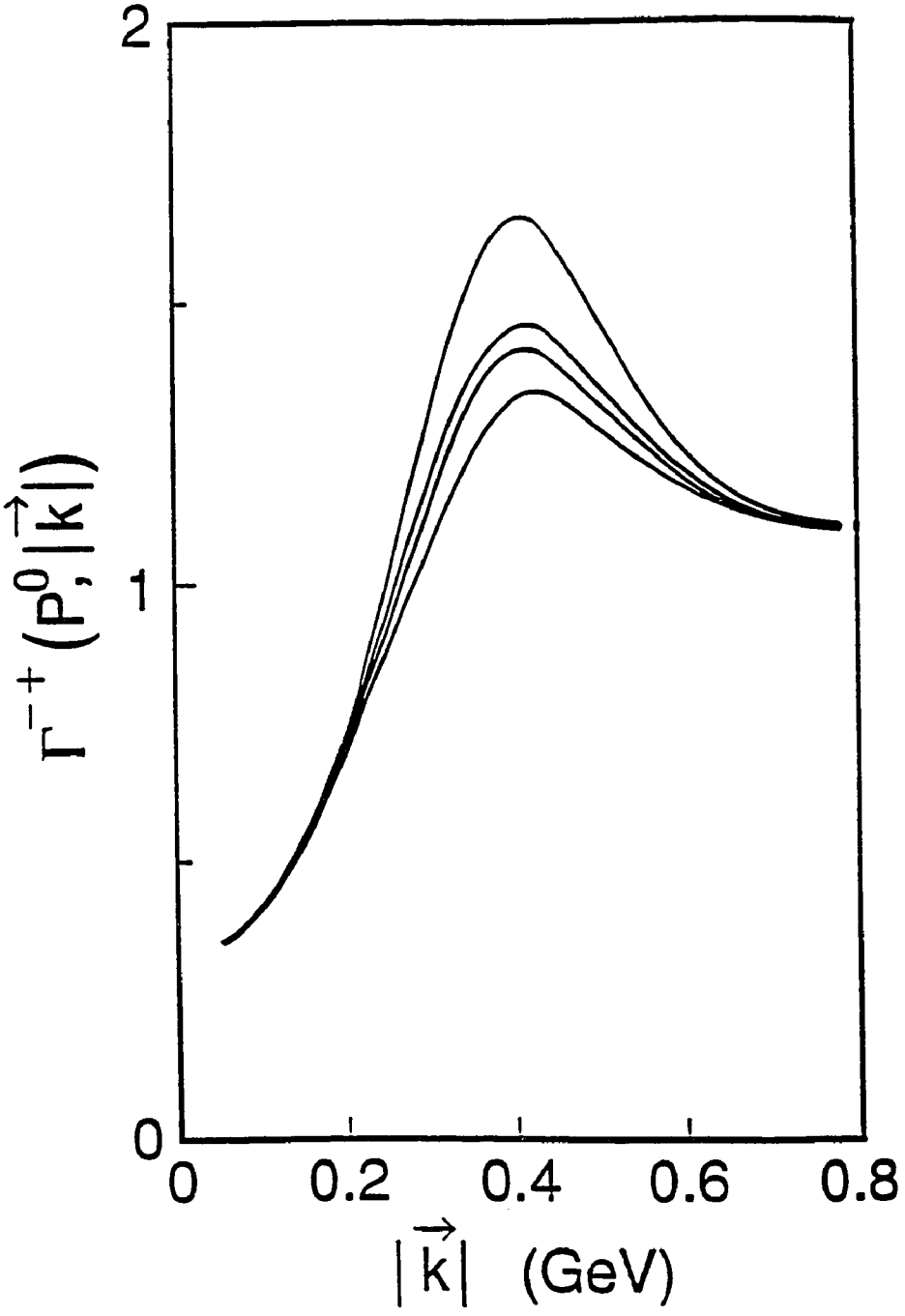

Fig. 3.4

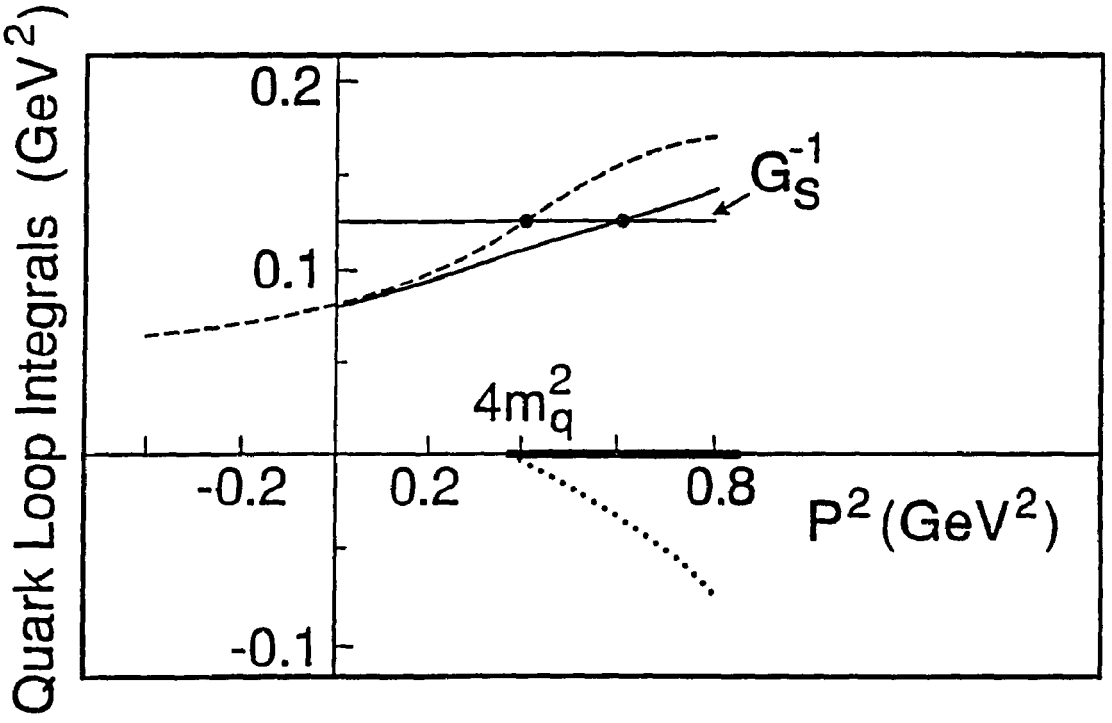

Fig. 3.5

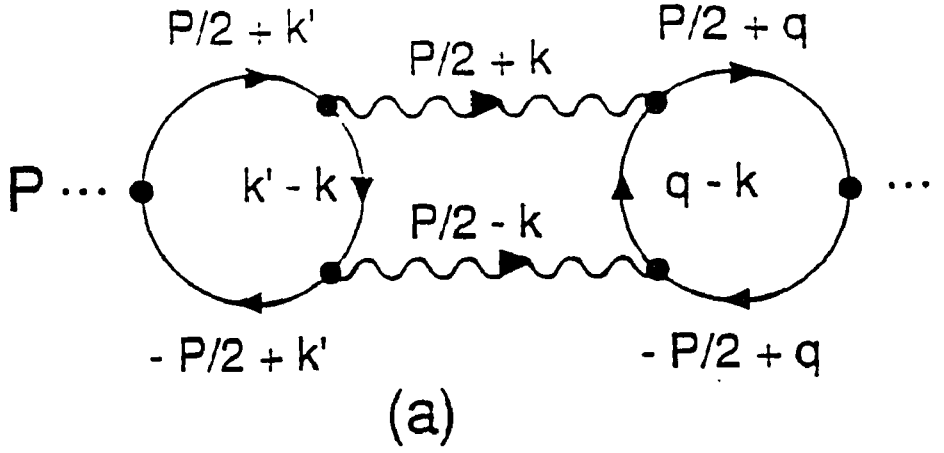

(a)

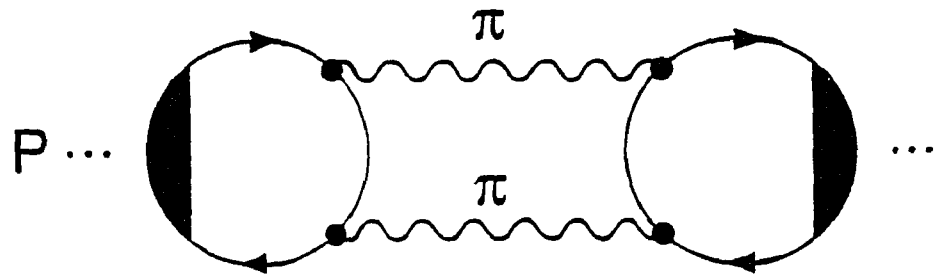

(b)

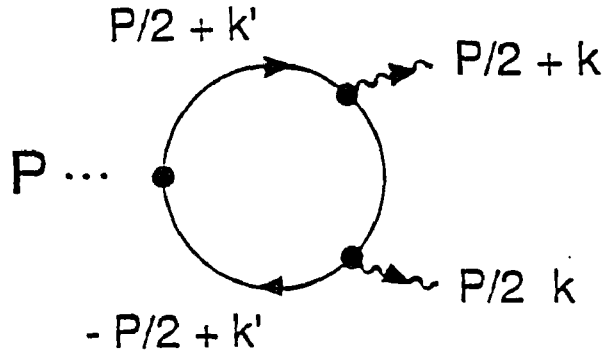

(c)

Fig. 3.6

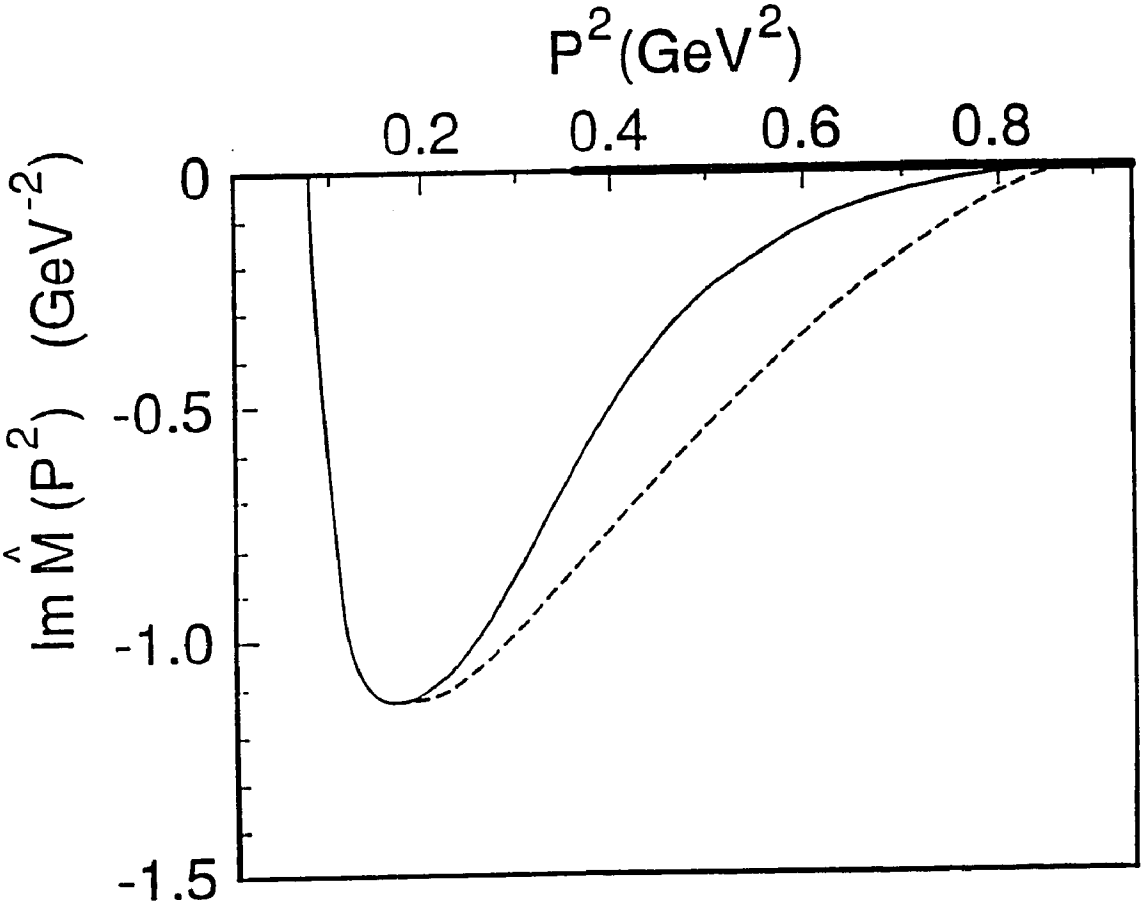

Fig. 3.7

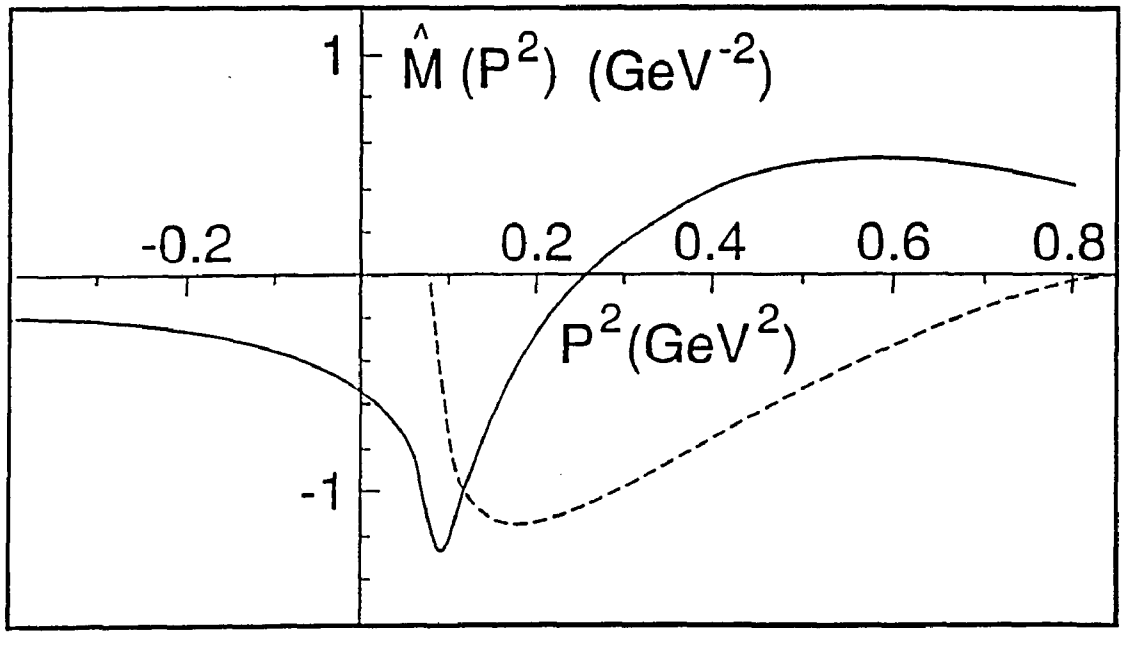

Fig. 3.8

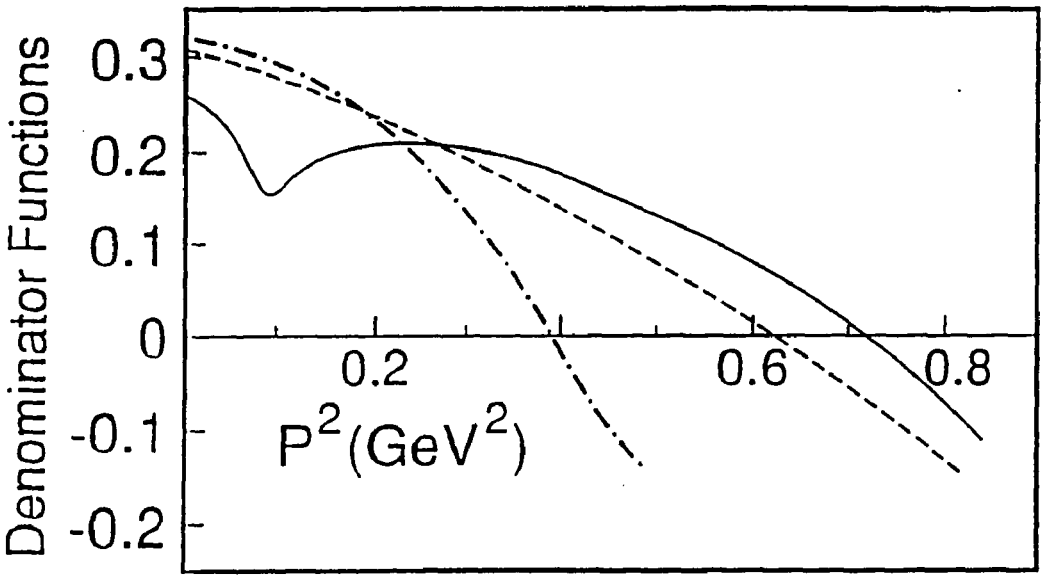

Fig. 3.9

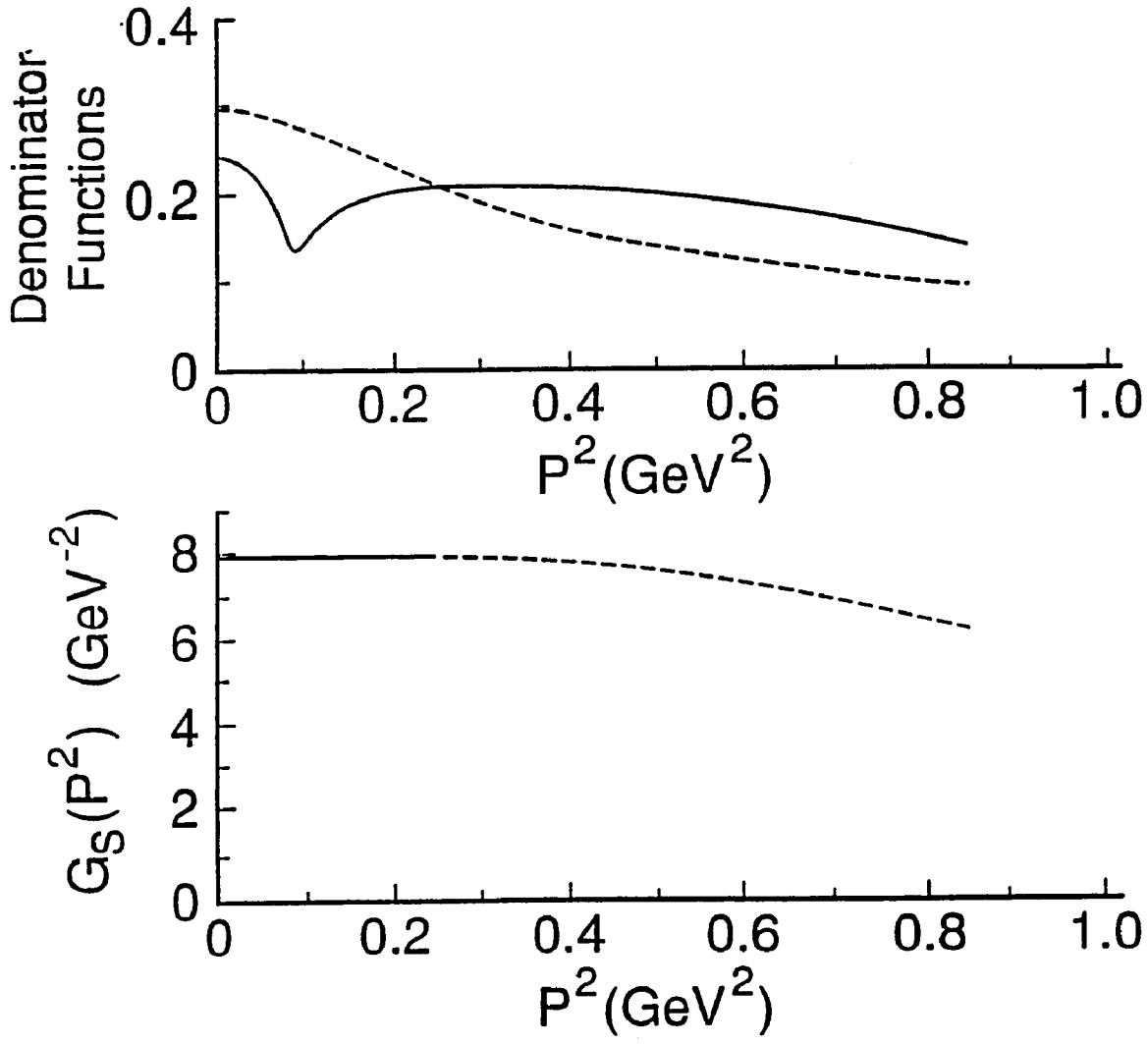
Denominator Functions
0.4
0.2
0
0
0.2
0.4
0.6
0.8
1.0
$P^2(GeV^2)$
$G_S(P^2)$ (GeV^{-2})
8
6
4
2
0
0
0.2
0.4
0.6
0.8
1.0
$P^2(GeV^2)$

Fig. 3.10

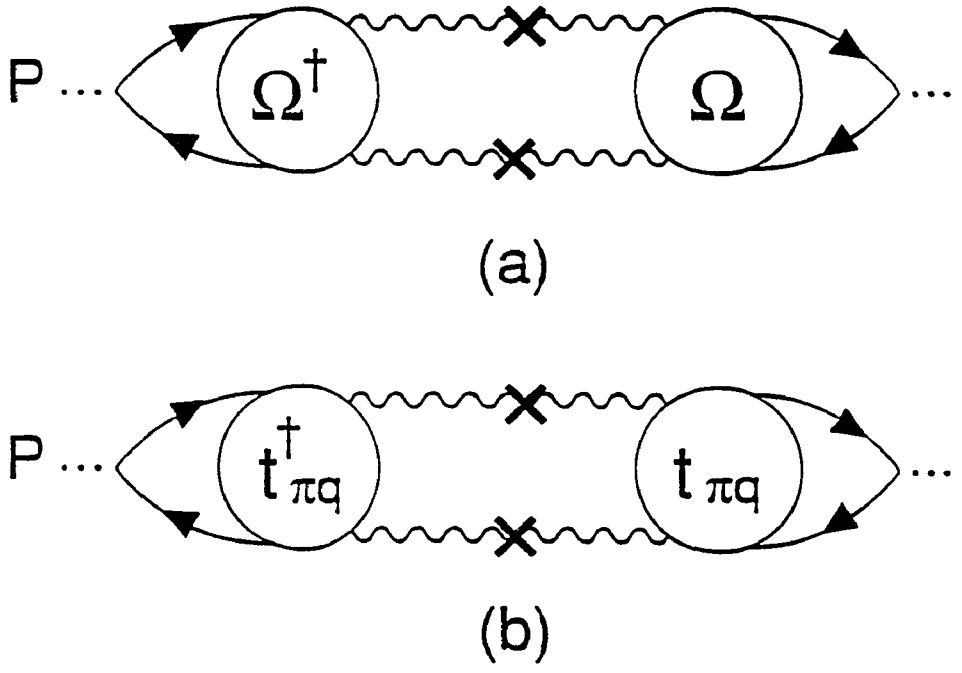

Fig. 4.1

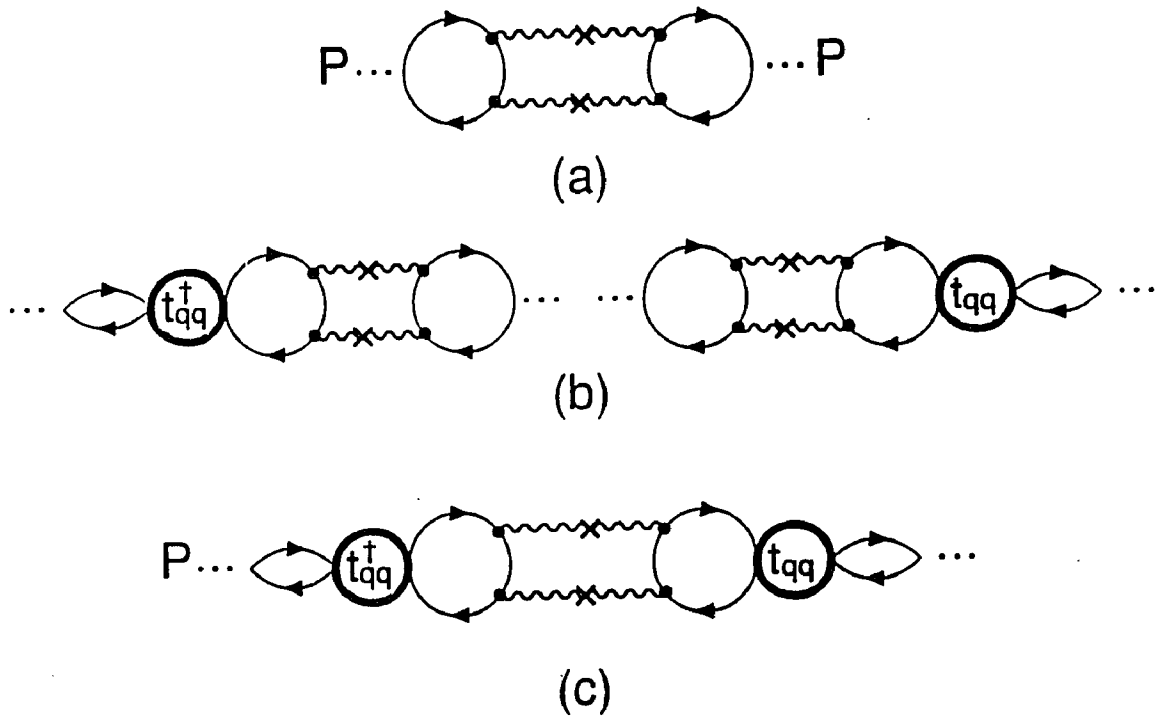

Fig. 4.2

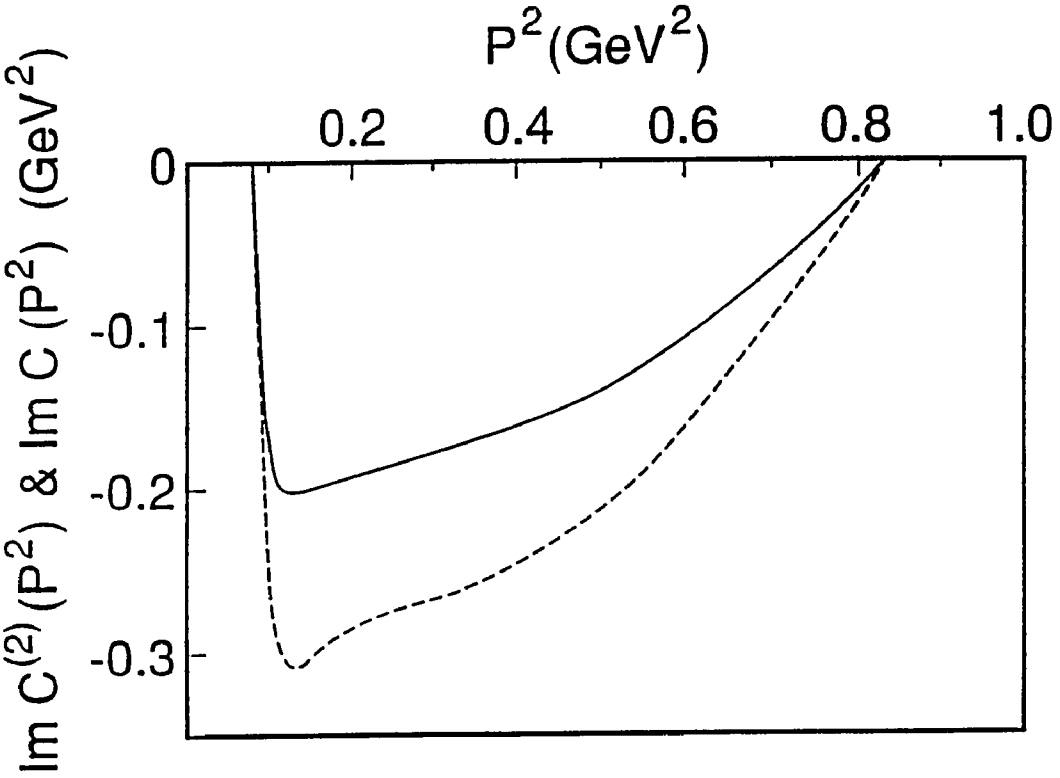

Fig. 4.3

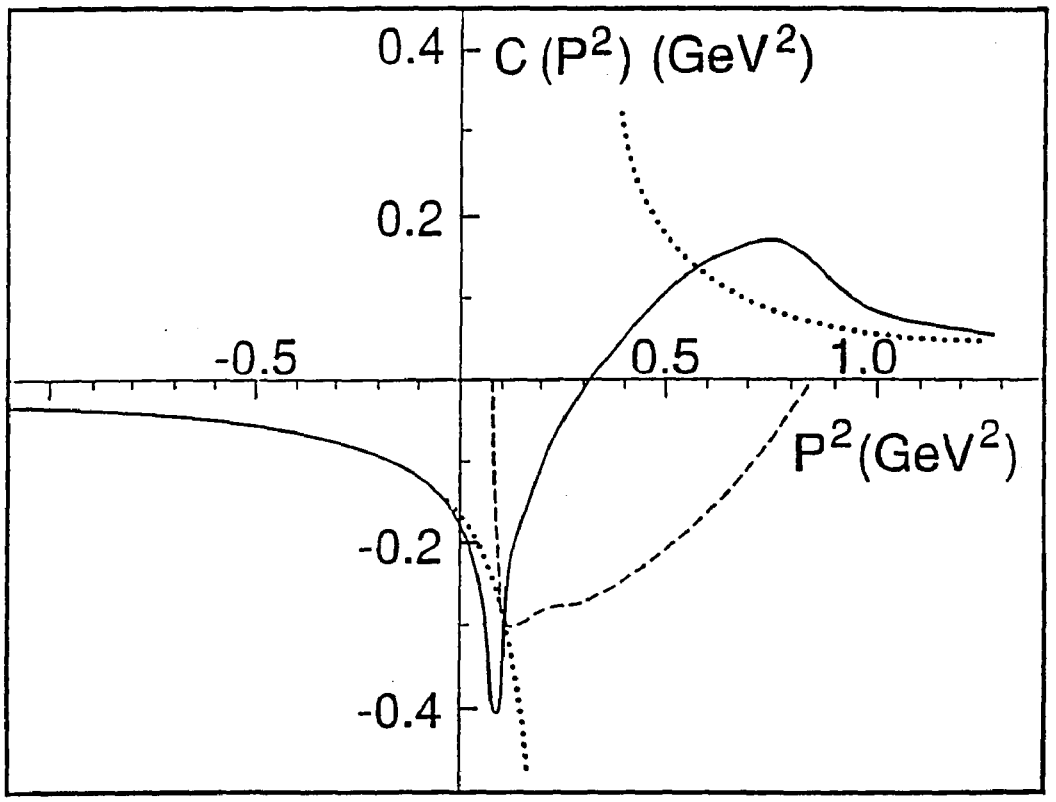

Fig. 4.4

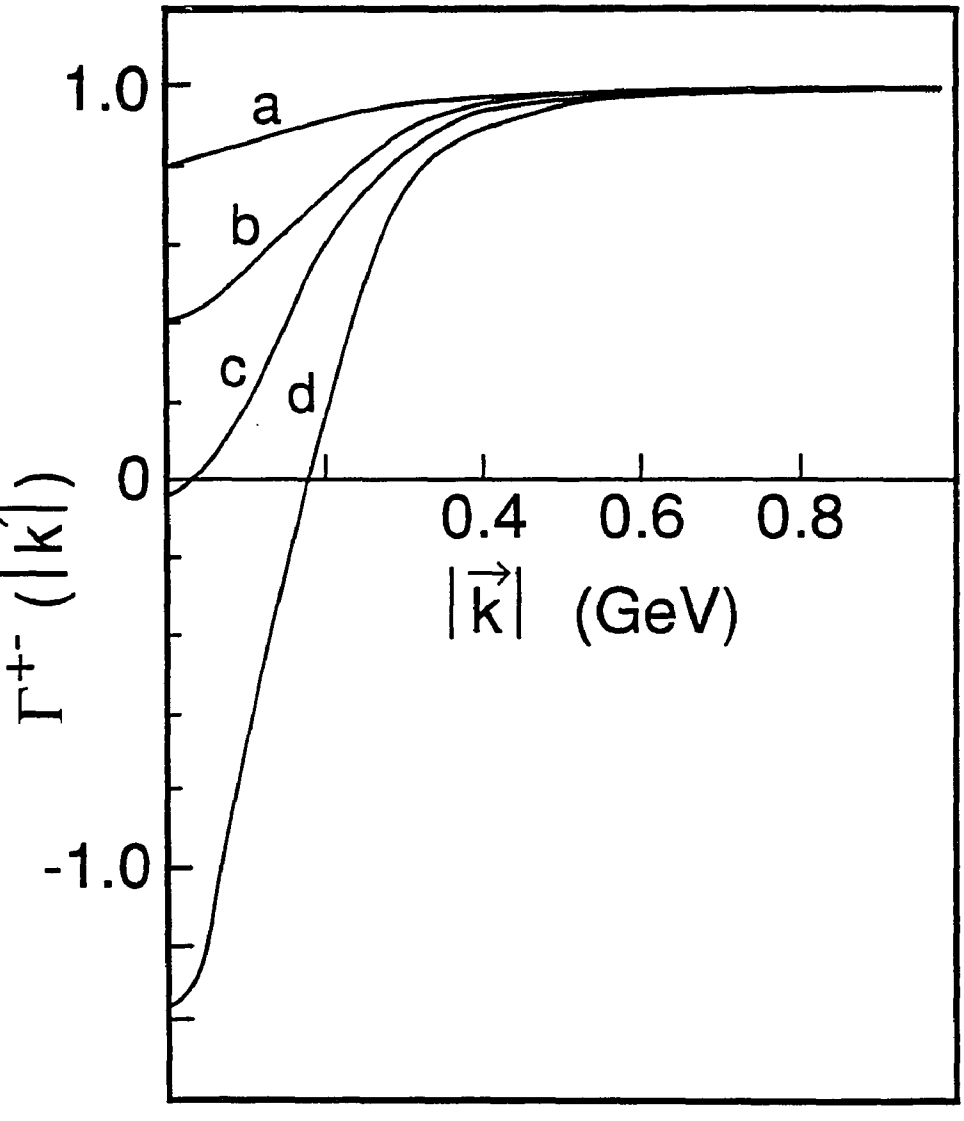

Fig. 5.1(a)

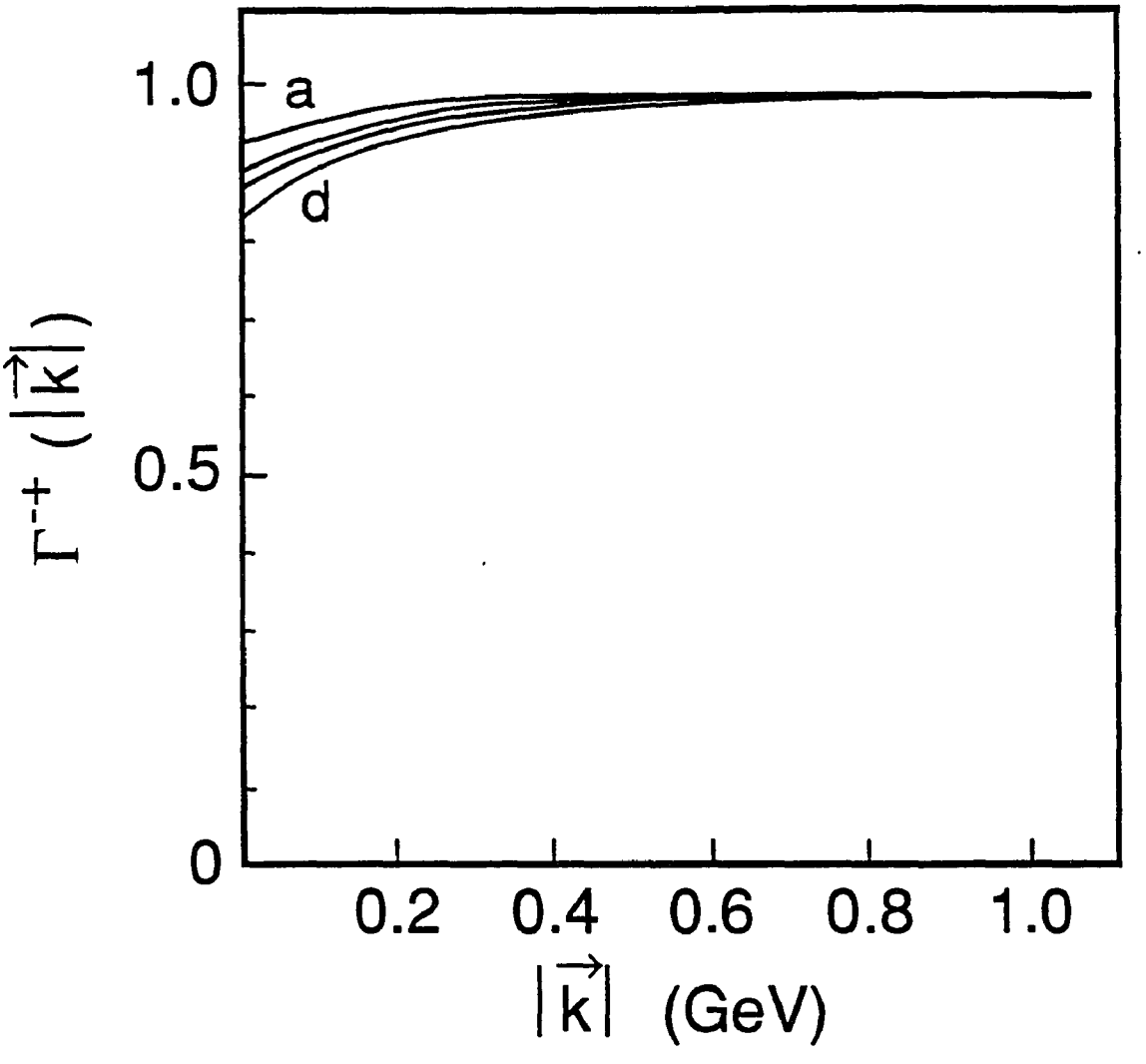

Fig. 5.1(b)

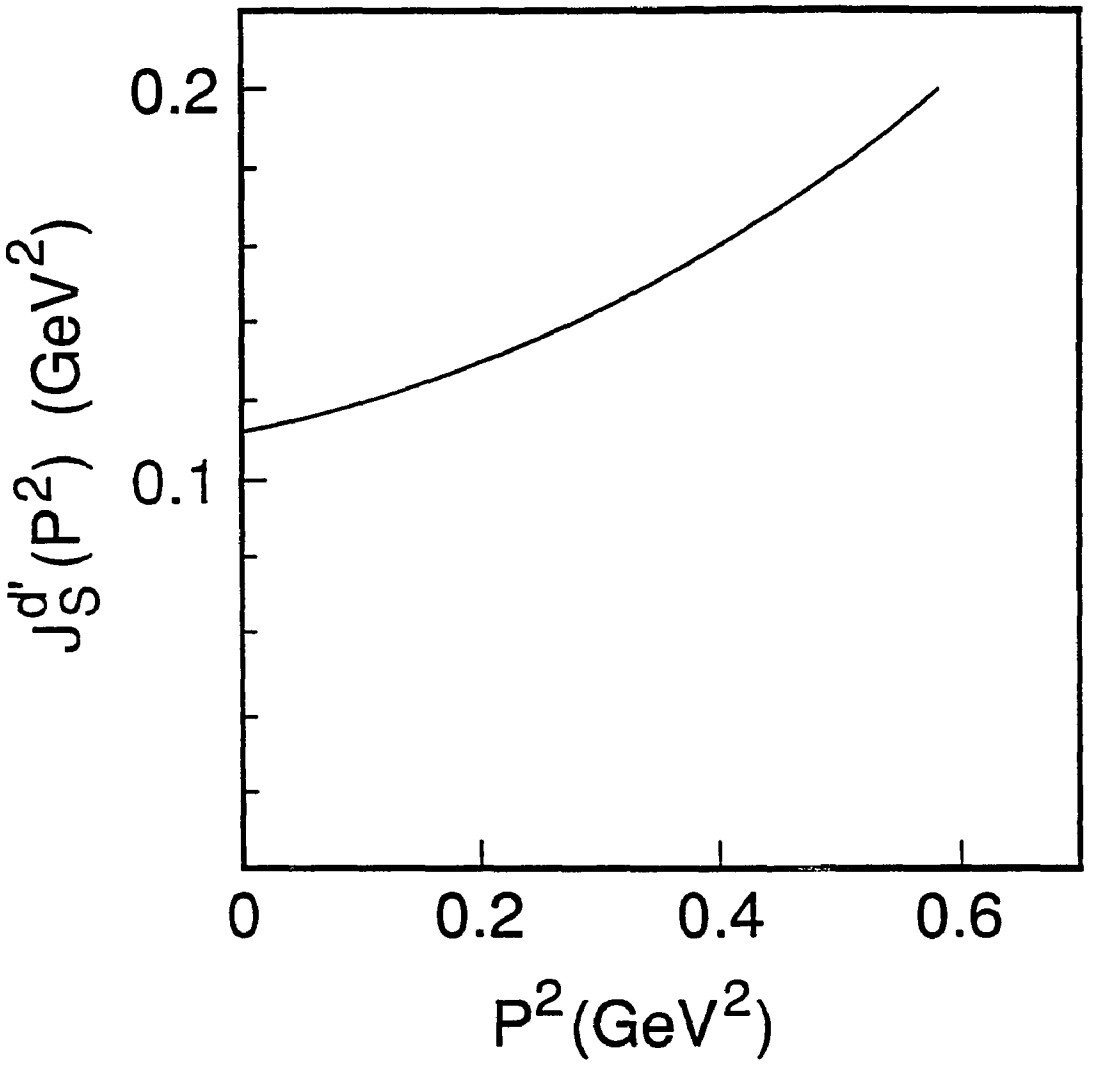

Fig. 5.2

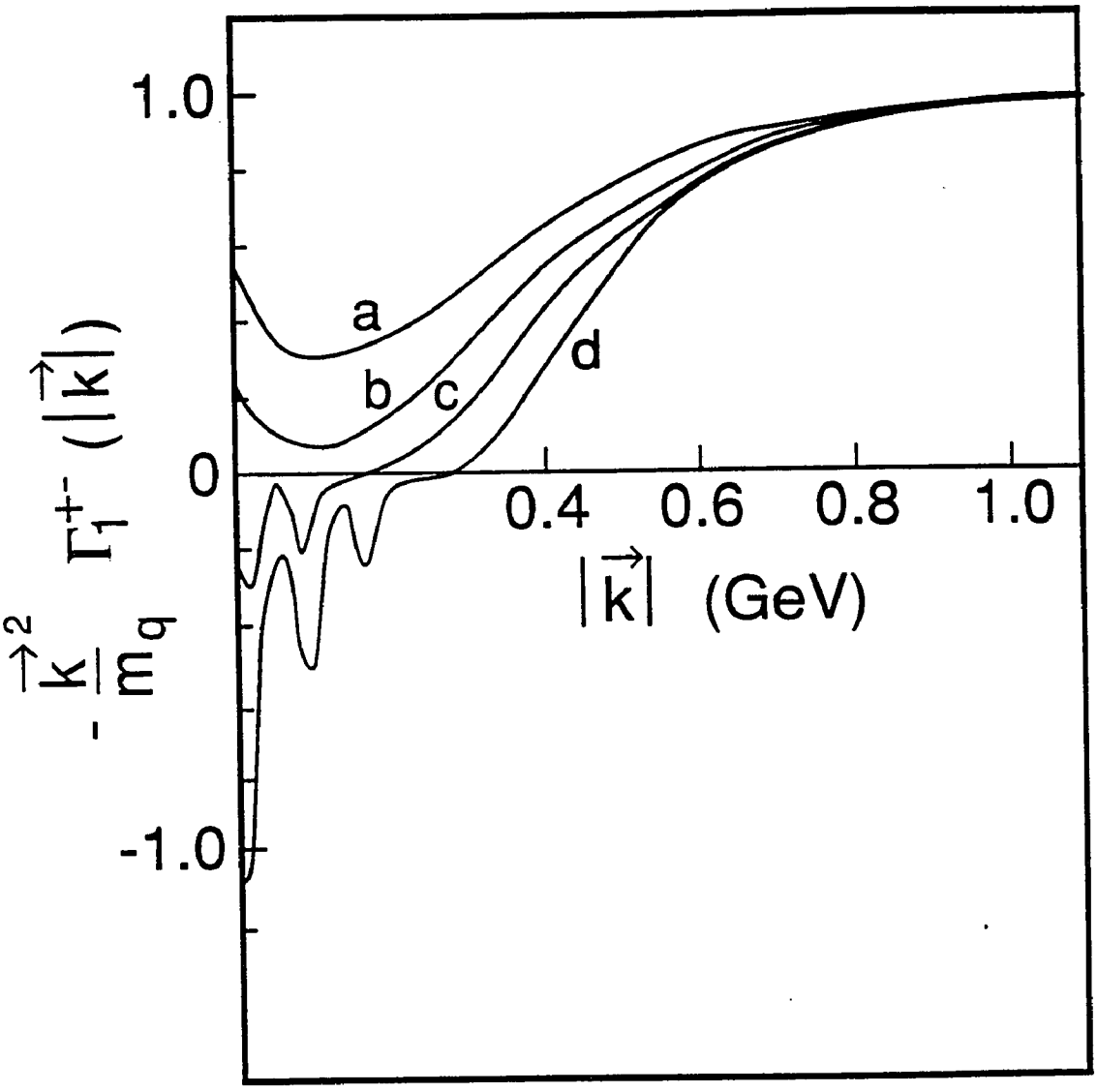

Fig. 5.3(a)

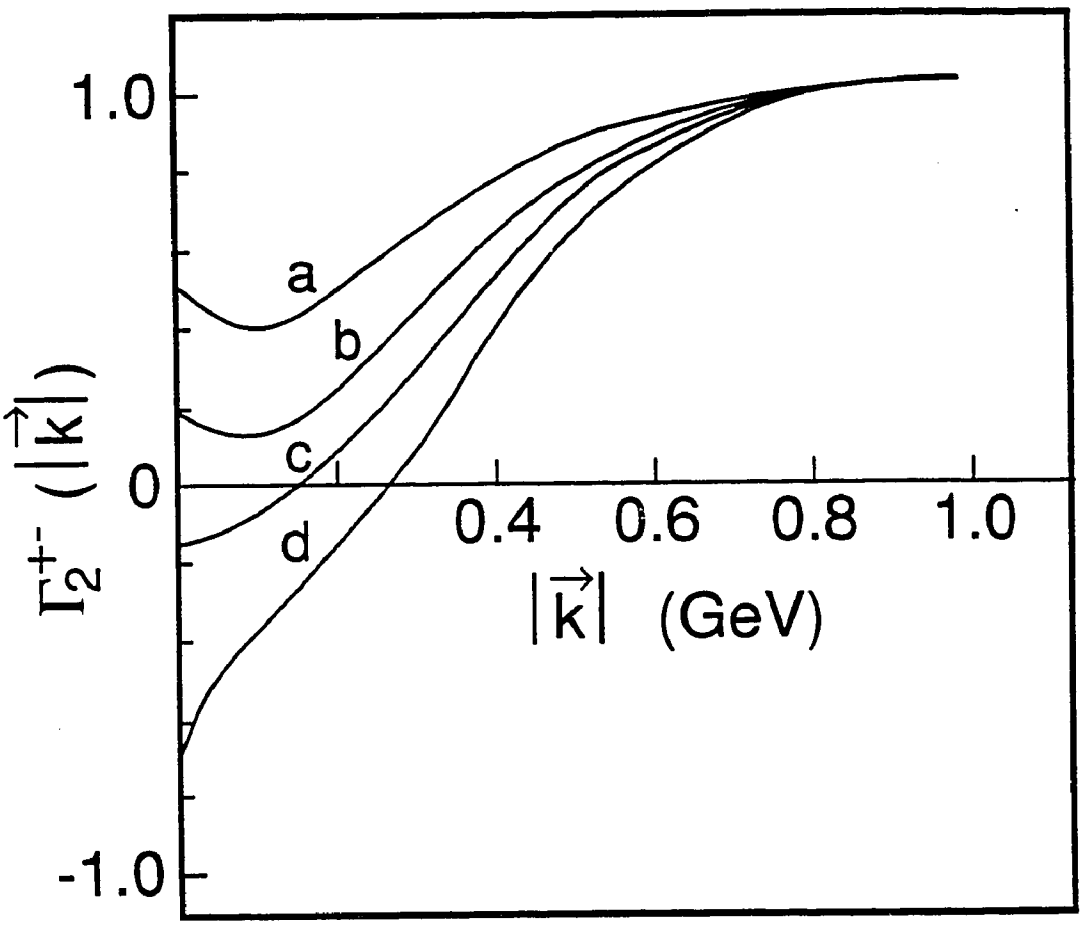

Fig. 5.3(b)

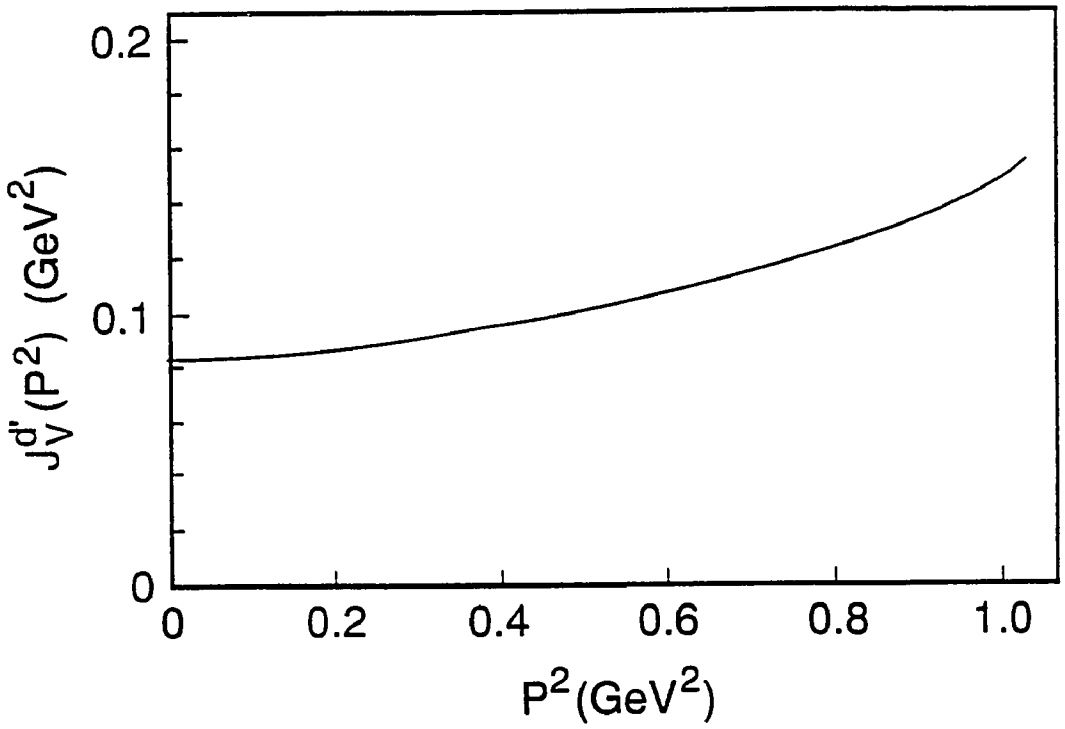

Fig. 5.4

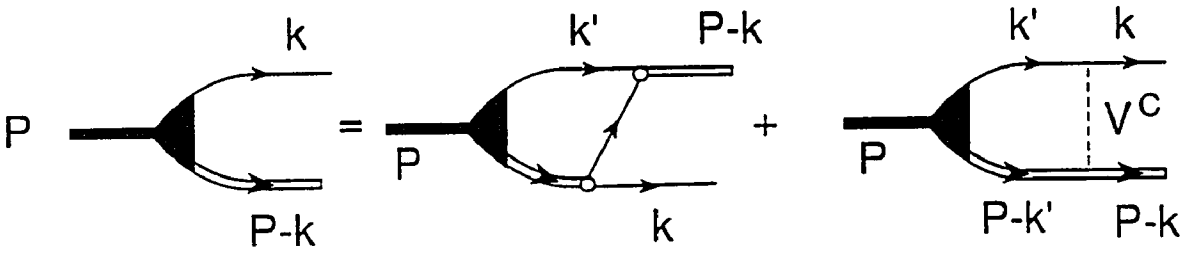

Fig. 6.1

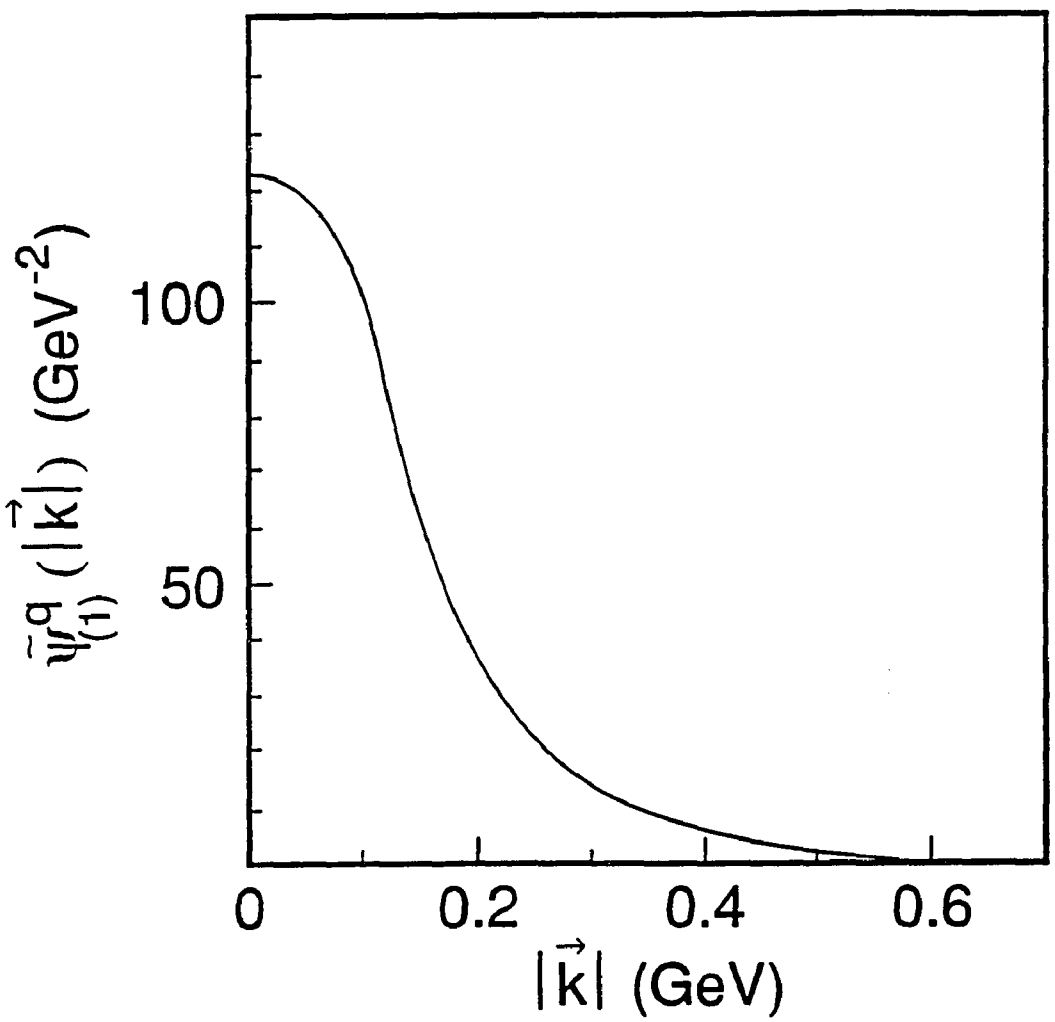

Fig. 6.2(a)

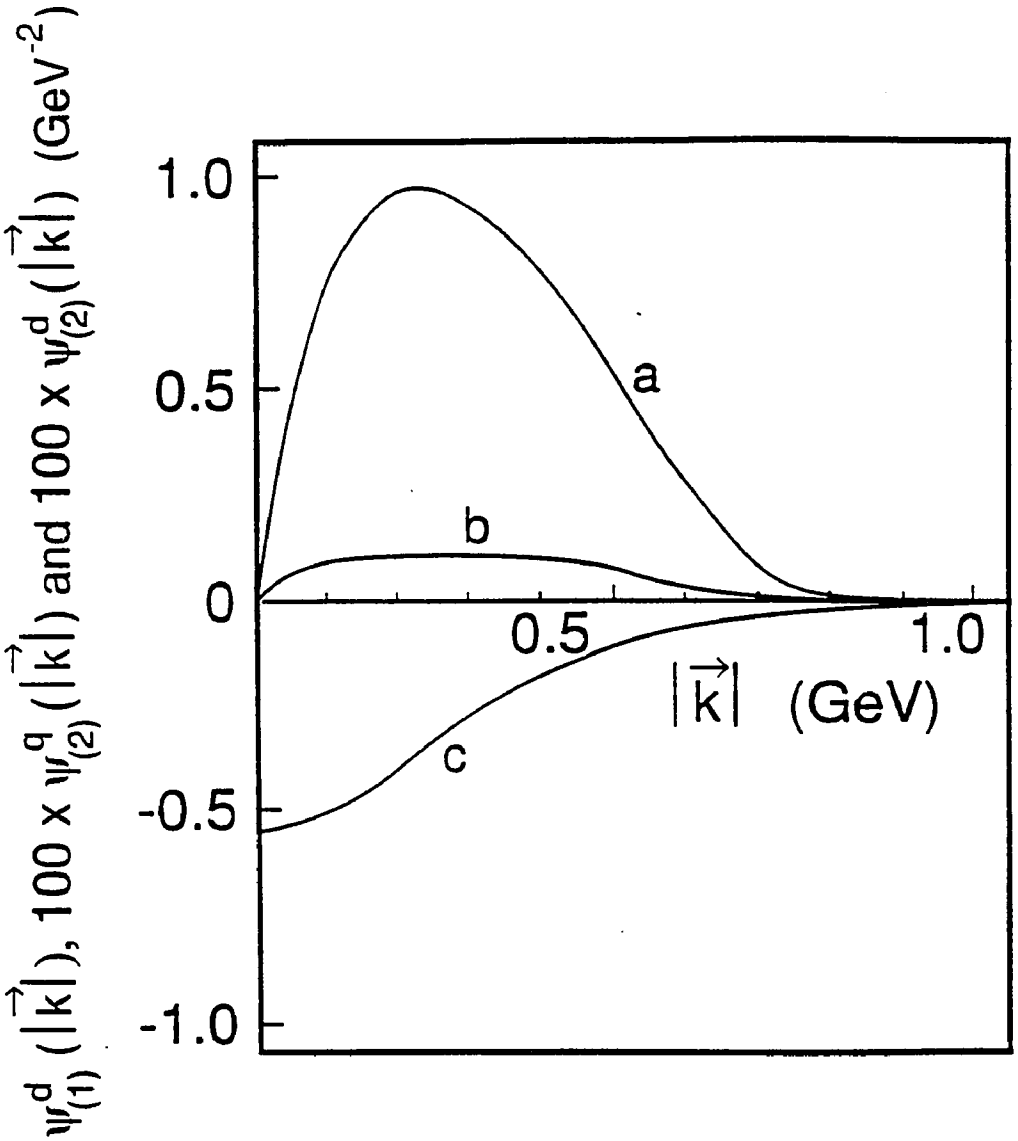
$\psi^d_{(1)}(|\vec{k}|)$, 100 x $\psi^q_{(2)}(|\vec{k}|)$ and 100 x $\psi^d_{(2)}(|\vec{k}|)$ (GeV^{-2})
1.0
0.5
0
-0.5
-1.0
0.5
1.0
$|\vec{k}|$ (GeV)
a
b
c

Fig. 6.2(b)

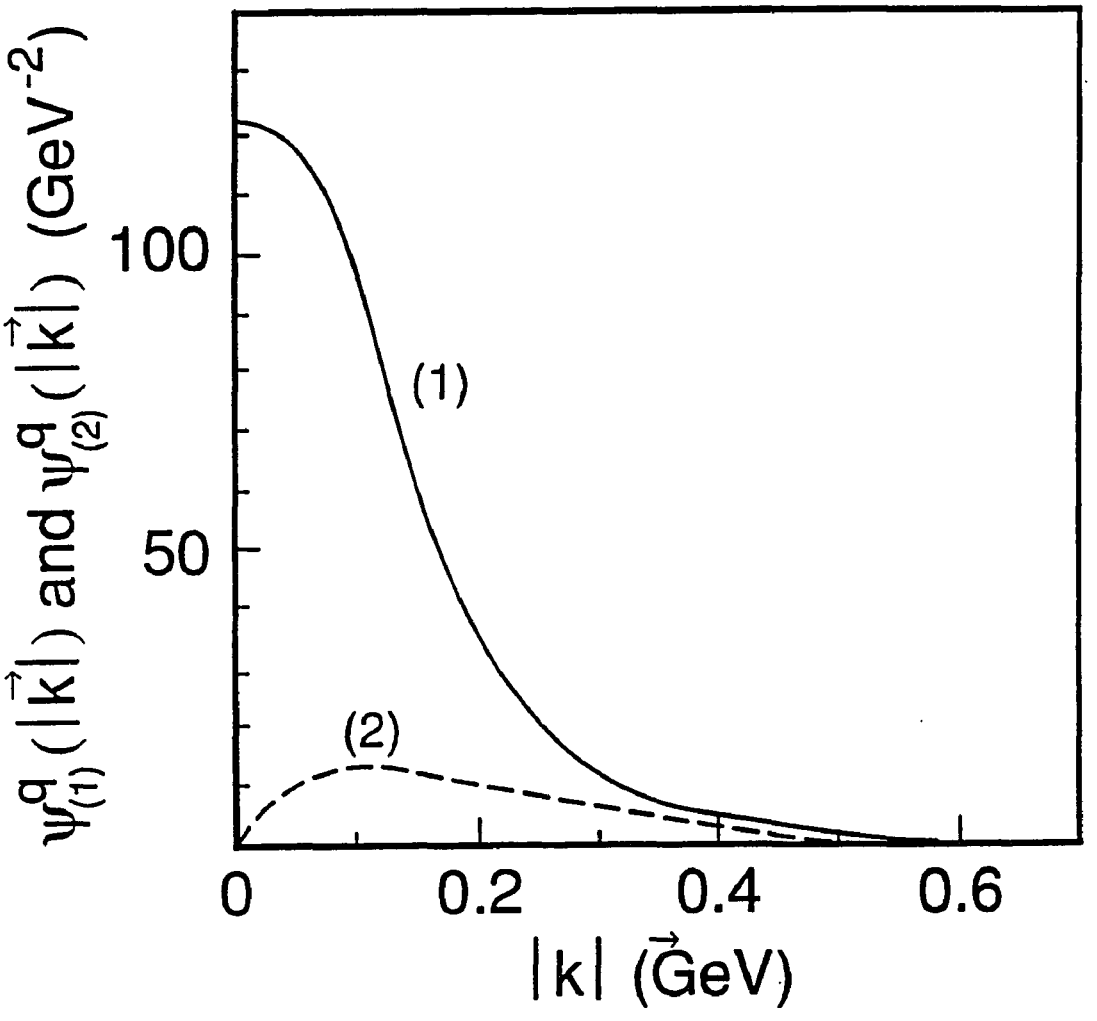

Fig. 6.3

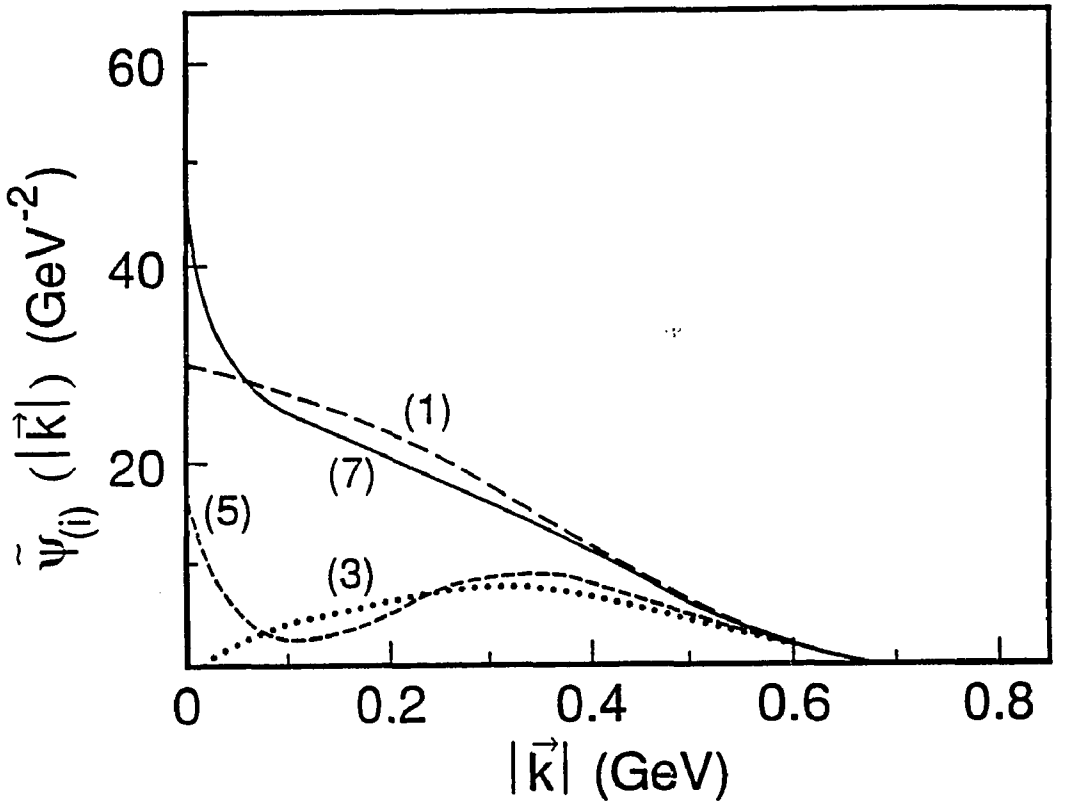

Fig. 6.4

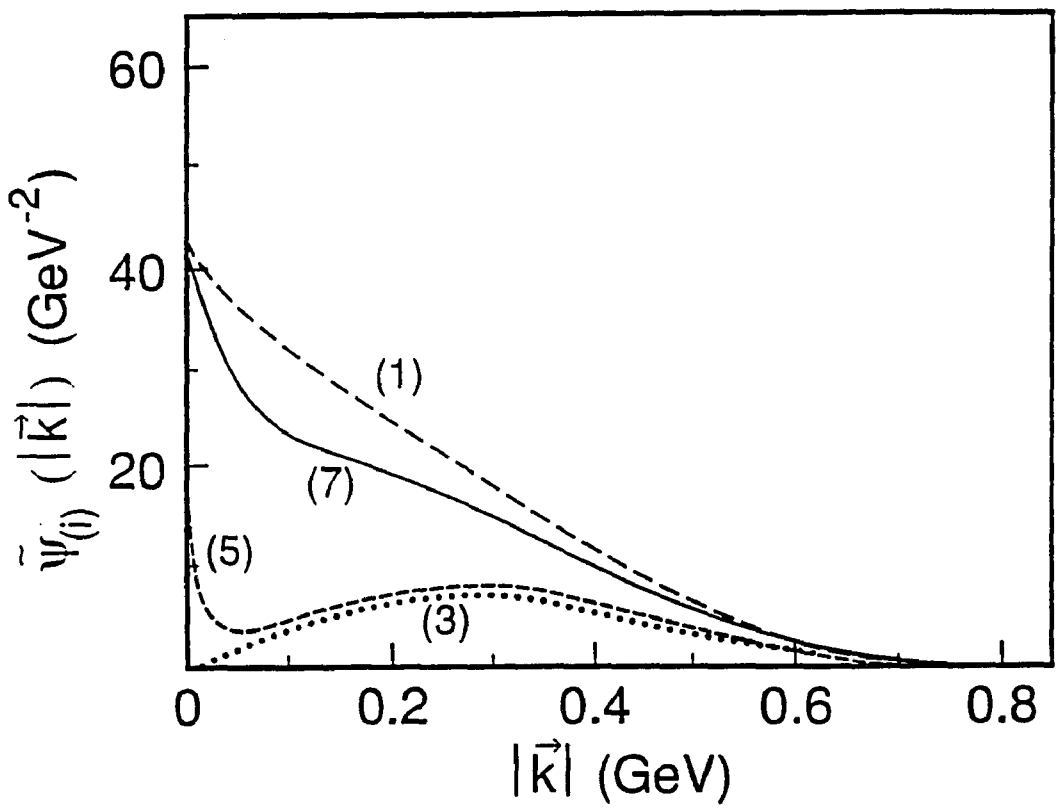

Fig. 6.5

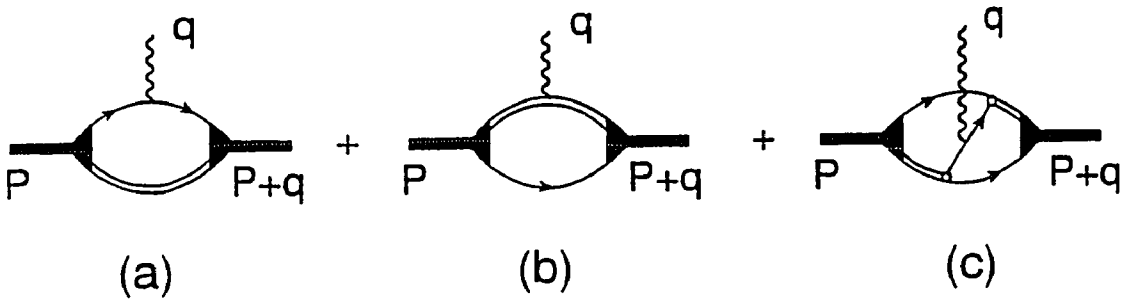

Fig. 7.1

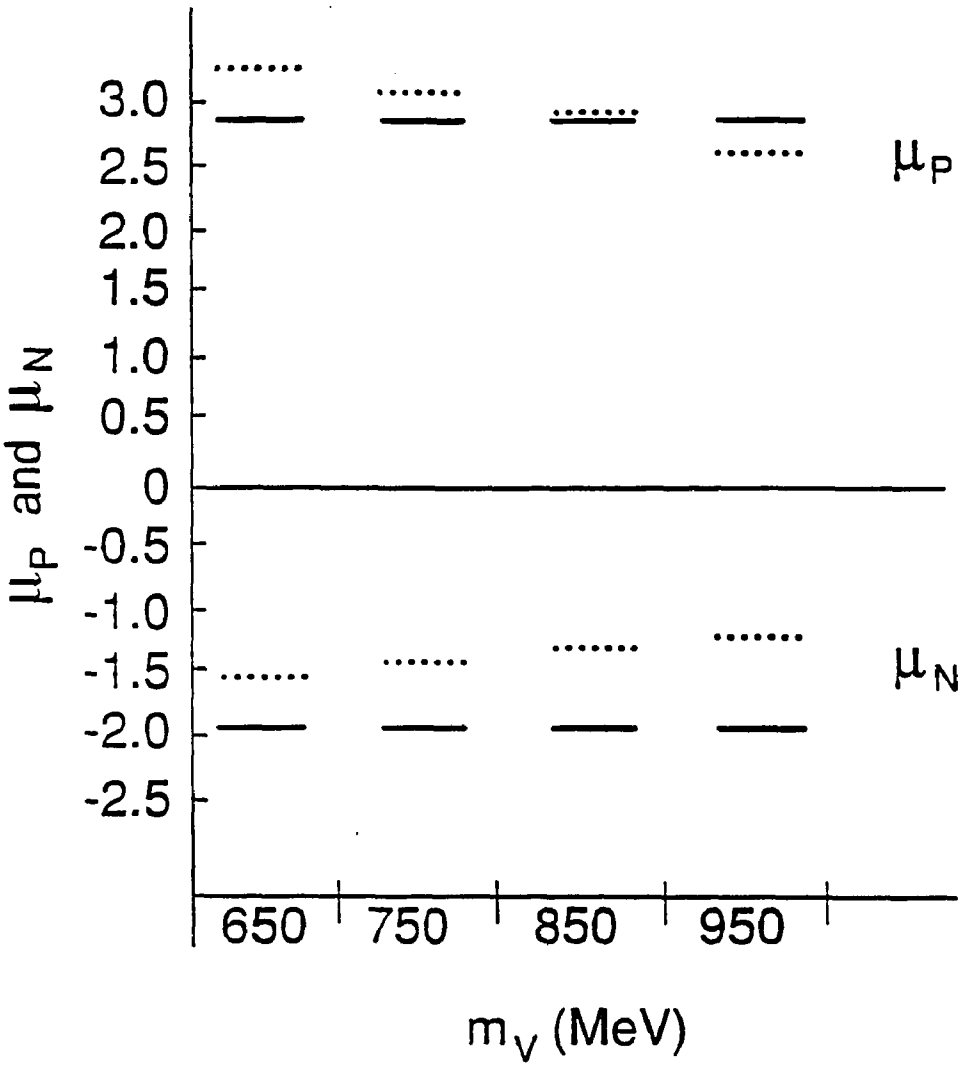
3.0
2.5
2.0
1.5
1.0
0.5
0
-0.5
-1.0
-1.5
-2.0
-2.5
μP and μN
μP
μN
650
750
850
950
mV (MeV)

Fig. 7.2

Appendix A

In this Appendix we describe the calculation of the diagram shown in Fig. 1(b). There the wavy lines denote pions with isospin indices, α and β. The Feynman amplitude, in the Bjorken-Drell convention, is with $q = p - p' = r - r'$

$$-iM(q^2) = (-1)^2 (iG_S)^2 g_{\pi qq}^4 n_c^2 \, Tr[\tau_\alpha(1)\tau_\beta(1)] \cdot Tr[\tau_\alpha(2)\tau_\beta(2)]$$

$$\times \int \frac{d^4k}{(2\pi)^4} D(k) \left\{ \int \frac{d^4k}{(2\pi)^4} Tr\,[\, S(p)\, S(p')\, \gamma_5\, S(r-k)\, \gamma_5\,] \right\} \qquad (A.1)$$

$$\times D(k') \left\{ \int \frac{d^4r}{(2\pi)^4} Tr\,[\, S(r)\, S(r')\, \gamma_5\, S(r-k)\, \gamma_5\,] \right\} .$$

Here, we use the notation $D(k) = i[k^2 - m_\pi^2 + i\epsilon]^{-1}$ and $S(p) = i[\not{p} - m_q + i\epsilon]^{-1}$

Further, n_c is the number of colors. With $n_f=2$ being number of flavors, we may write

$$-i\,M(q^2) = (-1)^2 (iG_S)^2 q_{\pi qq}^4 n_c^2 (n_f^2 - 1) \int \frac{d^4k}{(2\pi)^4} D(k) D(k') F^2(k^2, k\cdot q, q^2), \qquad (A.2)$$

where $F(k^2, k\cdot q, q^2)$ is a form factor,

$$F(k^2, k\cdot q, q^2) = \int \frac{d^4p}{(2\pi)^4} Tr\,[\, S(p)\, S(p-q)\, \gamma_5\, S(p-k)\, \gamma_5\,], \qquad (A.3)$$

$$= 8 m_q i^3 \int_0^1 dx \int_0^1 dy \int_0^1 dz\, \delta(1-x-y-z) \int \frac{d^4p}{(2\pi)^4} \frac{m_q^2 + q\cdot k - p^2 + 2p\cdot k}{[p^2 - 2p\cdot l - B^2]^3} , \qquad (A.4)$$

with $l = kz - qy$, $B^2 = m_q^2 - q^2y - k^2z$. Completing the square in the denominator, we find, with $A = B^2 + l^2$,

$$F(k^2, k\cdot q, q^2) = 8m_q i^3 \int_0^1 dy \int_0^{1-y} dx \left\{ [m_q^2 + q\cdot k + 2k\cdot l - l^2 - A] I_3(A) - I_2(A) \right\} \qquad (A.5)$$

where, upon introducing a Euclidean momentum-space cut-off, Λ,

$$I_2(A) = \frac{i}{16\pi^2} \left\{ \ln\left[\frac{\Lambda^2 + A}{A}\right] - \frac{\Lambda^2}{\Lambda^2 + A} \right\} , \qquad (A.6)$$

and

$$I_3(A) = \frac{-i}{48\pi^2} \left\{ \frac{(\Lambda^2 + A)^2 - (2\Lambda^2 A + A^2)}{A(\Lambda^2 + A)^2} \right\} . \qquad (A.7)$$

The discontinuity across the right-hand cut, for $q^2 < 4m_q^2$, is

$$-i\,\mathrm{Disc}[M(q^2)] = (-1)^2 (iG_S)^2 q_{\pi qq}^4 n_c^2 (n_f^2 - 1)\, i^2\, F^2(m_\pi^2, -q/2, q^2)$$

$$\times \int \frac{d^4k}{(2\pi)^4} \left[\delta^+(k'^2 - m_\pi^2)\, \delta^+(k^2 - m_\pi^2) \right] . \qquad (A.8)$$

The last integral in Eq. (A.9) has the value $\theta(q^2 - 4m_\pi^2)[1 - 4m_\pi^2/q^2]^{1/2}(1/32\pi^3)$, so that the result for imaginary part of $M(q^2)$ is (upon including a symmetry factor of 2)

$$\mathrm{Im}\,M(q^2) = \frac{8}{\pi} G_S^2 m_q^2 q_{\pi qq}^4 n_c^2 (n_f^2-1)\,\theta(q^2-4m_\pi^2)\left[1-\frac{4m_\pi^2}{q^2}\right]^{1/2} g^2(q^2)\ , \qquad (A.9)$$

where

$$g(q^2) = \int_0^1 dy \int_0^{1-y} dx \left\{ [x(3-2x)m_\pi^2 + q^2(2y-2y^2-\frac{1}{2}-2xy)]\, I_3(A) - I_2(A) \right\}\ , \qquad (A.10)$$

with

$$A = m_q^2 + m_\pi^2 x(x-1) + q^2 y(y+x-1)\ . \qquad (A.11)$$

We remark that $\mathrm{Im}M(q^2) \leq 0$, since $g(q^2)$ of Eq. (A.11) is pure imaginary. [See Eqs. (A.7) and (A.8).] Values for $\mathrm{Re}M(q^2)$ and $\mathrm{Im}M(q^2)$ are given in Fig. 7. If we make use of $M(q^2)$ rather than $G_{\pi S}^2 J_\pi(q^2)$, we have $D(q^2) = 1 - G_S J_S(q^2) + M(q^2)J_S(q^2)$. [See Fig. 8.] The replacement of $G_{\pi S}^2 J_\pi(q^2)$ by $M(q^2)$ defines model B.

Appendix B

In Appendix B we will use the following definitions:

$$K = \frac{1}{\sqrt{2\,|\vec{k}|\,|\vec{k}|}}\ , \tag{B.1}$$

$$z = \frac{\vec{k}\cdot\vec{k}'}{|\vec{k}|\,|\vec{k}'|}\ , \tag{B.2}$$

$$z_0 = K^2(\vec{k}^2 + \vec{k}'^2 + m_q^2)\ , \tag{B.3}$$

$$\alpha = K(P_0 - k_0 - k_0')\ . \tag{B.4}$$

and

$$\beta = \log|\alpha - \sqrt{z+z_0}\,|\ , \tag{B.5}$$

Then the quantities defined by Eqs. (6.26) and (6.27) are

$$I_{2n+1} = K\,[\,I_{2n+1}(1) - I_{2n+1}(-1)\,]\ , \tag{B.6}$$

where we define

$$I_{2n+1}(z) = \int dz\ z^n\left[\alpha - \sqrt{z+z_0}\right]^{-1}\ , \tag{B.7}$$

and

$$I_{2n+2} = K^2\,[\,I_{2n+2}(1) - I_{2n+2}(-1)\,]\ , \tag{B.8}$$

where

$$I_{2n+2}(z) = \int dz\ z^n \left\{ \sqrt{z+z_0} \left[\alpha - \sqrt{z+z_0} \right] \right\}^{-1} . \qquad (B.9)$$

Integrals (B.7) and (B.9) are

$$I_1(z) = -2(z+z_0)^{1/2} - 2\alpha\beta , \qquad (B.10)$$

$$I_2(z) = -2\beta , \qquad (B.11)$$

$$I_3(z) = -\alpha z + \frac{2}{3}(z+z_0)^{1/2}(-3\alpha^2 - z + 2z_0) - 2\alpha(\alpha^2 - z_0)\beta , \qquad (B.12)$$

$$I_4(z) = -z - 2\alpha(z+z_0)^{1/2} - 2(\alpha^2 - z_0)\beta , \qquad (B.13)$$

$$I_5(z) = -\frac{\alpha}{2}(z+z_0)^2 - \frac{2}{5}(z+z_0)^{5/3} - 2(-\alpha+z_0)^2(z+z_0)^{1/2} + \alpha(z+z_0)(-\alpha^2+2z_0) + \frac{2}{3}\alpha(z+z_0)^{3/2}(-\alpha^2+2z_0) - 2\alpha(-\alpha^2+z_0)^2\beta \qquad (B.14)$$

$$I_6(z) = -\frac{2}{3}\alpha(z+z_0)^{3/2} - \frac{1}{2}(z+z_0)^2 + 2\alpha(-\alpha^2+2z_0)(z+z_0)^{1/2} + (z+z_0)(-\alpha^2+2z_0) - 2(-\alpha^2+z_0)^2\beta . \qquad (B.15)$$

References

[Ba 83] A.P.Balasandran, V.P.Nair, S.G.Rajeev and A.Stern, Phys. Rev. D27, 1153 (1983).

[Bi 93] J. Bijnens, C.Bruno and E.de Raphael, Nucl.Phys B390, 501 (1993).

[Bu 92] A.Buck, R.Alhofer and H.Reinhardt, Phys. Lett. B286, 29 (1992).

[Ca 89] R.T.Cahill, C.D.Roberts and J.Praschifka, Aust. J. Phys. 42, 129 (1989).

[Ce 86] L.S.Celenza and C.M.Shakin, Relativistic Nuclear Physics: Theories of Structure and Scattering (World Scientific, Singapore, 1986).

[Ce 92] L.S.Celenza, A.Pantziris, C.M.Shakin and Wei-Dong Sun, Phys. Rev. C45, 205 (1992).

[Ce 93a] L.S.Celenza, C.M.Shakin, Wei-Dong Sun, J.Szweda and Xiquan Zhu, J. Mod. Phys. E2, 603 (1993).

[Ce 93b] L.S.Celenza, C.M.Shakin and J.Szweda, Intl. J. Mod. Phys. E2, 437 (1993).

[Ce 93c] L.S.Celenza, C.M.Shakin, Wei-Dong Sun, J.Szweda and Xiquan Zhu, Brooklyn College Report BCCNT 93/07/232 (1993) - to be published in Annals of Physics.

[Ce 93d] L.S.Celenza, A.Pantziris, C.M.Shakin and J.Szweda, Phys. Rev. C 47, 2356 (1993).

[Ce 93e] L.S.Celenza, C.M.Shakin, Wei-Dong Sun and Xiquan Zhu, Phys. Rev. 48, 159 (1993).

[Du 77] J.W.Durso, M.Saavela G.E.Brown and A.D.Jackson, Nucl. Phys. A278, 445 (1977).

[Du 80] J.W.Durso, A.D.Jackson and B.J. Verwest, Nucl. Phys. A345, 471 (1980).

[Eb 86] D.Ebert and H.Reinhardt, Nucl. Phys. B271, 188 (1986).

[Gr 91] F.Gross and J.Milana, Phys. Rev. D43, 2401 (1991).

[Gr 92] F.Gross and J.Milana, Phys. Rev. D45, 969 (1992).

[Is 93a] N.Ishii, W.Bentz and K.Yazaki, Phys. Lett. B301, 165 (1993).

[Is 93b] N.Ishii, W.Bentz and K.Yazaki, Phys. Lett. B318, 26 (1993).

[Jo 78] K.Johnson,Phys. Lett B78, 259 (1978).

[Kl 92] S.P.Klevansky, Rev. Mod. Phys. 64, 649 (1992).

[Ma 89] R.Machleidt, in Advances in Nuclear Physics, Vol 19, eds. J.W. Negele and E.Vogt (Plenum, New york, 1989).

[Na 61] Y.Nambu and G.Jona-Lasinio, Phys.Rev. 122, 345 (1961); 124, 246 (1961).

[Re 90] H.Reinhardt, Phys. Lett. B234, 316 (1990).

[Se 86] B.D.Serot and J.D. Walecka, in advances in Nuclear Physics, Vol. 16, eds. J.W.Negele and E.Vogt (Plenum, New York, 1986).

[Sh 93a] C.M.Shakin, Wei-Dong Sun and J.Szweda, Brooklyn College Report: BCCNT 93/093/236 (1993) - submitted to Phys. Rev. D.

[Sh 93b] C.M.Shakin, Wei-Dong Sun and J.Szweda, Brooklyn College Report: BCCNT 93/081/233R (1993) - to be published in Annals of Physics.

[Vo 91] V.Vogl and W.Weise, Prog. Part. Nucl. Phys. 27, 195 (1991).

[We 94] H.J.Weber, Phys. Rev. D49, 3160 (1994).